REPORT NO.
UCB/EERC-88/12
SEPTEMBER 1988

EARTHQUAKE ENGINEERING RESEARCH CENTER

NONLINEAR ANALYSIS OF REINFORCED CONCRETE FRAMES UNDER CYCLIC LOAD REVERSALS

by

FILIP C. FILIPPOU
AHMAD ISSA

Report to the National Science Foundation

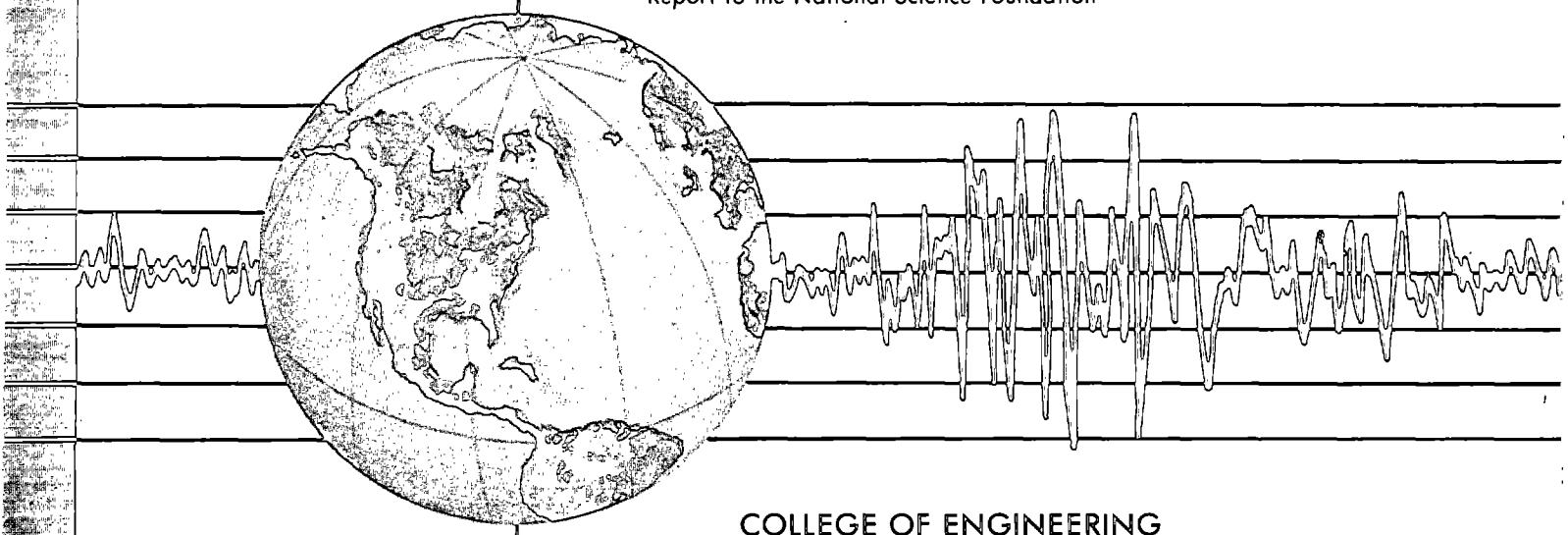

COLLEGE OF ENGINEERING

UNIVERSITY OF CALIFORNIA AT BERKELEY

1.6

For sale by the National Technical Information Service, U.S. Department of Commerce, Springfield, Virginia 22161

See back of report for up to date listing of EERC reports.

50272-101

REPORT DOCUMENTATION PAGE	1. REPORT NO. NSF/ENG-88048	2.	3 PB91-212589

4. Title and Subtitle
Nonlinear Analysis of Reinforced Concrete Frames Under Cyclic Load Reversals

5. Report Date
September 1988

6.

7. Author(s)
F.C. Filippou and A. Issa

8. Performing Organization Rept. No.
UCB/EERC-88/12

9. Performing Organization Name and Address
Earthquake Engineering Research Center
University of California, Berkeley
1301 S 46th St.
Richmond, CA 94804

10. Project/Task/Work Unit No.

11. Contract(C) or Grant(G) No.
(C)
(G) ECE-8657525

12. Sponsoring Organization Name and Address
National Science Foundation
1800 G. St. NW
Washington, DC 20550

13. Type of Report & Period Covered

14.

15. Supplementary Notes

16. Abstract (Limit: 200 words)

This report describes the static response in a study which endeavors to develop improved analytical methods for predicting the nonlinear static and dynamic response of multistory reinforced concrete frames. A new approach is proposed that consists of isolating the basic mechanisms controlling the hysteretic behavior of girders and columns into individual subelements which are connected in series to form the girder or column superelement. Two particular subelement models are developed: one describes the inelastic behavior along the girder accounting for the gradual spread of inelastic deformations at the girder ends, while the other models the fixed-end rotations that arise at the beam-column interface. The implementation of the superelement model requires the development of a numerical scheme which accounts for unbalanced moments between subelements. Such a scheme is developed within the framework of a special purpose analysis program for the nonlinear static and dynamic analysis of reinforced concrete moment-resisting frames.

Correlation studies show that the analytical predictions for the proposed models show excellent agreement with the experimental results. The predictions of the proposed model are compared with those of the widely used one-component model by investigating the local and global response of simple structural subassemblages under cyclic load reversals. It is concluded that the parameters of the one-component model can be adjusted to match reasonably well a given response.

17. Document Analysis a. Descriptors

b. Identifiers/Open-Ended Terms

c. COSATI Field/Group

18. Availability Statement	19. Security Class (This Report)	21. No. of Pages
Release Unlimited	unclassified	130
	20. Security Class (This Page) unclassified	22. Price

NONLINEAR ANALYSIS OF REINFORCED CONCRETE FRAMES UNDER CYCLIC LOAD REVERSALS

by

Filip C. Filippou

Assistant Professor of Civil Engineering

Ahmad Issa

Research Assistant

A Report on Research Conducted under
Grant ECE-8657525 from the
National Science Foundation

Report No. UCB/EERC-88/12
Earthquake Engineering Research Center
College of Engineering
University of California Berkeley, California

September 1988

ABSTRACT

This study endeavors to develop improved analytical methods for predicting the nonlinear static and dynamic response of multistory reinforced concrete frames. This report is limited to the study of the static response.

A new approach in describing the nonlinear hysteretic behavior of reinforced concrete frame elements is proposed. This approach consists of isolating the basic mechanisms controlling the hysteretic behavior of girders and columns into individual subelements which are connected in series to form the girder or column superelement. Two particular subelement models are developed in this study: one describes the inelastic behavior along the girder accounting for the gradual spread of inelastic deformations at the girder ends, while the other models the fixed-end rotations that arise at the beam-column interface due to bond deterioration and slippage of reinforcing bars in the beam-column joint region. The properties of these elements can be derived from basic principles or refined finite element models.

Because several subelements are connected in series and each of these follows a different hysteretic rule, internal unbalanced moments might arise between these elements at any given load step. The implementation of the proposed superelement model thus requires the development of a numerical scheme which accounts for these unbalanced moments between subelements. Such a scheme is developed in this study within the framework of a special purpose analysis program for the nonlinear static and dynamic analysis of reinforced concrete moment-resisting frames.

To establish the validity of the proposed models correlation studies of analytical predictions with experimental evidence of the load-displacement response of beam-column subassemblages under static load reversals are conducted. The analytical predictions generally show excellent agreement with the experimental results.

The predictions of the proposed model are also compared with those of the widely used one-component model. The two models are compared by investigating the local and global response of simple structural subassemblages under cyclic load reversals. One of the key parameters of the one-component model, namely, the post-yield stiffness of the moment-rotation envelope curve is varied in these studies. It is concluded that the parameters of the one-component model can be adjusted to match reasonably well a given response. These parameters vary, however, with the type and history of loading as well as with the type of subassemblage. By contrast, the proposed model, while maintaining computational efficiency, is based on parameters which are directly connected with the physical properties of the structural elements and can be derived by well established rational methods.

ACKNOWLEDGEMENTS

This study was supported by Grant No. ECE-8657525 from the National Science Foundation with Dr. A.J. Eggenberger as program director. This support is gratefully acknowledged. Any opinions expressed in this report are those of the authors and do not reflect the views of the sponsoring agency.

The participation in the early stages of this work of Maria Gabriella Mulas from the Politecnico di Milano helped in the definition of the problem.

We wish to express our deep appreciation to Professor Vincenzo Ciampi of the University of Rome for helpful comments on the nonlinear analysis algorithm. Finally, we thank Professor Graham Powell for devoting time to a general discussion of nonlinear analysis algorithms.

TABLE OF CONTENTS

LIST OF FIGURES

CHAPTER 1

INTRODUCTION

1.1 General

Reinforced concrete (RC) structures designed according to present building codes as moment resisting space frames, shear-walls, coupled shear-walls or any combination thereof to withstand strong earthquake motions are expected to deform well into the inelastic range and dissipate the energy input by the base motion through stable hysteretic behavior of structural components. Since inelastic deformations are typically concentrated at certain critical regions within the structure (Fig. 1.1) [BER75-2], the accurate prediction of the mechanical behavior of the structure during earthquake excitations depends on the development of reliable analytical models which describe the hysteretic behavior of these regions.

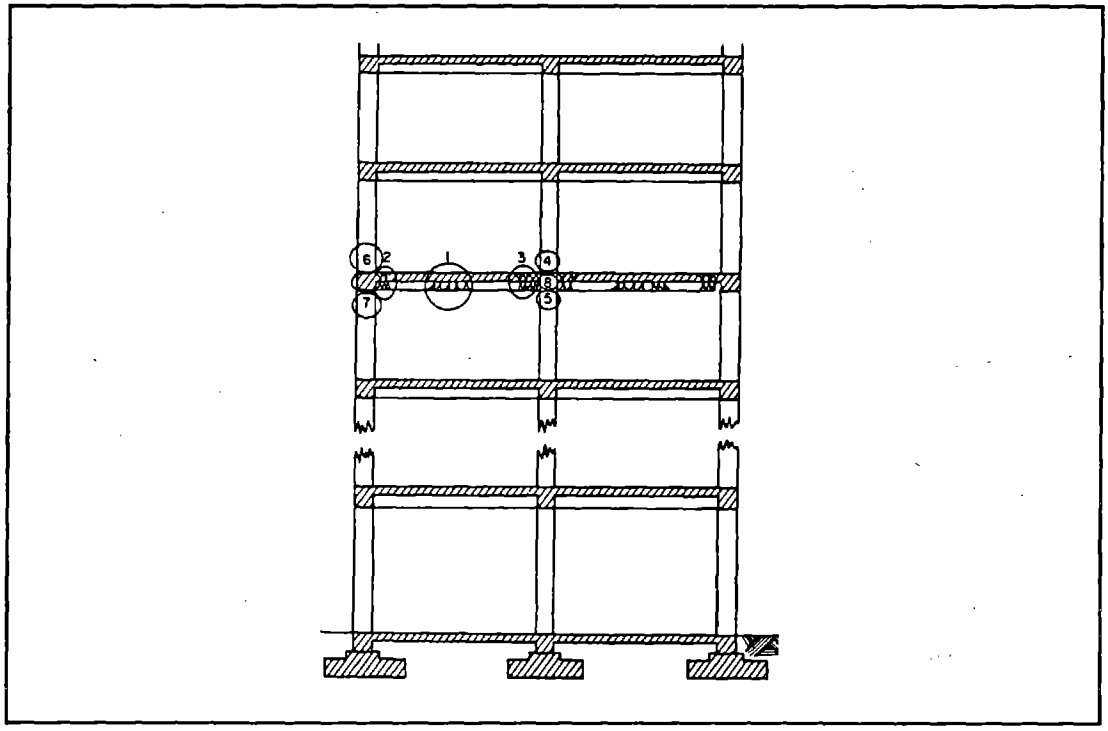

Fig. 1.1 *Critical regions in reinforced concrete frames subjected to cyclic excitations from [BER75-1]*

Ideally these models should be based on an accurate representation of material behavior taking into account the controlling states of stress or strain and identifying the main parameters which influence the hysteretic behavior of each critical region in order to predict the behavior up to failure of any structural component during the earthquake response. At the same time these models should be computationally efficient, so that the dynamic response of multistory structures under earthquake excitations can be determined within reasonable time.

Following present earthquake resistant design philosophy the energy input by the base motion should be dissipated in the largest possible number of inelastic regions within the structure. Ductile moment resisting space frames are designed so that yielding starts to develop at the girder ends. Columns of a ductile moment resisting space frame should remain elastic during the earthquake response, except at the base of the building, to avoid the formation of a partial sidesway collapse mechanism. Attention is thus focused on understanding and predicting the hysteretic behavior of critical regions in girders as well as that of beam-column or girder-wall joints (regions 1, 2, 3 and 8 in Fig. 1.1).

Various experimental studies of reinforced concrete structural subassemblages [DUR82-1], [JIR77-1], actual multistory buildings and dynamic tests of model frames have demonstrated that, when properly designed and detailed critical regions of RC structures are subjected to severe cyclic excitations, the major concern is the deterioration of stiffness.

The principal effects of stiffness deterioration are:

(1) an increase in the flexibility and period of vibration of the undamaged structure during large deformation reversals,

(2) a decrease in energy dissipation capacity,

(3) a significant redistribution of internal forces which could lead to excessive deformations in some regions.

Since induced seismic forces and deformations are sensitive to structural flexibility, natural period of vibration and energy dissipation capacity, the stiffness deterioration modifies the overall response of the structure.

1.2 Review of previous studies

Much effort has been devoted in the last twenty years to the development of models of inelastic response of RC elements subjected to large cyclic deformation reversals. Numerous models

incorporating information from experimental investigations and on-field observations of the hysteretic behavior of RC structural elements have been proposed. These range from the simple two-component model with bilinear hysteretic law to refined fiber or layer models based on sophisticated descriptions of the cyclic stress-strain behavior of concrete and reinforcing steel. Since this study focuses on relatively simple models which can be economically used in studying the seismic response of multistory frame structures, only the developments leading to a macroscopic model of inelastic response of RC elements will be briefly reviewed in the following.

The very first inelastic girder model was proposed by Clough et. al. in 1965 [CLO65-1]. In this model, known as the two-component model, a bilinear elastic-strain hardening moment-curvature relationship is assumed along the length of the girder. The beam model consists of two components acting in parallel: one which is linear elastic and one which is elastic-perfectly plastic with the plastic deformations concentrated in plastic hinges at the ends of the element. The elastic modulus of the first component is equal to the strain hardening modulus $p \cdot EI$ of the moment-curvature relation, where EI is the pre-yield section stiffness. The elastic modulus of the elasto-plastic component is equal to $q \cdot EI$ where $q = 1 - p$. One of the shortcomings of this model is the difficulty of accounting for the stiffness deterioration of RC elements during cyclic load reversals.

To overcome the problem of stiffness deterioration Giberson proposed another model in 1969 [GIB69-1]. This model is known as the one-component model. It consists of two nonlinear rotational springs which are attached at the ends of a perfectly elastic element representing the girder. All nonlinear deformations of the girder element are lumped in the two rotational springs. This is a simplification of experimental evidence which shows that inelastic deformations spread over a finite region at the ends of the girder. Giberson's model has the advantage that any kind of hysteretic law can be assigned to the nonlinear springs. This fact along with the simplicity of the model accounts for its wide use in analytical studies to date.

To describe the hysteretic behavior of the nonlinear springs at the ends of the one-component model a hysteretic law is needed. The first such law was proposed by Clough [CLO65-1]. A more refined hysteresis model was proposed by Takeda et. al. in 1972 [TAK72-1]. In this model the monotonic behavior is described by a trilinear skeleton curve which accounts for cracking of concrete and yielding of reinforcing steel. The hysteretic behavior is described through a number of rules for unloading and reloading and is based on data obtained from specimens tested in an earthquake simulator. Even though Takeda's hysteretic model was originally proposed for simulating the load-displacement relation of RC subassemblages, it has been widely used since in the description of the hysteretic moment-curvature or moment-rotation relation of RC members.

A different approach to the problem of modeling the seismic behavior of RC girders was proposed by Otani [OTA74-1]. In this case each beam or column member is divided into two linear elements, one linearly elastic and one inelastic, which act in parallel. One inelastic rotational spring is attached at each end of the member. These represent the fixed-end rotations at the beam-column interface due to slip of the reinforcement in the joint. In Otani's model the linear elastic element represents the entire elastic stiffness of the girder; the flexibility matrix of the inelastic element is derived as a function of the location of the point of contraflexure. This approach results in a non-symmetric flexibility matrix, unless one of the following assumptions is made: (a) the inelastic deformations are concentrated at the girder ends, or (b) the contraflexure point is assumed fixed at midspan of the member. Otani's study recognizes for the first time the importance of fixed-end rotations in predicting the seismic response of RC frame structures.

In 1976 Mahin and Bertero [MAH76-1] reviewed the various definitions of ductility factors in earthquake resistant design. One of the most important questions in this context is the accurate prediction of the rotational ductility demand in structural elements. The study points out how ductility factors for a beam represented by a two-component model must be modified to match those for a beam in which inelastic deformations spread into the member. Since the two-component model substantially underestimates the post-yielding stiffness of a member, the seismic response of the structure will not be predicted accurately. This is particularly true in the case of local response quantities such as inelastic rotations of girders and joints. It does not, therefore, appear reasonable to estimate ductility requirements of RC frame elements on the basis of the results of the two-component model.

Anderson and Townsend [AND77-1] investigated the effect of different hysteretic models on the dynamic response of RC frames. Four different models were used to describe the hysteretic behavior of critical regions of RC members: (a) a bilinear elastic-strain hardening model, (b) a bilinear degrading model with equal unloading and reloading stiffness, (c) a trilinear degrading model with different stiffness for unloading and reloading and (d) a degrading trilinear model for beam-column connections. They studied the effect of reinforcing bar slippage in the joint by inserting a small hinge element of predefined length between the rigid joint element and the flexible girder element. The study shows that the reduction in stiffness of reinforced concrete elements due to inelastic deformations can have a significant effect on the dynamic response of frame structures. Among the different hysteretic models used in the study the degrading trilinear connection model appears to be the most accurate. It is also shown that the use of a degrading stiffness model results in an increase in interstory displacements. This can have a significant effect on the load carrying capacity of the structure due to the P-Δ effect arising from high axial forces.

The first model which accounts for the spread of inelastic deformations into the member was introduced by Soleimani et. al. [SOL79-1]. In this model a zone of inelastic deformations gradually spreads from the beam-column interface into the member as a function of loading history. The rest of the beam remains elastic. The fixed-end rotations at the beam-column interface are modeled through point hinges which are inserted at the ends of the member. These are related to the curvature at the corresponding end section through an "effective length" factor which remains constant during the entire response history.

The effect of axial force on the flexural stiffness of a member was first accounted for in the model proposed by Takayanagi and Schnobrich [TAK79-1] in their study of the seismic response of coupled wall systems. The walls and coupling beams are represented by one-dimensional beam elements. The interaction of bending moment, shear and axial forces is taken into account in the wall elements, while the axial stiffness of the coupling beams is assumed to be infinite, since the horizontal displacements of both walls are almost equal. Otani's model is selected for the coupling beams. It is assumed that the inflection point is fixed at the midspan of the coupling beam. The beams are connected to the wall elements through a rigid link, which accounts for the finite dimensions of the wall. A spring is inserted between the beam element and the rigid link to model the rotations due to slip of the reinforcing bars anchored in the wall. The effect of shear in the coupling beams is also taken into account. A modified Takeda model is adopted for the hysteretic behavior of the beam elements. The model accounts for the "pinching" effect during reloading and the strength decay due to loss of shear resistance after crack formation and yielding of the reinforcement in the coupling beams.

The seismic response of a plane frame coupled with a shear wall was studied by Emori and Schnobrich in 1981 [EMO81-1]. They conducted nonlinear static analyses under cyclic load reversals and compared the results obtained using different beam models, namely, a concentrated spring model, a multiple spring model and a layer model. The first model is identical to Otani's model. The second is a linear element composed of several springs acting in series and interconnected by rigid links. It is thus capable of accounting for the shift of the contraflexure point during the response history. In the third model, which is a modification of the concentrated spring model, a layered element of length L_p is inserted at the ends of the beam. L_p is selected equal to the length of the region where major inelastic action is expected. The layer model can account for the interaction of bending moments and axial forces. It can not account, however, for the effects of shear and slip of reinforcement, unless a spring is inserted at the ends of the beam. Takeda's hysteresis rule has

been adopted in all models. The study concludes that the concentrated spring model predicts satisfactorily the inelastic response of RC girders, while a multiple spring model is needed to accurately describe the inelastic behavior of shear walls. If a detailed study of the inelastic response of plastic zones in columns is desired, the authors recommend the use of a layer model.

The applicability of point hinge models in studying the seismic response of structures was investigated in great detail by Anagnostopoulos [ANA81-1]. His study is limited to flexural members subjected to end moments and uniformly distributed gravity loads. The moment-curvature relation is assumed to be bilinear elastic-strain hardening. He notes that a point hinge model is incapable of reproducing the gradual change of stiffness of a member in the post-yielding range. The study then focuses attention on the problem of defining the strain hardening ratio of the moment-rotation relation of point hinge models. Anagnostopoulos shows that it is incorrect to set this ratio equal to the strain hardening ratio of the moment-curvature relation, since this considerably underestimates the post-yield stiffness of flexural members. He then proposes an iterative solution for determining the strain-hardening ratio of the moment-rotation relation of point hinge models.

A complete model for the analysis of seismic response of RC structures was proposed by Banon et. al. [BAN81-1]. The one-component model in its original form describes the nonlinear behavior of the girder. The hysteretic moment-rotation relation is based on a modified Takeda model. In order to reproduce the "pinching" effect due to shear and bond deterioration a nonlinear rotational spring is inserted at each member end. The hysteretic model of the nonlinear springs is based on a bilinear skeleton curve with strength decay under large deformations and includes the effect of "pinching" during reloading. The authors also proposed a set of damage indicators in an effort to quantify the performance of a structure during an earthquake. These indicators describe the state of damage of each element due to large deformation reversals and low-cycle fatigue. The damage indicators are used in the development of a probabilistic model of member resistance. The study concludes that the one-component model is sufficiently accurate in modeling the inelastic response of RC members subjected to severe deformation reversals. It also shows that it is possible to accurately predict the state of damage of RC members using parameters based on deformation ductility and cumulative energy dissipation due to low-cycle fatigue.

The effect of different hysteresis models on the nonlinear dynamic response of a simple concrete specimen was studied by Saiidi [SAI82-1]. He analyzed four models: elastic-perfectly plastic, elasto-plastic with strain hardening, Clough's model and a new Q-hysteresis model. The first two are very simple, but quite unrealistic for reinforced concrete; the other two are more accurate and differ mainly in the representation of stiffness degradation during unloading and reloading. The performance of the different hysteretic models was evaluated by comparing the results with those

obtained using Takeda's model, since its agreement with a large number of experimental data is excellent. Poor agreement with Takeda's model is exhibited by both elasto-plastic models; Clough's model shows relatively good agreement and the Q-hysteresis model shows excellent agreement. The study concludes that stiffness degradation effects during unloading and reloading are very important in determining the overall response of RC structures, because they affect the amount of energy dissipated by the structure.

In 1983 Meyer et. al. [MEY83-1] developed another spread plasticity model. The flexibility coefficients of the new model are identical to those of Soleimani's model. The authors proposed a slightly different way of calculating the stiffness of the plastic zone during reloading and used Takeda's model to describe the hysteretic behavior. The same model was used in describing the inelastic behavior of beams and columns, with no account of the effect of axial forces on flexural rigidity. Fixed-end rotations are not taken into account in the study. The analytical results are compared with a series of experimental data and show excellent agreement.

An integrated experimental and analytical study on the effect of bond deterioration on the seismic response of RC structures was published by Otani et. al. in 1985 [OTA85-1]. The model adopted for beams and columns is the one-component model. Takeda's model is used to describe the hysteretic behavior of the elements. A rotational spring is inserted at each member end to model the slip of reinforcement due to bond deterioration; the hysteretic behavior of the spring is described by Takeda's model modified so as to account for the "pinching" effect during reloading. No strength decay is introduced in the monotonic skeleton curve, since experimental data did not provide such evidence.

A model for assessing structural damage in RC structural elements was proposed in a study by Park and Ang [PAR85-1]. Damage is expressed as a linear function of the maximum deformation and the hysteretic energy absorbed during cyclic load reversals.

In their study of the nonlinear response of plane rectangular frames and coupled shear walls Keshavarian and Schnobrich [KES85-1] extended the spread plasticity model proposed by Soleimani to column elements. The model accounts for the interaction between bending moment and axial force in determining the strength and stiffness of column elements. The study compares the predictions of different models: in addition to the spread plasticity model, these include the one-component, two-component and multiple spring model. In performing the nonlinear static and dynamic analysis of the structure the element stiffness is linearized at the beginning of each load step. Any nonlinearity which takes place during the load increment is not accounted for and the resulting unbalance forces are neglected. The study concludes that the one-component model is

well suited for describing the inelastic behavior of RC girders. It is also noted that the two-component model has the same versatility as the one-component model and yields similar results. The multi-layer model is found very expensive for nonlinear dynamic analysis of multistory structures. Finally, the study points out that the fluctuation of axial forces in coupled shear walls and in exterior columns of frame structures significantly affects the forces and deformations in individual walls and columns.

In a recent study Roufaiel and Meier [ROU87-1] proposed an extension of the spread plasticity model presented in [MEY83-1]. The new model includes the effect of shear and axial forces on the flexural hysteretic behavior based on a set of empirical rules. The hysteretic moment-curvature relation is described by Takeda's model. The variation of axial loads due to overturning moments is not accounted for. The predictions of the model were compared with available experimental data and show very good agreement. A set of new damage parameters was proposed which seem to correlate well with the residual strength and stiffness of specimens tested in the laboratory.

1.3 Objectives and scope

The general objective of this research is to develop improved analytical methods for predicting the nonlinear static and dynamic response of multistory reinforced concrete frames subjected to large cyclic deformation reversals. This report is limited to the study of the static response. The dynamic response will be presented in a following study.

To achieve the general objective a new reinforced concrete girder element is proposed. The element is composed of a number of subelements which are connected in series and represent the different sources of hysteretic behavior of reinforced concrete girders. In particular, two subelement models are proposed in the study: one describes the inelastic behavior along the girder accounting for the gradual spread of inelastic deformations at the girder ends, while the other models the fixed-end rotations that arise at the beam-column interface due to bond deterioration and slippage of reinforcing bars in the beam-column joint region.

An efficient numerical technique which accounts for the unbalance of internal forces in the different subelements during a given load increment is proposed and an algorithm for implementing this numerical strategy is described.

The reinforced concrete girder model is incorporated into a computer program for nonlinear static and dynamic analysis of reinforced concrete frames. The predictions of the model are compared

with experimental results obtained from beam-column subassemblages subjected to cyclic deformation reversals. The accuracy of various models in describing the local and global response of simple structural subassemblages is investigated. The study concludes with a number of parametric studies which assess the sensitivity of the results to changes in key model parameters.

CHAPTER 2

MODELS OF REINFORCED CONCRETE FRAME ELEMENTS

2.1 Introduction

When medium to high rise reinforced concrete moment resisting frames are subjected to severe seismic excitations, the behavior of members in the lower part of the building is controlled by lateral loads. In a typical lower story the combined action of high lateral and relatively small gravity loads gives rise to the moment distribution shown in Fig. 2.1. Since it is not economically feasible to design reinforced concrete (RC) structures to remain elastic during severe earthquake ground motions, the maximum girder moments are likely to exceed the yield moment of the cross-section in critical regions of the structure and lead to inelastic deformations. In lower stories critical regions are usually located at the ends of girders and columns and at beam-column joints. In upper stories inelastic deformations can also take place near the midspan of the girders. Critical regions can be classified according to the actions governing their behavior [BER79-1]. Since the seismic response of the entire structure depends on the hysteretic behavior of these regions, accurate models of such behavior need to be developed.

Ideally these models should be based on an accurate representation of the material behavior of reinforcing steel and concrete and take into account the controlling states of stress and strain in order to identify the main parameters influencing the hysteretic behavior of each critical region. The problems arising from the transfer of stresses between reinforcing steel and surrounding concrete under cyclic load reversals also need to be addressed. While such models can be developed based on the finite element method [ASC82-1], their implementation in dynamic response analyses of large structural systems is prohibitively expensive.

A different solution approach consists of developing macroscopic models of reinforced concrete elements. These are based on approximations of the physical behavior of RC members and vary in their complexity [CEB83-1], [ZER88-1]. In determining the seismic response of multistory buildings point hinge models have been most widely used because of their simplicity [UME82-1]. In these the inelastic behavior of reinforced concrete elements is represented by concentrated springs located at the ends of the member. Since it is computationally most convenient

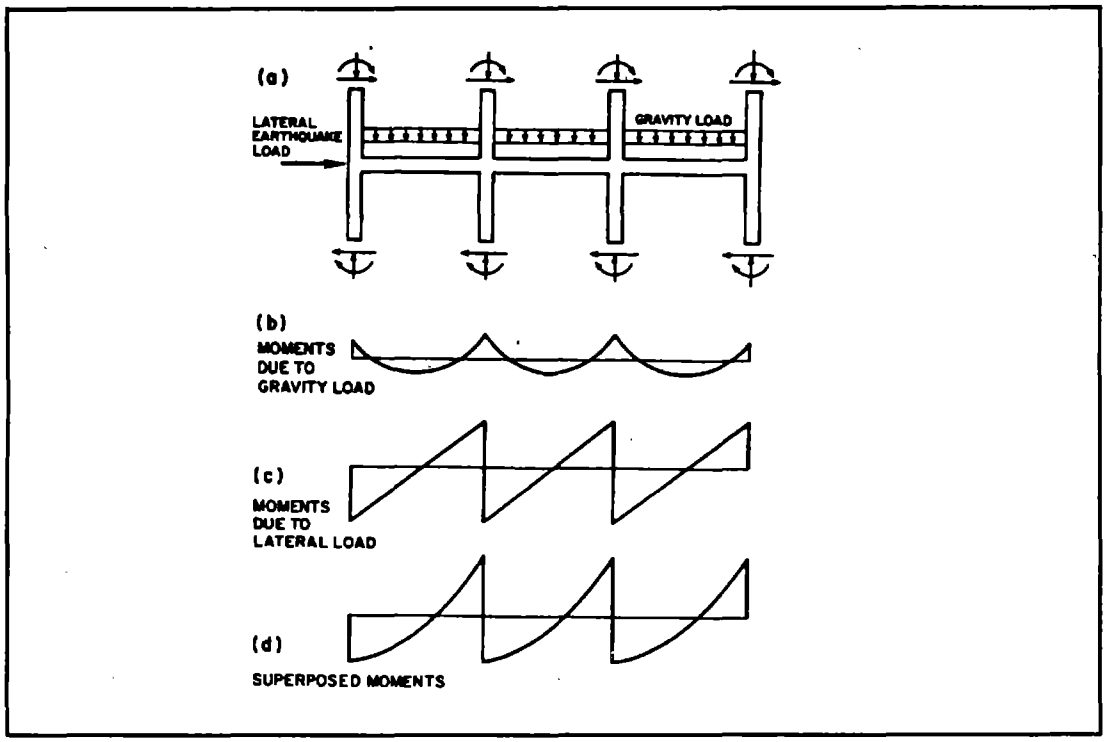

Fig. 2.1 ***Bending moments in lower story of moment resisting frame under combination of gravity and earthquake loading***

to use a single spring to model the inelastic behavior of any type of critical region, several parameters need to be defined to describe the monotonic behavior of the springs. These depend on the actions which control the inelastic behavior of the member and are established empirically.

To describe the behavior of RC members under cyclic load reversals phenomenological models of hysteretic behavior are typically used. While only a few parameters are needed to describe the hysteretic behavior when flexure governs the response, many more parameters become necessary in members with complex interactions of bending moments, shear and axial forces. These parameters are typically established from a limited set of experimental data making the general applicability of such models questionable. It appears doubtful that a single hysteretic model can approximate the actual behavior of RC regions over the wide range of possible interactions of bending moment, shear and axial force in structures subjected to earthquake excitations.

Another way of describing the inelastic behavior of RC members is proposed in the present study. This approach consists of identifying the basic mechanisms which control the hysteretic behavior of each type of critical region and, if possible, isolating these in individual subelements.

Each girder and column element is then made up of a number of such elements. This approach is, in many respects, similar to the model proposed by Otani [OTA74-1] and will be presented in greater detail in the following.

Since the present study is limited to the analysis of planar moment resisting frames (Fig. 2.2), the following basic elements are needed for determining the nonlinear response of such structures to cyclic deformation reversals: a girder element, a column element, a beam-column joint and a foundation element. The girder element should also include the effect of the slab. Shear wall or infill panel elements are not dealt with in this study, since attention is focused on the behavior of bare frames. It is assumed that floor diaphragms are infinitely rigid so that a single degree of freedom represents the lateral displacements of an entire story (Fig. 2.2).

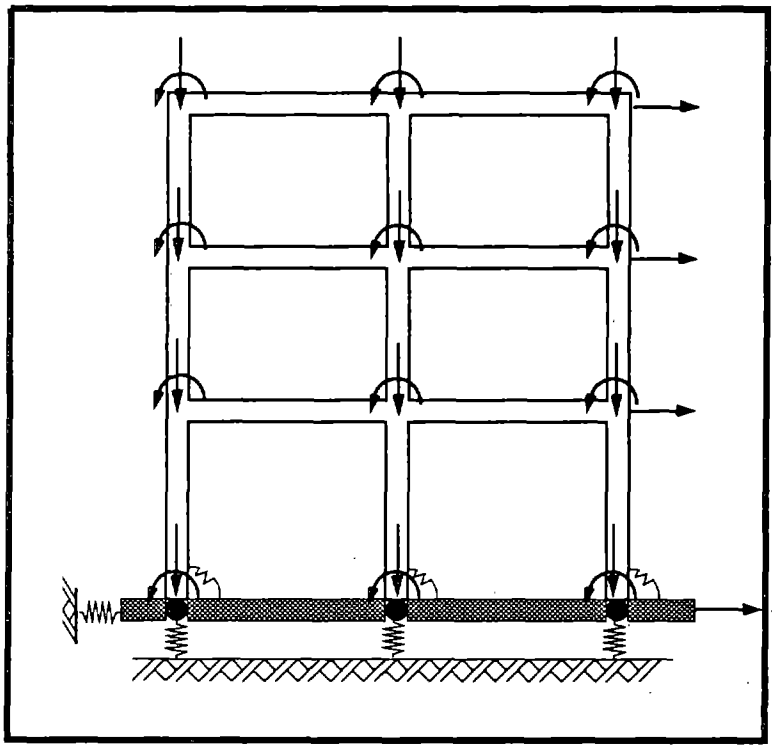

Fig. 2.2 Proposed modeling of planar moment resisting R/C frames

Because the beam-column joint element proposed in this study describes deformations which arise at the beam-column interface (e.g. shear sliding, reinforcement pull-out), it can be combined with the element which accounts for deformations along the girder span to form a girder super-element. In this case the moment resisting frame consists of only three types of elements: (a) a

girder superelement, (b) a column element and (c) a foundation element. This subdivision implies that the beam-column joint panel zone remains rigid. If it is desired to include the deformations due to shear cracking in beam-column joints, a panel zone element needs to be added for the purpose.

In reinforced concrete structures subjected to large cyclic deformation reversals bond deterioration and shear effects give rise to slippage of reinforcing bars anchored in beam-column joints. This leads to an interaction between forces and moments acting at the ends of beams and columns which frame into a particular joint [FIL83-1]. If it is desired to explicitly account for the interaction between girder and column moments at beam-column joints, a special joint element needs to be developed. Such interaction is not explicitly accounted for in the present study. A way of implicitly accounting for this effect is presented in section 1.2.3.

Information about the different elements used in the present study is given in the following sections. First, the girder superelement is described in detail. This is followed by descriptions of the column and foundation element. Finally, a brief derivation of the stiffness matrix of the entire frame structure is given.

2.2 Reinforced concrete girder element

In moment resisting frames designed according to current building codes to resist severe earthquake excitations inelastic deformations are expected to take place at the ends or at midspan of girders and at beam-column joints, while columns are designed so as to remain elastic except at the base of the building.

The behavior of critical regions in girders is governed by flexure, shear and the transfer of stresses between reinforcing steel and concrete. When these regions are subjected to cyclic deformation reversals, considerable stiffness deterioration is observed. This can be attributed to several factors the most important of which are:

(1) concrete cracking and splitting along reinforcing bars,

(2) cyclic deterioration of bond between reinforcing steel and surrounding concrete,

(3) shear sliding in regions with cracks running through the entire depth of the member,

(4) crushing and spalling of concrete.

(5) Bauschinger effect of reinforcing steel,

These factors are also responsible for the stiffness deterioration observed in interior and exterior beam-column joints. In this case, however, the hysteretic behavior is governed by the large change in bending moments from one face of the joint to the other causing a combination of high shear and bond stresses. Large bending moments at the girder ends induce yielding of the reinforcement, which, combined with the diagonal cracks induced by shear, leads to slippage of reinforcing bars in the joint. This manifests itself as bar pull-out at the beam-column interface and results in concentrated rotations known as fixed-end rotations at the girder ends. Experimental studies show that fixed-end rotations due to bond deterioration in the joint can contribute up to 50% to overall deflections of beam-column subassemblages after yielding of the reinforcement [SOL79-1]. Because earthquake resistant design of moment resisting frames is based on the strong column-weak girder design philosophy, fixed-end rotations do not typically occur at the ends of columns which are designed to remain elastic.

In addition to fixed-end rotations, the shear stress transfer in the joint leads to diagonal cracks giving rise to panel zone deformations. In general, the mechanism of joint shear resistance is coupled with the problem of stress transfer between reinforcing steel and concrete [PAR84-1]. It is possible, however, to design and detail joints so that the nominal concrete shear stress in the joint remains smaller than a specified limit. This is the approach followed by current design recommendations [ACI85-1]. In this case diagonal cracking is kept to a minimum and the shear deformation of the panel zone remains small and can be neglected. By contrast, it is not possible to eliminate fixed-end rotations due to slippage of reinforcing bars in the joint, except by moving the plastic hinge a certain distance away from the beam-column interface through special detailing of the reinforcement [BER75-2, HAD86-1].

In order to model as accurately as possible the different mechanisms which contribute to the hysteretic behavior of critical regions in RC girders, the girder element is decomposed into several subelements as shown in Fig. 2.3:

(1) an elastic beam subelement which represents the behavior of the girder before yielding of the reinforcement,

(2) a plastic beam subelement with plastic hinges at the ends; the length of the plastic hinges is a function of the loading history; this element represents the behavior of the girder in the post-yielding range,

(3) a joint subelement which accounts for the fixed-end rotations and the sliding due to shear at the beam-column interface.

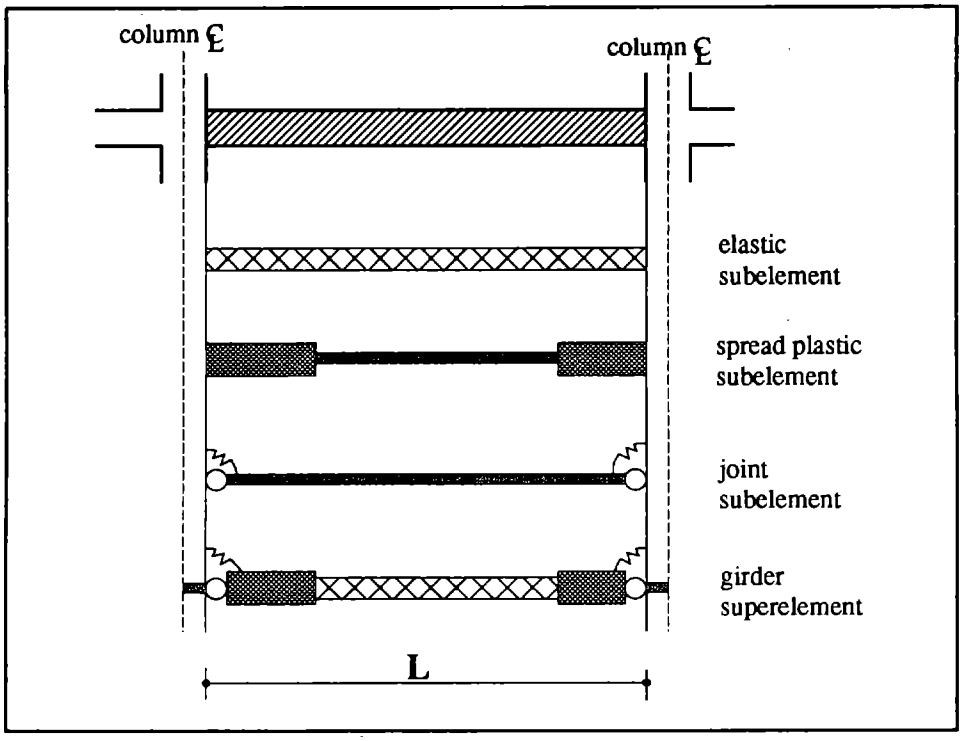

Fig. 2.3 Decomposition of girder into different subelements

Fig. 2.3 shows that the beam-column joint panel zone is considered infinitely rigid. It is assumed in this study that shear deformations of the joint panel zone remain small and can be neglected. This does not constitute, however, a limitation of the present work. If desired, panel zone deformations can be included in the analysis by adding a flexible panel zone element. Such an element has been developed by Kanaan and Powell for the nonlinear analysis of steel structures [KAN73-1].

2.2.1 Linear elastic beam subelement

The linear elastic beam subelement represents the behavior of the girder before yielding of the reinforcement. Its length is equal to the clear span L of the girder and it is assumed to have a constant section stiffness EI along the span. The assumption of a constant section stiffness along the entire span of the girder is clearly an approximation. Reinforcement layout typically varies along the length of the girder with different amounts of reinforcement at the top and bottom of the cross section. When the bending moments act such that the top of the section is subjected to tension, the compression zone is rectangular in shape having a width equal to the width of the web. Part of the slab reinforcement contributes to the tensile force thus significantly increasing the yield strength of the section, but not affecting much the stiffness before yielding. When the bending moments act

such that the bottom of the section is subjected to tension, the compression zone is either rectangular or often T-shaped. It is clear from the above that the effective slab width in tension and compression needs to be determined, if the strength and stiffness of the girder element is to be estimated accurately.

In this study the elastic section stiffness EI is set equal to the average of the positive (tension at the bottom) and negative (tension at the top) section stiffness at the two girder ends. The elastic section stiffness is determined as the secant stiffness of the moment-curvature relation at yielding of the tension reinforcement. Only the effect of slab in compression has been included in determining the strength and stiffness of the girder based on the effective width specified in ACI 318-83 [ACI83-1]. A better model of the effect of slab in tension and compression has been recently developed [PAN87-1]. It should be noted that girders spanning between interior columns typically have a symmetric arrangement of reinforcement with respect to the girder midspan. By contrast, exterior girders are likely to have different amounts of reinforcement at each end. In the latter case the average stiffness is determined from the positive and negative section stiffness at each end. The approximation of a constant average section stiffness is certainly unsatisfactory, if it is desired to study the response of the structure under service loads. In the present study attention is focused on predicting the response of the structure under large deformation reversals. Such response is not significantly affected by the stiffness of the structure before yielding.

With the assumption of a constant average section stiffness along the entire length of the elastic beam subelement the flexibility matrix with respect to the member chord is given by the well known expression

$$[f]_{el} = \frac{L}{EI}\begin{bmatrix} 2 & -1 \\ -1 & 2 \end{bmatrix} \tag{2.1}$$

2.2.2 Rigid-plastic beam subelement

The rigid plastic beam subelement accounts for the inelastic deformations of the girder after yielding of the reinforcement. Two different plastic subelements are included in the current study:

(a) The first model assumes that all inelastic deformations are concentrated in a hinge of zero length located at each end of the girder. The two hinges are connected by an infinitely rigid bar to form the concentrated plastic beam subelement. The combination of the flexibility matrix of this element with that of the elastic subelement results in the one-component model originally proposed by Giberson [GIB74-1].

(b) The second model accounts for the gradual spread of inelastic deformations into the girder as a function of loading history. In this an inelastic zone of gradually increasing length is located at each end of the girder. The two inelastic zones are connected by an infinitely rigid bar to form the spread plastic beam subelement. The combination of the flexibility matrix of this element with that of the elastic subelement results in a model similar to that originally proposed by Soleimani et. al. [SOL79-1].

The effect of shear manifests itself in two ways at the girder ends:

(1) It affects the inclination of cracks and the curvature distribution in the inelastic zone region at the girder ends [PAR75-1]. This effect can be taken into account by modifying the hysteretic law of the plastic subelement. In the case of the spread plasticity element it can also be accounted for by modifying the curvature distribution in the inelastic zone region. This shear effect in neglected in the present study.

(2) The transfer of shear across the crack at the beam-column interface can give rise to significant shear sliding. Because of the unequal amounts of top and bottom reinforcement, the tensile force in the bottom does not suffice to yield the top steel in compression. Thus when the applied end moment subjects the bottom steel to tension the crack remains open across the entire depth of the section and shear is only resisted by dowel action of the top and bottom reinforcement [FIL83-1]. To include the effect of shear sliding at the girder ends a special subelement needs to be added to those shown in Fig. 2.3. This effect is neglected in the present study.

The effect of bond deterioration along the reinforcing bars also manifests itself in two ways:

(1) It affects the stress, strain and curvature distribution in the inelastic zone region at the girder ends. This effect can be accounted for by modifying the curvature distribution in the inelastic zone region as will be described later.

(2) It gives rise to concentrated rotations at the beam-column interface. This phenomenon is taken into account in the present study by the joint subelement which is described in Section 1.2.3.

2.2.2.1 Concentrated rigid-plastic beam subelement

In the concentrated plastic subelement the inelastic deformations which take place at the girder ends after yielding of the reinforcement are represented by a rigid plastic hinge of zero length. The hinge, which is depicted as a nonlinear spring in Fig. 2.4(a), is only activated when the moments at the girder ends first exceed yielding. Since all inelastic deformations are lumped at the plastic

hinges at the two ends of the girder and the elastic deformations are accounted for in the linear elastic beam subelement, the part of the concentrated plastic subelement which connects the two hinges is infinitely rigid.

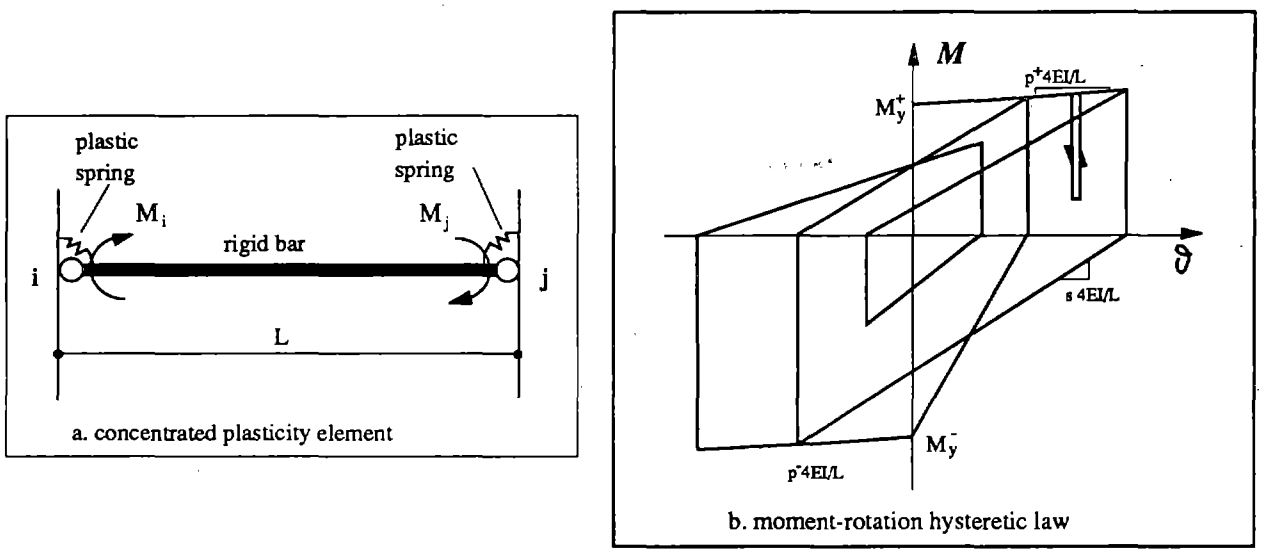

Fig. 2.4 Concentrated plasticity beam subelement

It can be easily shown that the off-diagonal elements of the flexibility matrix are zero in this case. The matrix thus reduces to the simple form

$$[f]_{pl} = \begin{bmatrix} f_i & 0 \\ 0 & f_j \end{bmatrix} \tag{2.2}$$

where f_i and f_j are the flexibility coefficients of the rotational springs at ends i and j, respectively. The problem of determining the flexibility of the rotational springs has occupied many researchers to date. Otani presented a detailed discussion of the problem [OTA74-1]. In order to avoid load path dependency of the flexibility coefficients it is usually assumed that the bending moments are distributed such that the point of inflection remains fixed during the entire load history. In most studies to date the point of inflection is assumed to remain fixed at girder midspan. In this case each half of the member can be viewed as a cantilever beam (Fig. 2.5). If the effect of gravity loads is neglected, the moment distribution is linear (Fig. 2.5b). This corresponds to the cantilever beam being loaded with a concentrated load P at the tip (Fig. 2.5c).

To determine the flexibility coefficients f_i and f_j of the concentrated plasticity model the plastic rotation at the root of the cantilever due to the actual curvature distribution is first established for different values of the load P. This is rather straightforward, if the moment-curvature relation (M-φ)

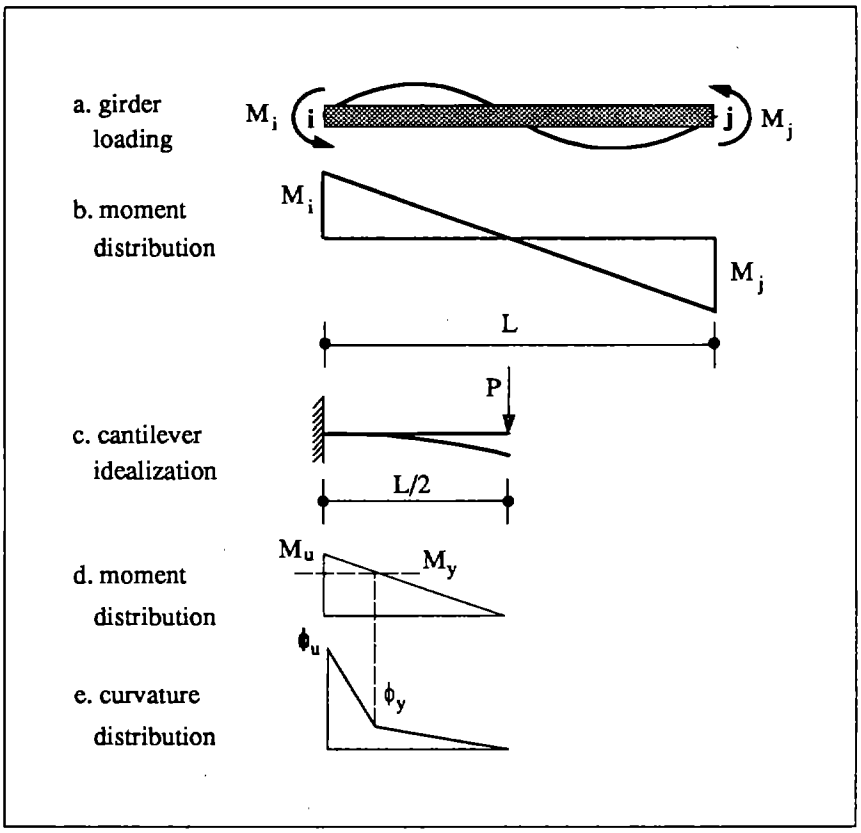

Fig. 2.5 Derivation of parameters of concentrated plasticity subelement

is known for all sections along the cantilever span. To simplify the calculation the (M-φ) relation is assumed to be bilinear with a single post-yield stiffness (Figs. 2.5d and 2.5e). In spite of the approximations made in Fig. 2.5 the procedure results in a nonlinear flexibility coefficient of the equivalent concentrated spring, because of the gradual spread of inelastic deformations into the cantilever beam. To simplify the moment-rotation relation of the equivalent end spring the actual behavior is replaced by a bilinear moment-rotation relation with constant post-yield stiffness as shown in Fig. 2.4(b). The post-yield stiffness is calculated by equating the plastic rotations for the case that the section at the root of the cantilever reaches the ultimate moment capacity (Fig. 2.5d). In this case the post-yield stiffness k_{sp} of the equivalent rotational spring is

$$k_{sp} = \frac{M_u - M_y}{\theta_{pl}} \tag{2.3}$$

where M_u is the ultimate and M_y the yield moment of the cantilever beam, respectively. θ_{pl} is the plastic rotation of the equivalent concentrated spring. This is equal to the plastic rotation at the root of the cantilever beam which can be readily determined from the curvature distribution in Fig. 2.5e.

Eq. (2.3) results in an infinite spring stiffness k_{sp} for the case that the end moment does not exceed the yield moment. This is in agreement with the definition of a concentrated rigid-plastic spring subelement which only accounts for the inelastic girder deformations after yielding of the reinforcement.

It is customary to express the rotational spring stiffness k_{sp} in relation to the stiffness term k_{11} of the elastic stiffness matrix of a prismatic beam element. Thus

$$k_{sp} = \frac{4EI}{\gamma L_c} \tag{2.5}$$

The flexibility matrix of the concentrated plastic beam subelement can now be written by considering Eq. (2.5) at ends i and j of the element.

$$[f]_{pl} = \begin{bmatrix} \frac{\gamma_i L}{4EI} & 0 \\ 0 & \frac{\gamma_j L}{4EI} \end{bmatrix}$$

$$[f]_{pl} = \frac{L}{6EI} \begin{bmatrix} 1.5\gamma_i & 0 \\ 0 & 1.5\gamma_j \end{bmatrix} \tag{2.6}$$

The coefficients γ_i and γ_j vary as a function of the moment-rotation history of the rotational springs. The moment-rotation relation of the springs is completely defined by two envelope curves which represent the behavior of the springs under positive and negative monotonic loading and a hysteretic model which describes the behavior of the springs under cyclic load reversals (Fig. 2.4b).

The monotonic envelope curves are represented by a bilinear relation which has infinite stiffness for moments not exceeding the yield moment of the end section and a single post-yield stiffness for moments larger than the yield moment. The yield moment M_y^+ when the bottom reinforcement is subjected to tension is different from the yield moment M_y^- when the top reinforcement is subjected to tension. The post-yield stiffness $p^+ \cdot 4EI/L$ for positive bending moments is also assumed to be different from the post-yield stiffness $p^- \cdot 4EI/L$ for negative bending moments.

The hysteretic behavior of the rotational springs under cyclic moment reversals is described by Clough's hysteretic model shown in Fig. 2.4(b) [CLO65-1]. This model is characterized by the following hysteretic rules:

(a) The unloading stiffness is equal to the initial stiffness before yielding. Since the behavior of the spring is rigid-plastic, this means that the unloading stiffness is infinite and the spring is deactivated during unloading.

(b) Reloading takes place along a line which connects the point at which unloading was completed with the point on the envelope curve in the opposite direction of loading with the maximum previous excursion into the inelastic range.

The advantage of this model lies in its computational simplicity combined with reasonable accuracy in representing the hysteretic response of R/C critical regions whose behavior is controlled by bending. One of the limitations of this model arises from the very steep unloading slope, as was already pointed out by Saiidi in [SAI82-1]. Advantages and limitations of the model will be discussed in detail in Chapter 4 by comparing analytical predictions with experimental results.

It should be mentioned here that in the original model reloading after partial unloading takes place along the line which connects the point at which unloading stopped with the point on the envelope curve in the same direction of loading with the largest previous inelastic deformation (line a-c in Fig. 2.6). Since this behavior is not realistic, the hysteretic model has been modified so that reloading after partial unloading follows an infinite slope until reaching the last reloading curve connecting the last point of complete unloading with the point on the envelope curve with maximum previous inelastic deformation (line a-b in Fig. 2.6). Upon reaching point b the moment-rotation relation follows the last reloading curve (line b-c in Fig. 2.6).

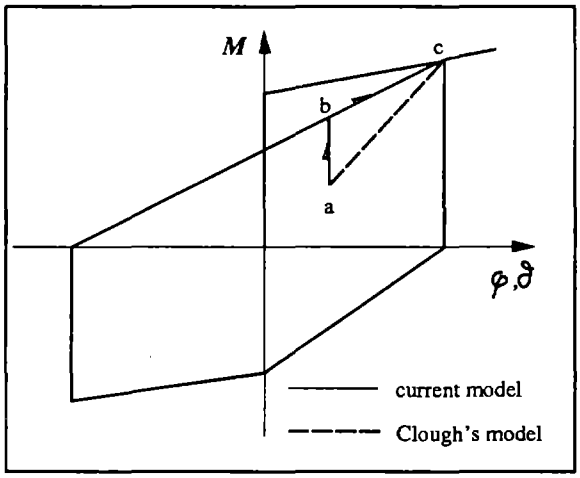

Fig. 2.6 Hysteretic behavior of current model vs. Clough's model

Based on the hysteretic model of Fig. 2.4(b) the coefficients γ_i and γ_j assume the following values:

(a) $\gamma = 0$ during initial loading and unloading.

(b) $\gamma = 1/p$ during strain hardening, where $p \cdot 4EI/L$ is the post-yield stiffness of the moment-rotation relation of the concentrated rotational springs.

(c) $\gamma = 1/s$ during reloading where $s \cdot 4EI/L$ is the reloading stiffness of the moment-rotation relation of the concentrated rotational springs.

Since the linear elastic and concentrated plastic beam subelements are connected in series, the flexibility matrix of the combined element is obtained by simply adding the flexibility matrices of the two subelements (Eqs. 2.1 and 2.6). Inverting the flexibility matrix of the combined element results in the stiffness matrix of the one-component model, as originally proposed by Giberson [GIB69-1].

The main advantage of the concentrated plasticity model is its simplicity and computational efficiency. It has, however, some serious limitations: most importantly it does not account for the gradual spread of inelastic deformations into the girder. This results in an underestimation of stiffness in the early stages of inelastic deformation. Another limitation of the model lies in the assumption that the point of inflection is fixed at midspan during the entire response history. This is not realistic, particularly, if one considers that the yield moments at the ends of a girder bent in double curvature are not equal, because of unequal areas of top and bottom reinforcement. The significance of these factors will be discussed in detail in Chapter 4 by comparing the predictions of the model with experimental evidence.

2.2.2.2 Spread rigid-plastic beam subelement

A more refined model of the nonlinear behavior of RC girders was first proposed by Soleimani et. al. in [SOL79-1]. A slightly different formulation of the original model is presented here. Since the deformations of the girder before yielding of the reinforcement are accounted for in the elastic beam subelement, the spread rigid-plastic subelement only accounts for the inelastic girder deformations which take place when the end moments exceed the yield moment.

The spread rigid-plastic beam subelement consists of two regions of finite length where the plastic deformations of the girder take place. These regions are connected by an infinitely rigid bar (Fig. 2.7(a)). The length of each plastic zone varies during the response history as a function of the moment distribution in the girder. The model thus accounts for the gradual spread of inelastic deformations into the girder and the shift of the inflection point during the response time history.

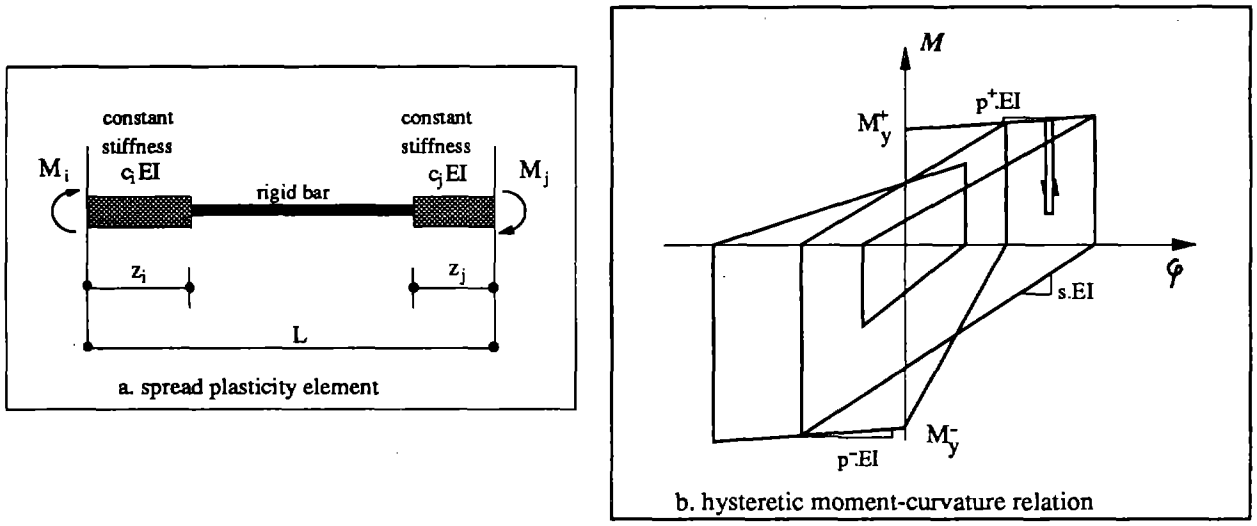

Fig. 2.7 Spread rigid plastic beam subelement

In the following the salient features of the spread rigid-plastic beam subelement and the derivation of the flexibility coefficients are presented. Most of this information can be found in slightly different form in [SOL79-2].

In presenting the features of the spread plastic subelement and the approximations involved in its development it is instructive to look at the case of a cantilever beam loaded by a concentrated load at its tip (Fig. 2.8a). The moment distribution in the cantilever beam (Fig. 2.8b) is identical to the moment distribution caused by lateral loads in the girders of a moment resisting frame between the point of inflection and the beam-column interface, if the effect of gravity loads is neglected (Fig. 2.1).

We are interested in calculating the load-displacement relation at the tip of the cantilever beam after yielding of the reinforcement at the end section. The moment distribution in this case is shown in Fig. 2.8(b). This gives rise to the curvature distribution in Fig. 2.8(c). Curvatures are rather irregular, because of the effects of cracking and tension stiffening between cracks. The strains in the top and bottom reinforcing steel are also affected by the presence of shear stresses in the beam. It is difficult to account for all these effects when developing simple models of the inelastic behavior of RC members. Several solutions have been proposed in the past. Some researchers have proposed beam shape functions with special weighting schemes which account for the concentration of inelastic deformations at the ends of the girder. Since the shape functions do not change with the response time history, these proposals represent generalizations of the point hinge models and share many of their limitations. Other researchers have subdivided the beam into a number of slices along

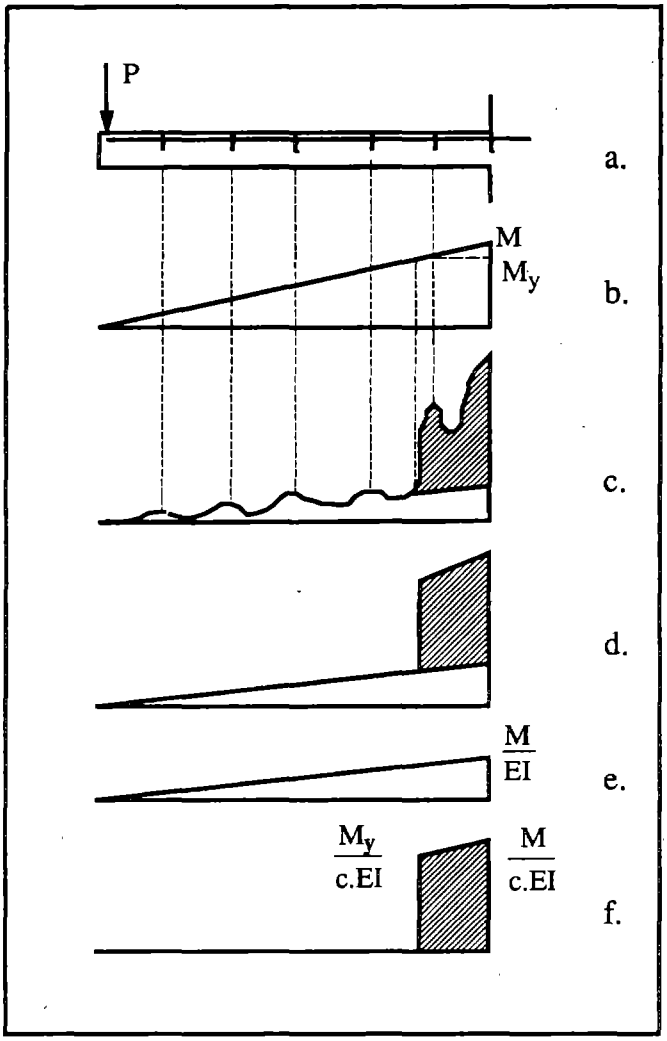

Fig. 2.8 ***Development of spread plasticity model in the case of a cantilever beam loaded by a concentrated load at the tip***

the span. This approach requires tracing the behavior of each slice during the response time history and is rather costly for nonlinear dynamic analyses of multistory structures. Even so, many of the aforementioned effects of bond deterioration and shear are not taken into account.

A possible approximation, which lies between the extremes of point hinge models, on the one hand, and multi-slice models, on the other, consists of idealizing the curvature distribution as shown in Fig. 2.8(d). This approximation is based on the assumption of an average section stiffness $c \cdot EI$ along the plastic zone of the cantilever beam, where EI is the secant stiffness of the end section at yielding of the reinforcement. Subtracting the elastic curvatures which are already accounted for

in the elastic subelement (Fig. 2.8(e)) results in the curvature distribution in Fig. 2.8(f). This curvature distribution lies at the heart of the following derivation of the flexibility matrix of the spread plastic subelement. It will be shown later, that the assumption of an average effective stiffness of the plastic zone is of considerable importance to the computational efficiency of the model, because it leads to a symmetric stiffness matrix.

The quality of the approximation of an average section stiffness $c \cdot EI$ along the plastic zone of the subelement depends on the value of c. The determination of the value of c is relatively simple in the case of a cantilever beam under monotonically increasing load. By neglecting the effect of tension stiffening and assuming that all plastic zone sections exhibit the same bilinear moment-curvature relation we can readily derive c (Fig. 2.8f). Under a monotonic load P which gives rise to the moment distribution in Fig. 2.8b all sections in the plastic zone length are in the strain-hardening range and have the same stiffness. In this case $c \cdot EI$ is simply equal to the post-yield stiffness of the bilinear moment-curvature relation. It is important to note that the reinforcement layout will not typically vary along the plastic zone length, as long as the zone does not extend beyond the quarter span point. Thus the assumption that all sections in the beam plastic zone possess the same moment-curvature relation is quite accurate.

The determination of the value of c becomes more involved, if not impossible, if we consider the effect of load reversals. A number of complications arise in this case:

(a) The point of inflection shifts from one load step to the next. In this case part of the plastic zone is in the loading stage, while another part is unloading (Fig. 2.9).

(b) Different sections in the plastic zone exhibit a different amount of stiffness degradation during reloading. This case is shown in Fig. 2.10 in its simplest form. The cantilever beam in Fig. 2.8 is first loaded in one direction so that part of the beam enters into the strain hardening range. The load at the tip is then reversed. Upon loading in the opposite direction sections along the inelastic zone exhibit different amounts of stiffness deterioration. While it is possible to derive a closed form expression for the curvature distribution in the simple case of Fig. 2.10 (dashed line), such an endeavor is fruitless after the second reloading cycle, even for a bilinear moment-curvature relation.

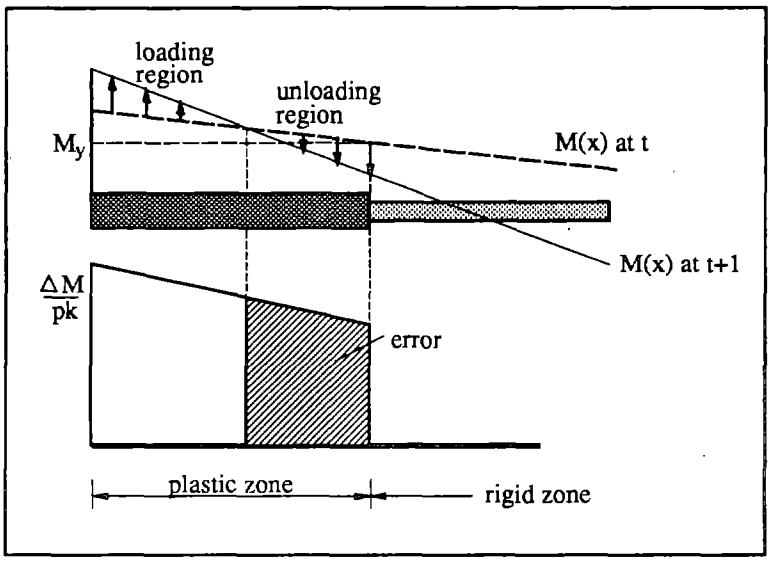

Fig. 2.9 ***An unusually large shift in the point of inflection during a given load step causes unloading along some portion of the plastic zone length***

To accurately represent the hysteretic behavior of the plastic zone during a complex load history requires tracing the response of each section during the entire response time history. Since this is undesirable from the standpoint of computational efficiency, the following key assumptions are made in the spread rigid-plastic zone subelement:

(1) The state of the entire plastic zone is controlled by the state of the section at the beam-column interface. In Fig. 2.9 this means that the entire plastic zone is in the loading stage. This assumption gives rise to a discrepancy between actual and assumed curvature distribution, as shown in Fig. 2.9. This error can be minimized by reducing the size of the load increment and thus avoiding drastic shifts in the point of inflection during a given load step.

(2) The stiffness of the plastic zone is represented by an average effective stiffness $c \cdot EI$ which depends on the stiffness of the section at the beam-column interface.

These two key assumptions associate the behavior of the entire plastic zone with that of the section at the beam-column interface. This reduces substantially the computational effort required for describing the hysteretic behavior of the spread plastic subelement. Instead of a number of sections along the plastic zone, the load history needs to be traced at the two end sections of the element only. In addition, the model has to keep track of the length of the plastic zone at the two ends of the element. The second assumption has the added advantage that it results in a symmetric stiffness matrix.

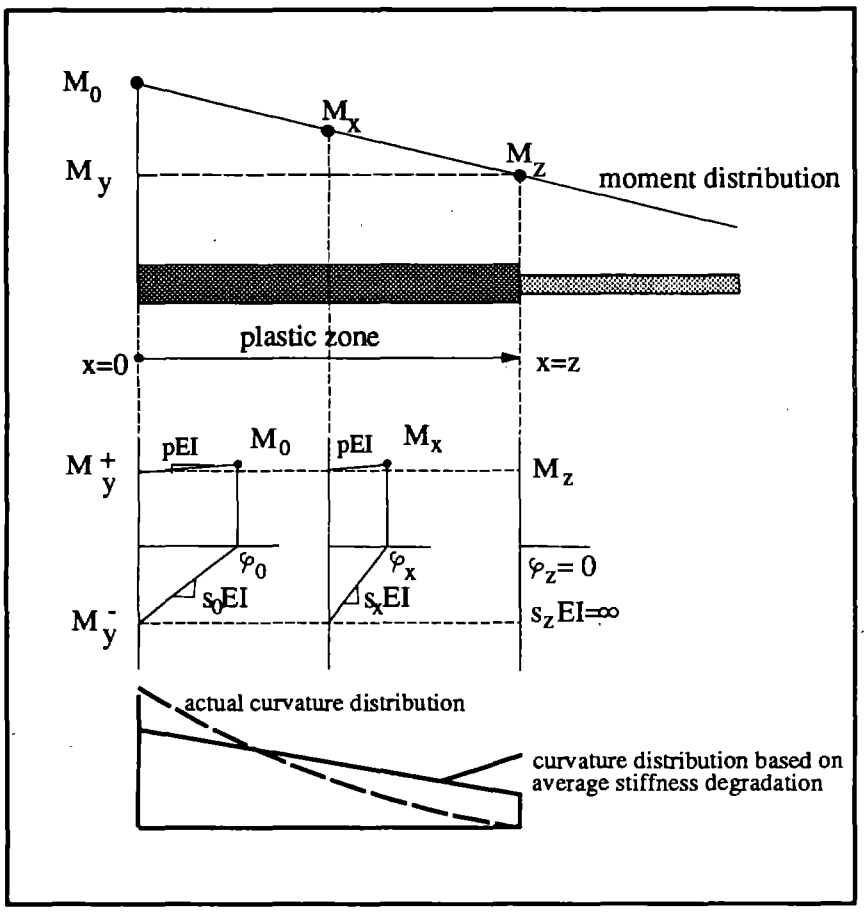

Fig. 2.10 Variation of stiffness deterioration along the plastic zone length during first unloading and reloading

Since the effective stiffness $c \cdot EI$ of the plastic zone depends on the behavior of the section at the beam-column interface, a hysteretic moment-curvature relation of the end section is needed. This relation is based on two bilinear envelope curves (Fig. 2.7b). Under positive bending moments (tension at the bottom) the section yields at a moment equal to M_y^+, while under negative moments (tension at the top) the yield moment is M_y^-. The post-yield stiffness $p^+ \cdot EI$ for positive bending moments is also assumed to be different from the post-yield stiffness $p^- \cdot EI$ under negative bending moments, as shown in Fig. 2.7b. To describe the behavior of the section under cyclic moment reversals the model originally proposed by Clough [CLO65-1] is adopted in this study. The original model has been modified in the same way as described for the moment-rotation relation of the concentrated rigid-plastic subelement (Fig. 2.6b).

Using this model to describe the hysteretic moment-curvature relation of the section at the beam-column interface the value of c is determined as follows:

(1) During strain-hardening of the end section we can assume according to (1) that the entire plastic zone is in the strain-hardening range. Thus $c = p$ where $p \cdot EI$ is the post-yield stiffness of the moment-curvature relation. c thus assumes two different values p^+ or p^- depending on the sign of the end moment.

(2) During unloading of the end section it is assumed that the entire plastic zone is unloading. Since elastic unloading is accounted for by the elastic subelement, this implies that the plastic zone is infinitely rigid and $c = \infty$.

(3) The complications which arise during reloading have already been described. Fig. 2.10 shows that each section has a different reloading stiffness, which is a function of the section's previous response history. In order to limit the number of sections at which the response history needs to be traced the second key assumption of the spread plastic subelement is introduced: it is assumed that the effective stiffness of the plastic zone $c \cdot EI$ is equal to the average of the section stiffness at the two ends of the plastic zone. Since one end is elastic, this implies that only the response time history of the section at the beam-column interface needs to be traced. In this case c is equal to

$$\frac{1}{c} = \frac{1}{2}\left[\frac{1}{s_0} + \frac{1}{\infty}\right] = \frac{1}{2s_0}$$

where $s_0 \cdot EI$ is the reloading stiffness of the section at the beam-column interface (Fig. 2.10).

The effect of gravity loads has so far not been accounted for. This effect is considered in the present study in an approximate manner. The girder end moments and shear forces due to incremental lateral load analysis are added to the end moments and corresponding shear forces resulting from a static analysis of the structure under gravity loads. The plastic zone length at each load step is determined from these end moments and shear forces under the assumption that the shear force remains constant along the entire plastic zone length. This implies that the actual gravity load pattern is approximated by the third point loading shown in Fig. 2.11.

This approximation has the computational advantage that the calculation of the current length of the plastic zone z_c can be based on the bending moment and shear force at the girder end, which are readily available. The plastic zone length z_c is then calculated according to (Fig. 2.11b)

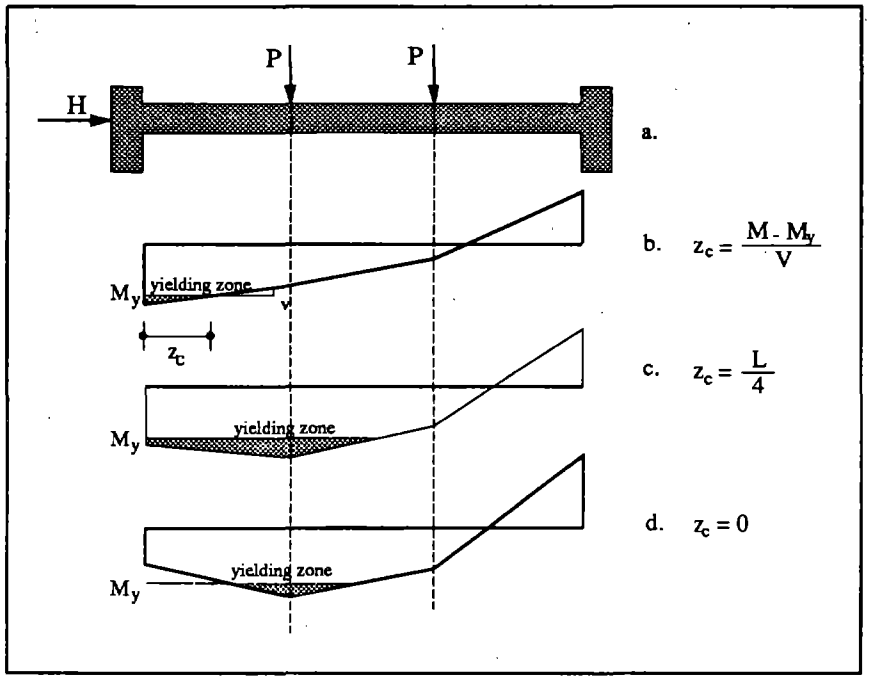

Fig. 2.11 Calculation of plastic zone length in typical cases

$$z_c = \frac{M - M_y}{V} \tag{2.7}$$

where M and V are the current values of bending moment and shear force, respectively, at the end of the girder. Eq. (2.7) results in very large values of the plastic zone length if the value of the end shear force is very small. This can happen in the upper stories of high-rise frames where the end shear forces due to lateral loads are small and sometimes act opposite to the shear forces due to gravity loads. Similarly, Eq. (2.7) does not make sense, if the value of the shear force becomes negative (Fig. 2.11c). To prevent unrealistically large values of the plastic zone length in these cases an upper limit z_{max} is placed on the extent of the plastic zone (Fig. 2.11c):

$$z_{max} = 0.25 \cdot L \tag{2.8}$$

where L is the clear span of the girder. The limit on the extent of the plastic zone is particularly important on account of the likely change in the reinforcement layout that takes place at the quarter span point.

Since the calculation of the plastic zone length depends on the moments and forces at the girder ends, the spread plastic subelement is unable to recognize yielding that might take place

along the girder span (Fig. 2.11d). Plastic zones can, therefore, only form at the girder ends. If hinges are expected to form along the span, then the girder has to be subdivided into several such elements along its length.

It should be noted here that no increase of the current plastic zone length will occur in the extreme case depicted in Fig. 2.12. Consistent with the first key assumption of the model that the behavior of the plastic zone is controlled by the behavior of the corresponding end section, spreading of the plastic zone can only take place while the end section is in the strain-hardening range. Since the end section is unloading in the case of Fig. 2.12, the further extension of the plastic zone length due to the considerable decrease in the magnitude of the shear force from one step to the next will not be detected by the model. It should be mentioned, however, that the case depicted in Fig. 2.12 is highly unlikely, when using a reasonably small load step size.

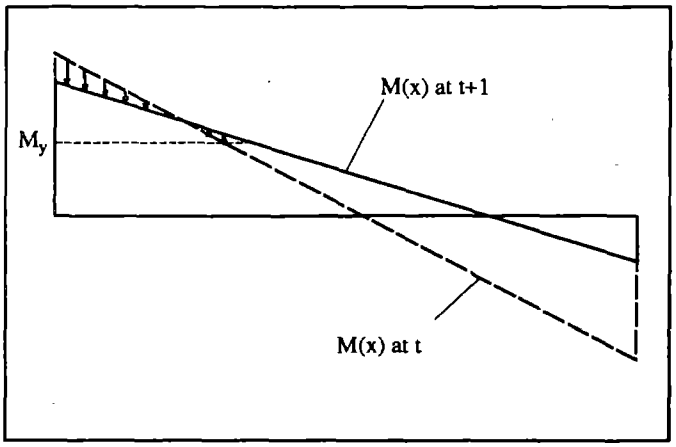

Fig. 2.12 Spread of the plastic zone while end section is unloading (not accounted for in the model)

We are now in a position to derive the flexibility matrix of the spread plastic subelement. It can be written in the general form

$$[f]_{pl} = \begin{bmatrix} f_{11} & f_{21} \\ f_{12} & f_{22} \end{bmatrix} \tag{2.9}$$

As will be shown in the following, the assumption of an average plastic zone stiffness results in a symmetric flexibility matrix and thus

$$f_{12} = f_{21}$$

It is interesting to note here that the off-diagonal terms f_{12} and f_{21} of the flexibility matrix of the spread plastic subelement are not zero, as is the case in the concentrated plasticity element. This results in coupling between the moments which act at the ends of the element. The importance of this phenomenon will be discussed in detail in Chapter 4.

To derive the coefficients of the tangent flexibility matrix of the spread plastic subelement use is made of the principle of virtual work (Fig. 2.13). It is assumed that the current length of the plastic zone at ends i and j of the element is z_i and z_j, respectively. The average stiffness of the plastic zone at ends i and j is c_i and c_j, respectively (Fig. 2.13a). The application of a moment increment ΔM_i at end i (Fig. 2.13b) results in the incremental curvature distribution shown in Fig. 2.13(c). A virtual unit moment at end i results in the moment distribution shown in Fig. 2.13(d).

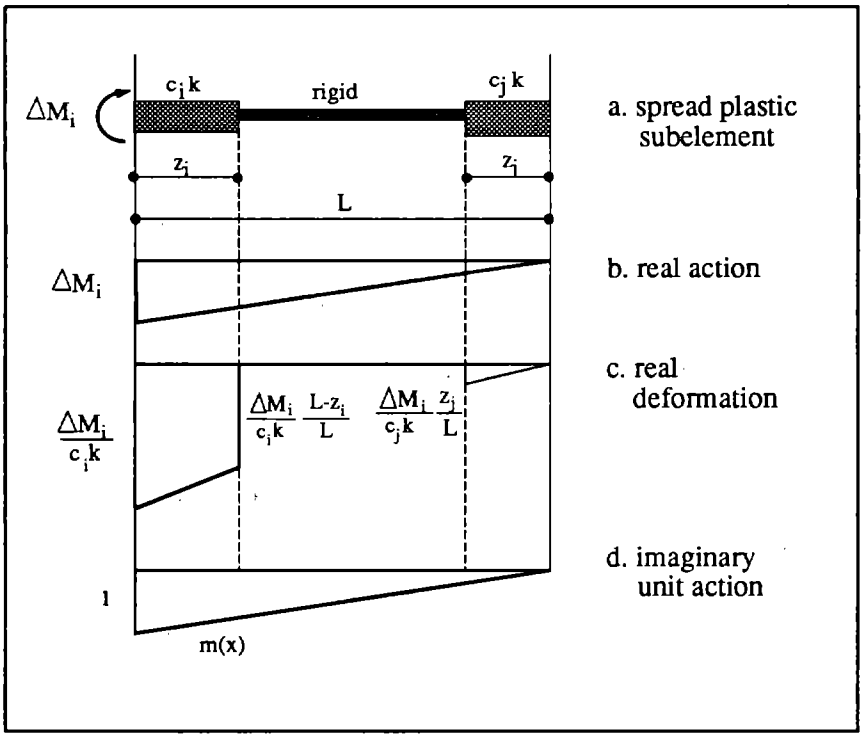

Fig. 2.13 Derivation of flexibility coefficients of spread plasticity subelement

By applying the principle of virtual work we have:

work external (WE) = work internal (WI)

$$WE = f_{11} \cdot \Delta M_i$$

$$WI = \int_L m(x) \cdot \Delta\phi(x) dx$$

where $m(x)$ is the moment distribution due to the virtual unit moment at end i (Fig. 2.13d) and $\Delta\varphi(x)$ is the curvature distribution due to the applied end moment increment ΔM_i (Fig. 2.13c).

$$WI = \left(\frac{\Delta M_i}{c_i k} - \frac{\Delta M_i}{c_i k}\frac{L - z_i}{L}\right)\frac{z_i}{2}\frac{1}{L}\left(L - \frac{z_i}{3}\right) + \frac{\Delta M_i}{c_i k}\frac{(L - z_i)}{L}\frac{z_i}{L}\left(L - \frac{z_i}{2}\right) + \frac{1}{2}\frac{\Delta M_i}{c_j k}\left(\frac{z_j}{L}\right)z_j\frac{2}{3}\frac{z_j}{L}$$

where $k = EI$. By defining

$$\frac{z}{L} = \xi$$

$$\frac{1}{c} = \gamma$$

we obtain

$$WI = \frac{\Delta M_i}{k} L\gamma_i\left\{[1 - (1 - \xi_i)]\frac{\xi_i}{2}\left(1 - \frac{\xi_i}{3}\right) + (1 - \xi_i)(\xi_i)\left(1 - \frac{\xi_i}{2}\right)\right\} + \frac{\Delta M_i}{6k} L\gamma_j 2\xi_j^3$$

$$= \frac{\Delta M_i}{k} L\gamma_i\left\{\xi_i\frac{\xi_i}{2}\left(1 - \frac{\xi_i}{3}\right) + (\xi_i - \xi_i^2)\left(1 - \frac{\xi_i}{2}\right)\right\} + \frac{\Delta M_i}{6k} L\gamma_j 2\xi_j^3$$

$$= \frac{\Delta M_i}{k} L\gamma_i\left\{\frac{\xi_i^2}{2} - \frac{\xi_i^3}{6} + \xi_i - \frac{\xi_i^2}{2} - \xi_i^2 + \frac{\xi_i^3}{2}\right\} + \frac{\Delta M_i}{6k} L\gamma_j 2\xi_j^3$$

Equating the external with the internal work and canceling ΔM_i on both sides of the equation results in

$$f_{11} = \frac{L}{6k}\{(2\gamma_i(1 - (1 - \xi_i)^3) + \gamma_j 2\xi_j^3\} \tag{2.10}$$

By interchanging i and j we obtain f_{22}

$$f_{22} = \frac{L}{6k}\{(2\gamma_j(1 - (1 - \xi_j)^3) + \gamma_i 2\xi_i^3\} \tag{2.11}$$

Using the same procedure but replacing $m(x)$ by the moment function which results from the application of a virtual unit moment at end j results in the flexibility coefficient f_{12}.

$$f_{12} = \frac{L}{6k}\{-\gamma_i(3\xi_i^2 - 2\xi_i^3) - \gamma_j(3\gamma_j^2 - 2\xi_j^3)\} \tag{2.12}$$

By interchanging i and j we can obtain f_{21}. From Eq. (2.12) it can be seen that

$$f_{12} = f_{21}$$

2.2.3 Joint subelement

The joint subelement accounts for the fixed-end rotations which arise at the beam-column interface of R/C members due to bond deterioration and slippage of reinforcement in the joint and in the girder region adjacent to the joint. Detailed models of this phenomenon have been proposed in [FIL83-1] and [FIL85-1]. The model used in this study is a simple yet sufficiently accurate phenomenological description of the behavior of beam-column joints observed in previous experimental and analytical studies. The proposed model consists of a concentrated rotational spring located at each girder end. The two springs are connected by an infinitely rigid bar to form the joint subelement (Figs. 2.3 and 2.14(a)). The moment-rotation relation of the rotational springs is derived using the detailed model presented in [FIL83-1] which accounts for the geometry, material properties and reinforcement layout of the connection. A different moment-rotation relation can be prescribed at each connection.

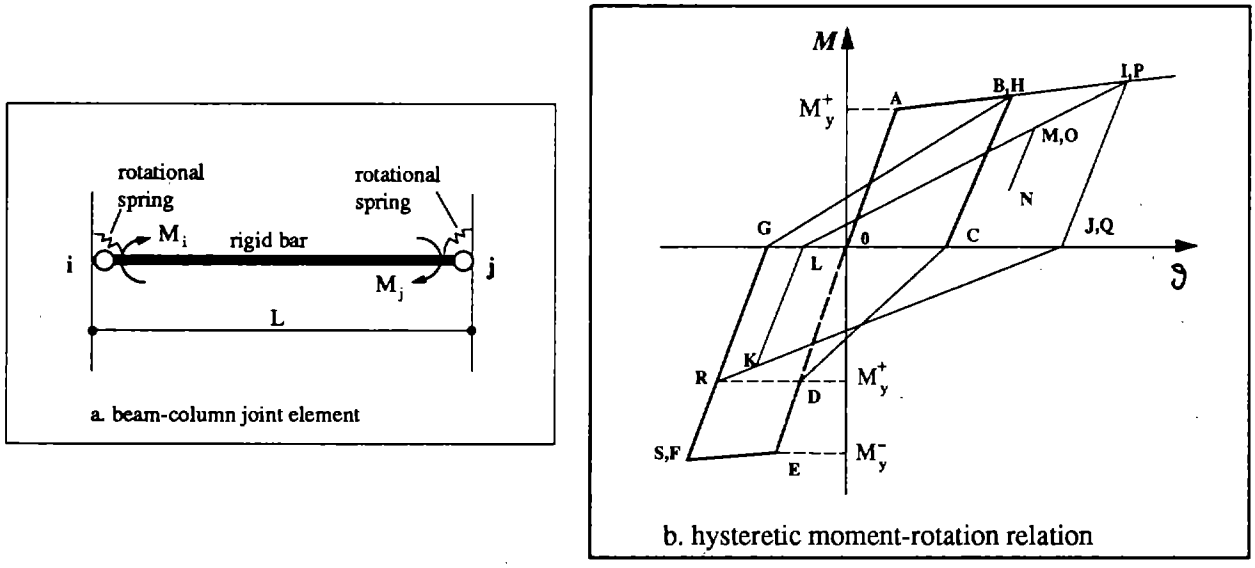

Fig. 2.14 Beam-column joint subelement

The moment-rotation relation of the rotational springs of the joint subelement is based on a bilinear elastic-strain hardening envelope curve (Fig. 2.14b). Following common design practice the area of the bottom reinforcing bars is typically less than the area of the top reinforcing bars; therefore two envelope curves need to be specified: one pertaining to the "strong side" of the end section -the top reinforcing bars are subjected to tension- and one pertaining to the "weak side" -the bottom bars are subjected to tension. These envelope curves exhibit different pre-and post-yield stiffness under positive and negative bending moments. Naturally the yield moment M_y^+ under positive bending moments is different than the yield moment M_y^- under negative bending moments (Fig. 2.14b).

The envelope curves are established with the aid of the joint model proposed in [FIL83-1] once the dimensions of a particular joint and the arrangement of the reinforcement are known. This process takes place as follows: the beam-column joint model which represents a particular connection of the frame under investigation is subjected to monotonically increasing girder end moments. These give rise to concentrated rotations due to reinforcing bar pull-out at the beam-column interface. In the case of interior joints a single loading cycle permits the determination of envelope curves under both positive and negative end moments. This happens, because bending moments caused by lateral loads act at the girder ends of an interior joint so that the bottom bars are pulled at one beam-column interface and pushed at the other. In the case of exterior joints two different load cases of monotonically increasing girder end moments are required to establish the envelope curves under positive and negative end moments: in one case the **bottom bars** of the end section are subjected to tension, while in the other the **top bars** are subjected to tension.

The study in [FIL83-2] concluded that no unique envelope curve exists in the case of interior and exterior joints; instead, the envelope curve depends on the load history. Since the elastic stiffness and yield moment do not depend on the load history, this essentially implies that the strain hardening or possibly strain softening slope of the bilinear envelope curve of the rotational springs has to be established as a function of load history. Thus, in order to establish the envelope curve for a particular joint, the load history of this joint must be known in advance. This effect is, however, negligible in properly designed joints and is not taken into account in the present study. If considerable bond deterioration and slippage of reinforcement is expected in the joints of the structure, the effect of load history on the envelope curve of the joint subelement should be taken into account.

The flexibility matrix of the joint subelement takes the simple form

$$[f]_{jnt} = \begin{bmatrix} f_i & 0 \\ 0 & f_j \end{bmatrix} \tag{2.13}$$

where f_i and f_j are the flexibility coefficients of the concentrated rotational springs at ends i and j, respectively. These coefficients depend on the monotonic envelope curves of each joint and the model used to represent the hysteretic behavior.

The hysteretic behavior of the rotational springs is described by a special hysteretic model which was first proposed in [FIL83-1]. It is derived by modifying Clough's model to account for observations of beam-column joint behavior made during experimental and analytical studies . The rules of this hysteretic model can be summarized as follows (Fig. 2.14b):

(1) unloading takes place along a line parallel to the initial elastic stiffness under moments acting in the same direction (line B-C parallel to 0-A, line K-L, in turn, parallel to 0-E)

(2) reloading on the "weak side" of the joint (G-H) occurs along the line which connects the most recent point of zero moment (G) to the load reversal point on the envelope curve which has the largest previously imposed fixed-end rotation (H),

(3) reloading on the "strong side" of the joint (Q-R-S) follows initially a line Q-R which connects the most recent point of zero moment (point Q) to a point on the unloading curve which initiates at the load reversal point with largest previous fixed-end rotation (point R). This point has a moment equal to the yield moment of the "weak side" of the joint (M_y^+ in Fig. 2.14(b)). After reaching this point reloading proceeds along the unloading curve (R-S),

(4) incomplete reloading followed by unloading and reloading in the opposite direction takes place along the path J-K-L-M,

(5) incomplete reloading followed by incomplete unloading and reloading in the same direction takes place along the path L-M-N-O-P.

These hysteretic rules are derived from observations of the behavior of joints under cyclic load reversals made during experimental and analytical studies [FIL83-1] (Fig. 2.15):

(a) no pinching is observed in the hysteretic moment-rotation relation when the bottom reinforcing layer is subjected to tension ("weak side"). In this case the beam-column interface crack remains open through the depth of the end section during the entire moment reversal process. The girder end moment is thus resisted by a force couple in the top and bottom reinforcing steel. This observation is reflected in the second hysteretic rule,

(b) when the top reinforcing layer is subjected to tension ("strong side"), the moment resisted by the section at the beam-column interface cannot exceed the moment carried by the reinforcement with the bottom reinforcing bars yielding in compression, as long as the crack remains open. This moment is approximately equal to the yield moment in the opposite

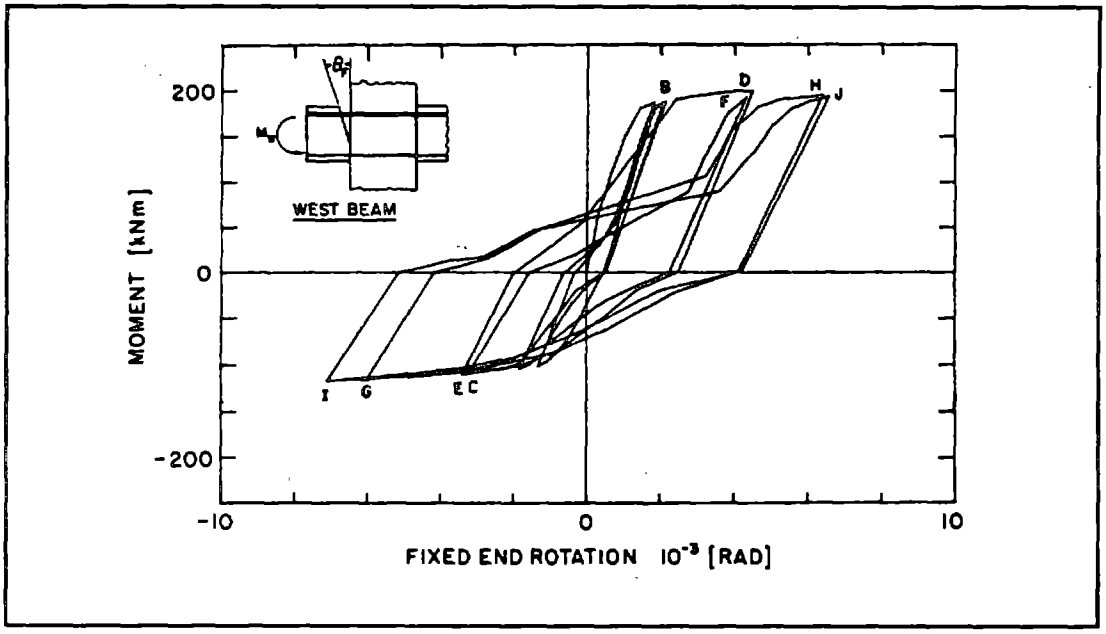

Fig. 2.15 Moment-rotation relation at beam-column joint interface from [FIL83-1]

direction of bending ("weak side"). Since the crack closes when the previously imposed pull-out of the bottom reinforcing bars is overcome, crack closure takes place approximately when the maximum previously imposed fixed-end rotation is exceeded. Once the crack closes, the resisting moment quickly reaches the envelope curve, since the concrete in contact now contributes a significant portion of the compressive force at the section. This observation is reflected in the third hysteretic rule,

(c) it is apparent from the results in [FIL83-2] that the unloading stiffness of the joint moment-rotation relation decreases with increasing deformation. Since, however, no general expression describing the observed decrease in unloading stiffness could be deduced, the simple hysteretic rule that the unloading stiffness remains equal to the initial elastic stiffness is postulated in the present model.

The proposed rules describe well the observed hysteretic behavior of beam-column joints while retaining simplicity and computational efficiency. More refined models of the hysteretic behavior of beam-column joints could be readily incorporated into the girder superelement by simply replacing the hysteretic law of the joint subelement.

It should be noted here that the proposed joint subelement does not explicitly account for the interaction between the moments and forces acting at the girder ends of interior beam-column joints. This interaction is small as long as bond along the reinforcing bars anchored in the joint is not

completely destroyed [FIL83-3]. It only becomes pronounced after many severe deformation reversals which are unlikely to occur in well proportioned frames. This interaction is, however, implicitly accounted for in the present model, since the derivation of the hysteretic rules and the parameters of the envelope curves are based on the refined model of [FIL83-1], which explicitly accounts for this interaction. At the same time the present model retains great simplicity in that the flexibility coefficients of each rotational spring in the frame can be derived independently.

2.2.4 Girder superelement stiffness matrix

The elastic, rigid plastic and joint subelements are connected in series to make up the girder superelement (Fig. 2.3). Other subelements describing effects which might also affect the hysteretic behavior of the girder, e.g. shear transfer at the beam-column interface, can be added in the same fashion. Since the constituent subelements are connected in series, the flexibility matrix of the girder superelement $[F]_g$ can be obtained by simply adding the flexibility matrices of the constituent subelements. Using in the following the convention that upper case letters denote quantities associated with the girder superelement while lower case letters denote quantities associated with the individual subelements we obtain

$$[F]_g = [f]_{el} + [f]_{pl} + [f]_{jnt} \tag{2.14}$$

$[f]_{el}$ denotes the flexibility matrix of the elastic subelement given by Eq. 2.1. $[f]_{pl}$ denotes the flexibility matrix of either the concentrated rigid plastic (Eq. 2.6) or the spread rigid-plastic subelement (Eqs. 2.9-2.12). Finally, $[f]_{jnt}$ denotes the flexibility matrix of the joint subelement given by Eq. 2.13.

It is important to note that the flexibility coefficients in $[f]_{pl}$ and $[f]_{jnt}$ change, because of nonlinearities associated with the moment-curvature or moment-rotation relation and the change of the plastic zone length. Thus $[f]_{pl}$ and $[f]_{jnt}$ in Eq. 2.14 represent the current tangent flexibility matrix of the rigid plastic and joint subelement, respectively.

The flexibility matrix of the girder superelement $[F]_g$ is inverted to obtain the current stiffness matrix $[K]_g$ in local coordinates. This is then transformed to global coordinates using the transformation matrix $[a]$

$$[K]_b = [a]^T [K]_g [a] \tag{2.15}$$

where $[K]_b$ is the tangent stiffness matrix in global coordinates and $[a]$ expresses the transformation of superelement local moments and rotations to nodal forces and deformations in the global coordinate system (Fig. 2.16)

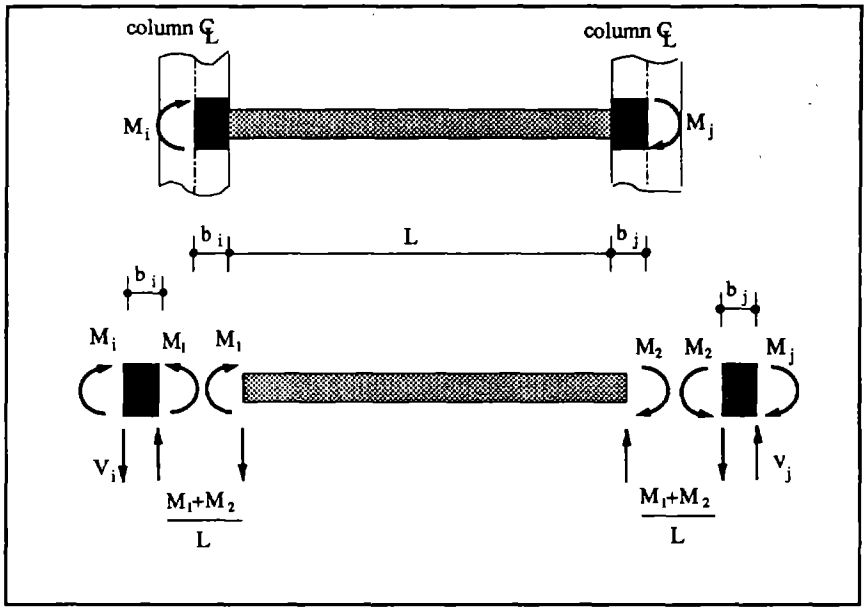

Fig. 2.16 ***Transformation of forces and moments between local and global coordinate system***

$$\begin{Bmatrix}\Theta_1\\ \Theta_2\end{Bmatrix} = [a]\begin{Bmatrix}\Theta_i\\ \Theta_j\\ v_i\\ v_j\end{Bmatrix} \tag{2.16a}$$

$$\begin{Bmatrix}M_i\\ M_j\\ V_i\\ V_j\end{Bmatrix} = [a]^T\begin{Bmatrix}M_1\\ M_2\end{Bmatrix} \tag{2.16b}$$

where

$$a = \begin{bmatrix}1+e_i & e_j & 1/L & -1/L\\ e_i & 1+e_j & 1/L & -1/L\end{bmatrix} \tag{2.17}$$

and

$$e_i = \frac{b_i}{L} \tag{2.18a}$$

$$e_j = \frac{b_j}{L} \tag{2.18b}$$

b_i and b_j is equal to half the width of the left and right end beam-column joint, respectively. L is the clear span of the member (Fig. 2.16).

By inverting the sum of the flexibility matrices of the elastic $[f]_{el}$ and the concentrated plastic subelement $[f]_{pl}$ given by Eqs. 2.1 and 2.6, respectively, the stiffness matrix of the one-component model as originally proposed by Giberson [GIB69-1] results.

The addition of the flexibility matrices of the elastic $[f]_{el}$ and the spread plastic subelement $[f]_{pl}$ given by Eqs. 2.1 and 2.10, respectively, yields the flexibility matrix of the spread plasticity model proposed by Soleimani et. al. [SOL79-1].

2.3 Reinforced concrete column element

In this study columns are assumed to remain elastic during the entire response time history except at the base of the building. In buildings designed according to the strong column-weak girder design philosophy of current codes of practice inelastic column deformations should remain small except at the base of the building. To account for the large inelastic deformations which are expected to occur at the base of the building a column base or foundation element is used, as described in the next section.

Columns are assumed to have uniform flexural EI and axial stiffness EA. It is, therefore, straightforward to write down the elastic bending stiffness matrix with respect to local coordinates

$$\begin{Bmatrix} M_1 \\ M_2 \end{Bmatrix} = \frac{EI}{h} \begin{bmatrix} 4 & 2 \\ 2 & 4 \end{bmatrix} \begin{Bmatrix} \Theta_1 \\ \Theta_2 \end{Bmatrix} \tag{2.19}$$

where EI is the gross uncracked stiffness and h is the clear height of the column. The local moments and rotations are defined similar to Fig. 2.16.

The column axial stiffness matrix with respect to local coordinates is given by

$$\begin{Bmatrix} P_1 \\ P_2 \end{Bmatrix} = \frac{EA}{h} \begin{bmatrix} 1 & -1 \\ -1 & 1 \end{bmatrix} \begin{Bmatrix} v_1 \\ v_2 \end{Bmatrix} \tag{2.20}$$

where v_1 and v_2 are the axial displacements at the ends of the column. Eq. 2.19 can be readily transformed to global coordinates by applying a transformation matrix similar to [a] in Eq. 2.17. This matrix can be derived from [a] by replacing L by h and considering b_i and b_j as half the depth of the beam-column joint at the lower and upper end of the column, respectively.

The transformation of Eq. 2.20 to global coordinates is much more direct, because the rigid offset zones have no effect on forces and deformations. Thus the local axial forces are equal one to one to the corresponding global forces and the local axial displacements v are equal one to one to the corresponding global vertical frame displacements.

The interaction of large axial forces in the lower story columns of multistory frames with large interstory drifts due to severe lateral loads may result in considerable second-order effects which should be taken into account. For simplicity and in view of the strong column-weak girder frame idealization, the local geometric stiffness with respect to the column chord end rotations is neglected. Consideration is given, however, to the global geometric stiffness related to the column end lateral displacements. Assuming a linear displacement function between the column ends (Fig. 2.17) results in the column centerline geometric stiffness matrix given in Eq. 2.21 with respect to global coordinates

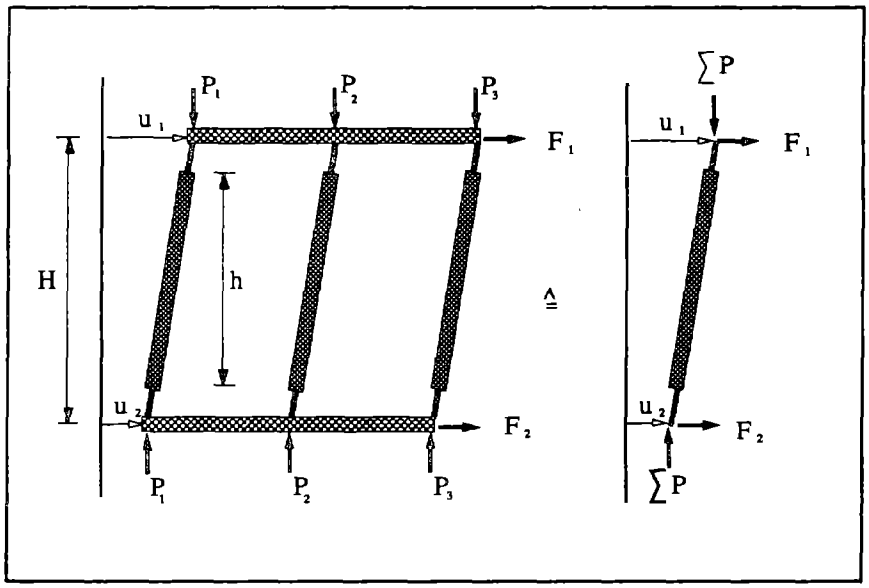

Fig. 2.17 Linear geometric stiffness matrix of column subelement

$$\begin{Bmatrix} F_1 \\ F_2 \end{Bmatrix} = \frac{P}{H} \begin{bmatrix} -1 & 1 \\ 1 & -1 \end{bmatrix} \begin{Bmatrix} u_1 \\ u_2 \end{Bmatrix} \tag{2.21}$$

u_1 and u_2 are the lateral displacements at the lower and upper column end, respectively, while P is the axial compressive force acting in the column. P accounts for the effect of gravity loads and overturning moments due to lateral loads. The axial load P is assumed to remain constant within a load step.

By assuming that the floor diaphragm is infinitely rigid in its plane all lateral displacements can be condensed into a single lateral degree of freedom at each story. In this case the geometric stiffness of the individual columns may be combined into the geometric stiffness of the entire story (Fig. 2.17). This is given by

$$\begin{Bmatrix} F_1 \\ F_2 \end{Bmatrix} = \frac{\Sigma P}{H} \begin{bmatrix} -1 & 1 \\ 1 & -1 \end{bmatrix} \begin{Bmatrix} u_1 \\ u_2 \end{Bmatrix} \tag{2.22}$$

u_1 and u_2 are the lateral displacements of the floor below and above the particular story, respectively, and ΣP is the sum of all axial forces in the columns of a particular story.

2.4 Foundation element

In order to account for the large inelastic deformations that can take place at the base of the first story columns of multistory frames subjected to severe earthquake excitations a spring element is inserted at the base of each first story column. This spring element, termed here a foundation element, is also capable of modeling vertical and lateral displacements of the base of the building associated with rocking and sliding of the foundation (Fig. 2.2). The stiffness matrix of the foundation element at the base of each first story column is simply given by

$$[K]_f = \begin{bmatrix} k_{sv} & 0 & 0 \\ 0 & k_{sh} & 0 \\ 0 & 0 & k_{sr} \end{bmatrix} \tag{2.23}$$

where k_{sv}, k_{sh}, k_{sr} is the vertical, horizontal and rotational stiffness of the spring at the base of the column, respectively. The vertical and horizontal stiffness are constant during the entire response time history. If the rotational spring stiffness were also assumed constant, then large moments would develop at the base of the first story columns due to P-Δ effects and the possible transformation of the frame into a cantilever beam after the necessary number of plastic hinges form in the relatively weaker girders. To avoid such large moments at the base of the first story columns, the rotational spring has a yielding feature. This limits the base moment to a value which corresponds to the yield moment capacity M_y of the column. M_y is determined with due consideration of the effect of axial

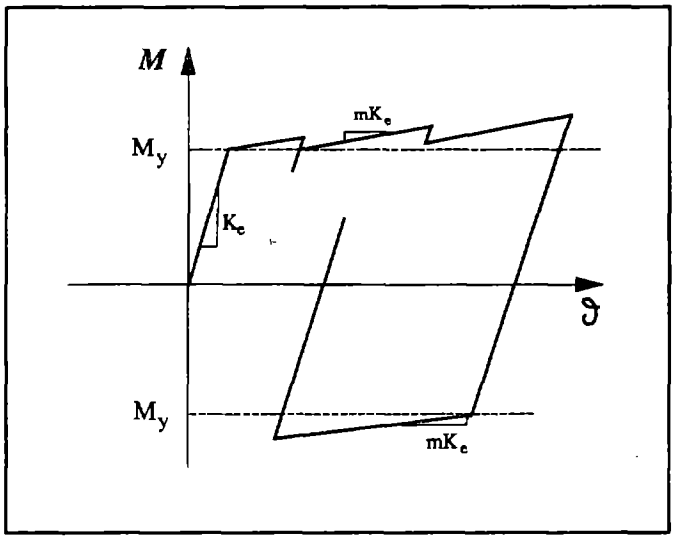

Fig. 2.18 Hysteretic moment-rotation relation of spring at the base of the building

forces due to gravity loads. The axial force variation in the columns during the response of the frame to earthquake excitations is neglected. The simple bilinear elasto-plastic hysteretic rule depicted in Fig. 2.18 describes the behavior of the rotational spring under moment reversals.

2.5 Structural stiffness matrix

The first step in the analysis of a moment resisting reinforced concrete frame is the development of a model of the actual structure. This process is schematically illustrated in Fig. 2.19. Fig. 2.19 shows how the girders and columns of the actual structure are modeled by the elements presented in the previous sections. After determining the stiffness matrix of all elements with respect to global coordinates the stiffness matrix of the entire structural model can be formed using the direct stiffness method. This process can be formally written as

$$[K] = \Sigma[K]_b + [K]_c + [K]_G + [K]_f \tag{2.24}$$

where $[K]$ is the stiffness matrix of the entire structure, $[K]_b$ is the beam element, $[K]_c$ is the column element and $[K]_f$ is the foundation element matrix with respect to global coordinates. $[K]_G$ represents the story geometric stiffness matrix defined in Eq. 2.22. The summation in Eq. 2.24 extends over all elements in the structure.

Since the different frame elements exhibit nonlinear behavior either through nonlinearities in material response or through changes in the inelastic zone length, the different stiffness matrices

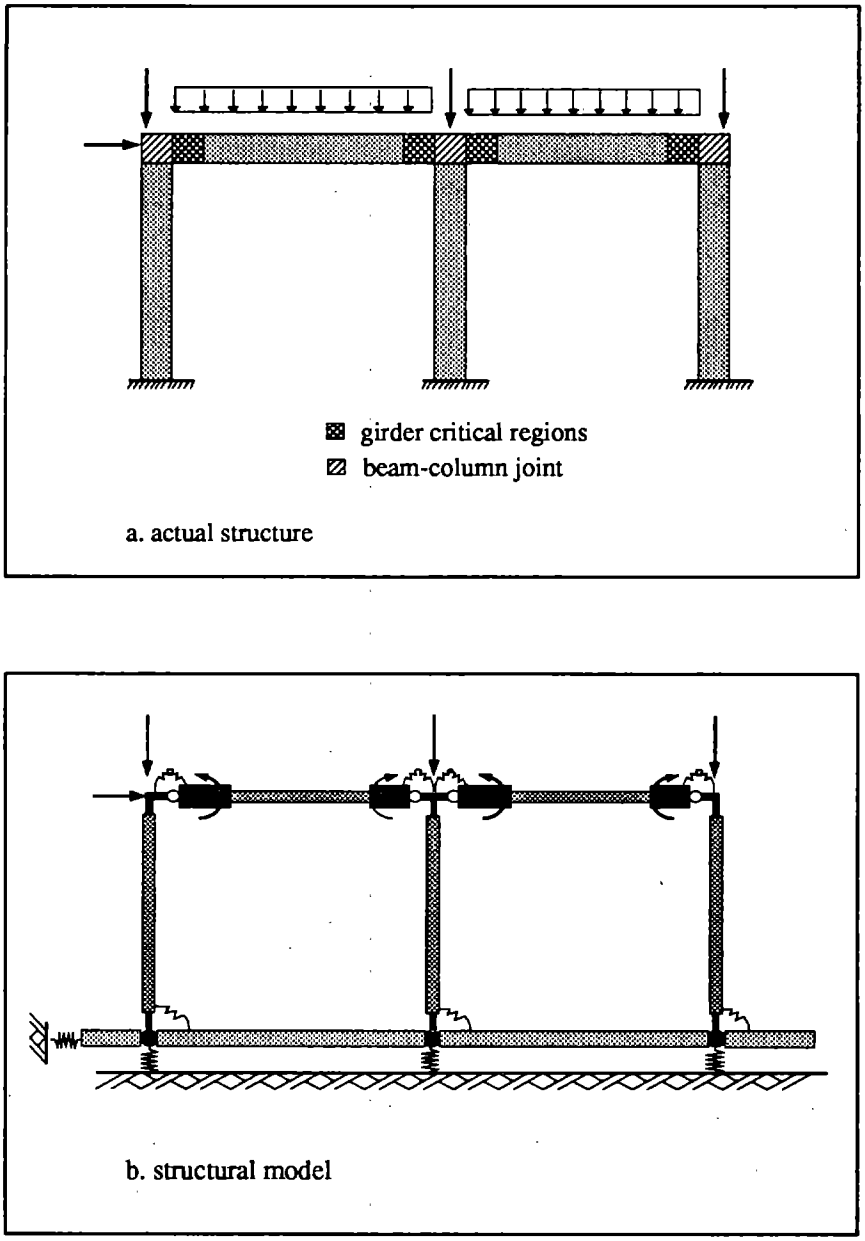

Fig. 2.19 Modeling of a one-story two-bay frame

in Eq. 2.24 really represent the tangent stiffness matrices of the various elements. The nonlinear response of the structure to cyclic load or deformation reversals can only be determined through an incremental step-by-step analysis. This process can be expressed by

$$[K]\Delta r = \Delta R \tag{2.25}$$

where $\Delta \boldsymbol{R}$ is the vector of load increments which are successively imposed on the structure and $\Delta \boldsymbol{r}$ is the vector of corresponding displacement increments. $[\boldsymbol{K}]$ is the current stiffness matrix of the structure.

After solving Eq. 2.25 for the unknown displacement increments $\Delta \boldsymbol{r}$ the response of the structure to the applied loads is obtained from

$$\boldsymbol{r}_{n+1} = \boldsymbol{r}_n + \Delta \boldsymbol{r} \tag{2.26}$$

where $\boldsymbol{r}_n$ is the vector of structural displacements at the beginning of the current load step and $\boldsymbol{r}_{n+1}$ the displacement vector at the end. The process is applied step-by-step by starting from a state of no loading and thus no corresponding displacements of the structure.

Depending on the magnitude of load increments it is more or less likely that the stiffness matrix $[\boldsymbol{K}]$ in Eq. 2.25 will change during the given load step. Thus, Eq. 2.25 has to be solved iteratively. The numerical and computational aspects associated with the solution of Eq. 2.25 will be presented in the next chapter.

CHAPTER 3

NONLINEAR ANALYSIS OF STATIC RESPONSE TO CYCLIC LOADS

3.1 Introduction

This chapter discusses the numerical implementation of the proposed frame elements within the framework of a special purpose program for the nonlinear static and dynamic analysis of planar R/C moment-resisting frames. Attention is focused herein on determining the response of moment-resisting frames under static cyclic loads. The proposed procedures of nonlinear analysis are equally applicable to dynamic response analysis.

To determine the response of the structure to cyclic static loads Eq. (2.25) needs to be solved. The solution of Eq. (2.25) yields the displacement increments $\Delta \boldsymbol{r}$ which result when the load increments $\Delta \boldsymbol{R}$ are imposed on the structure. This process is applied step-by-step starting from the unloaded state. Once a particular step is completed the displacement and load increments are added to the corresponding values at the end of the previous step. Since changes in the stiffness matrix of the structure are likely to take place within a given load step, Eq. (2.25) needs to be solved iteratively.

In order to find out whether the displacement increments $\Delta \boldsymbol{r}$ cause changes in the stiffness matrix of the structure during a particular load step the corresponding rotation increments $\Delta\Theta$ at the ends of each element need to be determined. This is done by applying Eq. (2.16a) which transforms the global structural degrees of freedom (dof's) to local element deformations. The usual procedure at this stage of the nonlinear analysis is the state determination of each element of the structure: the internal moments corresponding to the local rotation increments $\Delta\Theta$ are determined and the stiffness matrix of the element is updated, if necessary. If several elements are connected in series, as is the case in the present study, the state determination process is not straightforward. The basic problem lies in determining the rotation increments $\Delta\theta$ that result at the ends of each element in series by only knowing that the sum of all subelement rotations $\Delta\theta$ is equal to the superelement rotation $\Delta\Theta$. As long as no change in stiffness in any one of the elements in series occurs within the load step, the local rotations of each element can be determined from the stiffness of the particular element by making use of the fact that the end moments of all subelements are equal to the end moments of the superelement. If a change of stiffness in any of the elements in series occurs within the load step, then the determination of local subelement rotations requires the

development of a new nonlinear analysis procedure. Such a procedure is developed in this study. This will be presented in the following in the context of an initial stress formulation of the well-known Newton-Raphson method of nonlinear analysis.

3.2 Brief review of nonlinear solution methods

Several solution schemes have been proposed for solving the nonlinear problem formulated in Eq. (2.25). Some of these methods will be briefly referenced here as they relate closely with the nonlinear analysis procedure that will be proposed. An extensive review and evaluation of solution strategies for statically loaded nonlinear structures is presented in [BER73-1], [HAI74-1] and [SIM82-1].

The basic solution procedure of Eq. (2.25) is the well known Newton-Raphson method. In the Newton-Raphson method Eq. (2.25) is solved by a recurrence relation

$$[\boldsymbol{K}_T]^k \Delta \boldsymbol{r}_n^k = \Delta \boldsymbol{R}_n^{k-1} = (\Delta \boldsymbol{R}_E)_n - (\Delta \boldsymbol{R}_I)^{k-1} \tag{3.1}$$

and

$$\boldsymbol{r}_{n+1}^k = \boldsymbol{r}_{n+1}^{k-1} + \Delta \boldsymbol{r}_n^k \tag{3.2}$$

until a suitable norm of the vector on the right hand side of Eq. (3.1) becomes smaller than the specified tolerance. Index n refers to the load step, while index k refers to the iteration within a particular load step. $\Delta \boldsymbol{R}_n^{k-1}$ is the difference between $(\Delta \boldsymbol{R}_E)_n$, the externally applied load increments at step n, and $(\Delta \boldsymbol{R}_I)^{k-1}$, the internal resisting load increments. This iterative process is graphically depicted in Fig. 3.1.

The basic Newton-Raphson method is not necessarily the most economical solution scheme and does not always provide rapid or reliable convergence. To improve upon some of the limitations of the basic Newton-Raphson method several modifications have been proposed over the years. Some of these methods involve modifications in the formulation of the stiffness matrix in Eq. (3.1) and are then classified as Modified Newton or Quasi-Newton methods.

In cases where large unbalances between external applied loads and internal resisting forces develop the iteration process might fail to converge. Among the solution schemes that have been proposed to deal with these cases is the event-to-event method [SIM82-1]. In this method the solution advances from one stiffness change or event to the next. The purpose of this strategy is to follow the equilibrium path as closely as possible by updating the stiffness matrix and the state of each

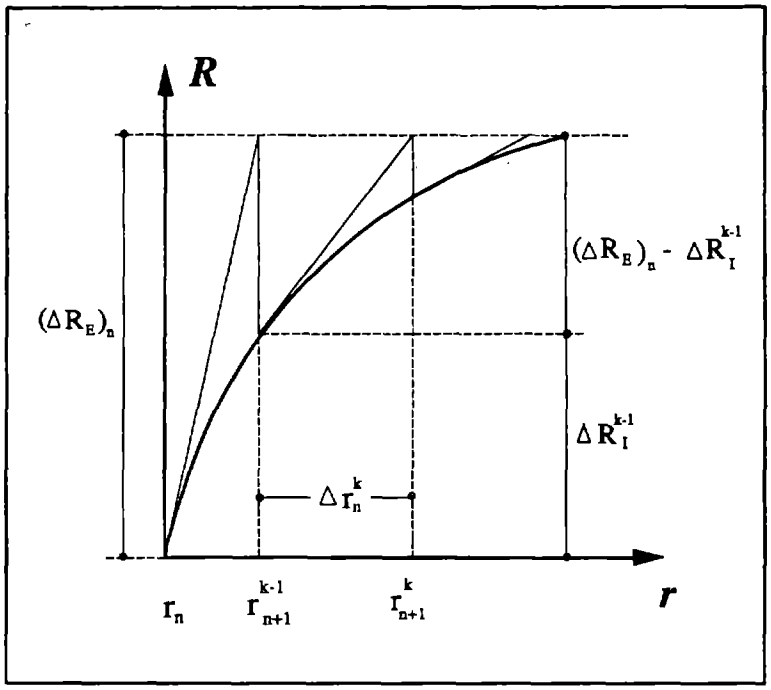

Fig. 3.1 Newton-Raphson method of nonlinear analysis

element each time a change of stiffness in one of the elements of the structure takes place. This is achieved by predicting the occurrence of the next change of stiffness (event) within a load step and then scaling the load increments by a factor such that the solution just reaches the predicted event.

In the present study the basic Newton-Raphson method is used in solving the nonlinear problem formulated in Eq. (2.25). The method is recast in a different form which is more suitable for the solution of nonlinear structures made up of several elements connected in series. Concepts from the event-to-event method are used in addressing the problem of state determination in the case of the gradual spread of the inelastic zone that takes place in the spread plastic beam subelement. The proposed algorithm has proved to be efficient and reliable in solving the nonlinear response analysis problems addressed in this report.

3.3 Proposed nonlinear analysis algorithm

Once the stiffness matrix of the entire structure is formed, the problem of determining the static response to cyclic load reversals takes the form of Eq. (2.25). Using the basic Newton-Rahpson method the solution of Eq. (2.25) takes the form of Eqs. (3.1) and (3.2).

It is possible to rewrite the basic Newton-Raphson solution scheme such that the displacement increments are always measured from the converged solution in the previous load step n. This results in an initial stress version of the Newton-Raphson method, which offers an advantage over the basic method in cases where several elements are connected in series. To perform the transformation we start from Eq. (3.2). Expressing Δr_n^k in terms of the solution estimates at iteration k and k-1 we get

$$\Delta r_n^k = r_{n+1}^k - r_{n+1}^{k-1} \tag{3.3}$$

Substituting Eq. (3.3) into Eq. (3.1) and solving for r_{n+1}^k we obtain

$$[K_T]^k (r_{n+1}^k - r_{n+1}^{k-1}) = (\Delta R_E)_n - (\Delta R_I)^{k-1}$$

$$[K_T]^k r_{n+1}^k = (\Delta R_E)_n - \{(\Delta R_I)^{k-1} - [K_T]^k \cdot r_{n+1}^{k-1}\} \tag{3.4}$$

By subtracting the term $[K_T]^k \cdot r_n$ from both sides of Eq. (3.4) we can solve for the displacement increments relative to the converged solution at the previous load step n.

$$[K_T]^k (r_{n+1}^k - r_n) = (\Delta R_E)_n - \{ (\Delta R_I)^{k-1} - [K_T]^k \cdot (r_{n+1}^{k-1} - r_n)\}$$

$$[K_T]^k \cdot \Delta \bar{r}_n^k = (\Delta R_E)_n - \{ (\Delta R_I)^{k-1} - [K_T]^k \cdot (\Delta \bar{r}_n^{k-1})\}$$

$$= (\Delta R_E)_n - (\Delta R_0)^{k-1} \tag{3.5}$$

$(\Delta R_0)^{k-1}$ is the initial load vector to be used in iteration k and $\Delta \bar{r}_n$ is the increment of the displacement vector with respect to the previous converged load step r_n. The graphical representation of the initial stress formulation of the Newton-Raphson method is shown in Fig. 3.2.

At the beginning of a new load step $(\Delta R_0)^{k-1}$ is equal to zero and the current displacement vector r_n and the current tangent stiffness matrix of the structure $[K_T]$ are known. Given an external load increment $(\Delta R_E)_n$ the solution process starts by solving Eq. (3.5) for the first iteration estimate of the displacement increments $\Delta \bar{r}_n$.

From $\Delta \bar{r}_n$ the global deformation increments Δr_m at the ends of each element of the structure can be extracted. Since the column elements are assumed to remain elastic, their stiffness does not change during the load step. Consequently, the nonlinear solution method will be presented with reference to the girder superelement.

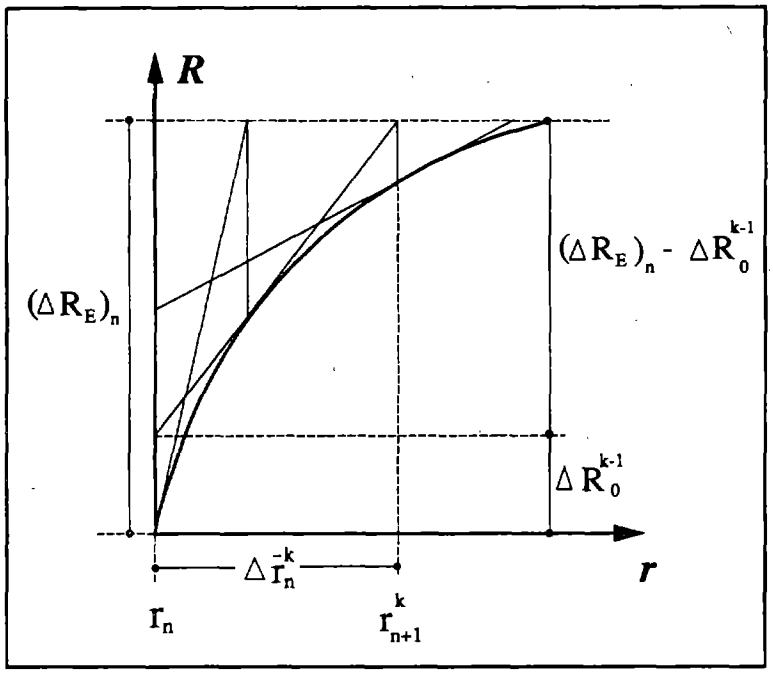

Fig. 3.2 Initial stress formulation of basic Newton-Raphson method

By transforming the global deformation increments Δr_m according to Eq. (2.18a), written in incremental form, the local rotation increments $\Delta\Theta$ at the ends of the girder superelement are obtained

$$\Delta\Theta = \begin{Bmatrix} \Delta\Theta_1 \\ \Delta\Theta_2 \end{Bmatrix} = [a] \cdot \Delta r_m = [a] \cdot \begin{Bmatrix} \Delta\Theta_i \\ \Delta\Theta_j \\ \Delta u_i \\ \Delta u_j \end{Bmatrix} \tag{3.6}$$

The corresponding moment increments at the end of the superelement are

$$\Delta M_E = [K]_g \cdot \Delta\Theta \tag{3.7}$$

where $[K]_g$ is the stiffness matrix of the girder superelement with respect to local degrees of freedom obtained by inverting the flexibility matrix given in Eq. (2.14).

The moment increments at the end of the superelement ΔM_E lead directly to the moment increments Δm_E at the ends of each subelement. Since all girder subelements are in series

$$\Delta M_E = (\Delta m_E)_{el} = (\Delta m_E)_{pl} = (\Delta m_E)_{jnt} \tag{3.8}$$

From the moment increments $\Delta \boldsymbol{m}_E$ and the current flexibility matrix of each subelement the rotation increments at the ends of each subelement can be determined

$$\Delta\theta_{el} = [f]_{el} \cdot (\Delta \boldsymbol{m}_E)_{el} \tag{3.9a}$$

$$\Delta\theta_{pl} = [f]_{pl} \cdot (\Delta \boldsymbol{m}_E)_{pl} \tag{3.9b}$$

$$\Delta\theta_{jnt} = [f]_{jnt} \cdot (\Delta \boldsymbol{m}_E)_{jnt} \tag{3.9c}$$

For the joint and concentrated plasticity beam subelements the process of state determination is rather straightforward: the local rotation increments at ends i and j, $\Delta\theta_{pl}$ and $\Delta\theta_{jnt}$, are added to the rotations at the end of the previous load step n, $(\theta_n)_{pl}$ and $(\theta_n)_{jnt}$, respectively, to obtain the current total rotations.

$$(\theta_{n+1})_{pl} = (\theta_n)_{pl} + \Delta\theta_{pl} \tag{3.10a}$$

$$(\theta_{n+1})_{jnt} = (\theta_n)_{jnt} + \Delta\theta_{jnt} \tag{3.10b}$$

Since the flexibility and stiffness matrices of these two subelements are diagonal, the rotational degrees of freedom at the ends of the subelement are uncoupled. Thus, the internal resisting moments

$$(\boldsymbol{m}_R)_{pl} = \begin{Bmatrix} m_{R,i} \\ m_{R,j} \end{Bmatrix}_{pl}$$

and

$$(\boldsymbol{m}_R)_{jnt} = \begin{Bmatrix} m_{R,i} \\ m_{R,j} \end{Bmatrix}_{jnt}$$

which correspond to total rotations

$$(\theta_{n+1})_{pl} = \begin{Bmatrix} \theta_{n+1,i} \\ \theta_{n+1,j} \end{Bmatrix}_{pl}$$

and

$$(\theta_{n+1})_{jnt} = \begin{Bmatrix} \theta_{n+1,i} \\ \theta_{n+1,j} \end{Bmatrix}_{jnt}$$

can be independently determined from the corresponding hysteretic moment-rotation relation and the load history at each end of the joint or concentrated plasticity beam subelement. The incremental vector of internal resisting moments ($\Delta \boldsymbol{m}_R$) can then be determined by subtracting from the current resisting moments those at the end of the previous load step

$$(\Delta \boldsymbol{m}_R)_{pl} = [\,(\boldsymbol{m}_R)_{n+1} - (\boldsymbol{m}_R)_n\,]_{pl}$$

$$(\Delta \boldsymbol{m}_R)_{jnl} = [\,(\boldsymbol{m}_R)_{n+1} - (\boldsymbol{m}_R)_n\,]_{jnl}$$

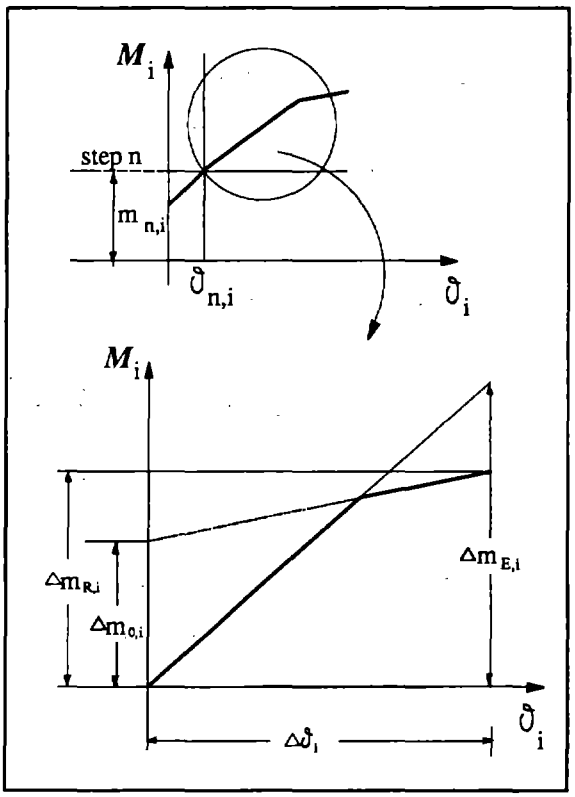

Fig. 3.3 ***State determination and initial moment calculation for joint and concentrated plasticity subelements***

If the difference between the increments of externally applied moments $\Delta \boldsymbol{m}_E$ and internal resisting moments $\Delta \boldsymbol{m}_R$ is larger than a specified tolerance at one or both ends, then the flexibility matrix of the corresponding subelement needs to be updated. Because of the change in stiffness, Eqs. (3.9) are no longer valid. Instead these relations have to be modified by introducing an initial moment vector $\Delta \boldsymbol{m}_0$ as follows

$$\Delta\theta_{pl} = [f_u]_{pl} \cdot (\Delta \boldsymbol{m}_R - \Delta \boldsymbol{m}_0)_{pl} \qquad (3.11a)$$

$$\Delta\theta_{jnt} = [f_u]_{jnt} \cdot (\Delta m_R - \Delta m_0)_{jnt} \tag{3.11b}$$

where $[f_u]$ is the updated flexibility matrix of the corresponding subelement.

Since the flexibility matrices of the joint and concentrated plasticity beam subelements are diagonal, the whole process of state determination, which consists of Eqs. (3.9)-(3.11) can be represented graphically for one end of the particular subelement, as shown in Fig. 3.3 for end *i*.

Solving Eqs. (3.11) for the initial moment vectors Δm_0 yields

$$(\Delta m_0)_{pl} = (\Delta m_R)_{pl} - [k_u]_{pl}\Delta\theta_{pl} \tag{3.12a}$$

$$(\Delta m_0)_{jnt} = (\Delta m_R)_{jnt} - [k_u]_{jnt}\Delta\theta_{jnt} \tag{3.12b}$$

For the spread plastic subelement a change of stiffness during a particular load step can be attributed to two effects: a change of stiffness in one or both plastic zones or a change in plastic zone length at one or both ends. It is important to note that the flexibility matrix of the spread plastic subelement is not diagonal and thus the rotational degrees of freedom are coupled in this case.

If only the effective section stiffness changes, the determination of initial moments remains practically the same as presented in Eqs. (3.11) and (3.12). The only difference is that the determination of internal resisting moments now depends on the curvatures at the end sections of the beam subelement instead of the end rotations. Using the concept of average plastic zone stiffness introduced in Chapter 2, the process of state determination is considerably simplified, since the curvature increment $\Delta\varphi$ at each end can be determined from the corresponding external moment increment Δm_E independently from the curvature increment at the other end. Thus

$$\Delta\phi_i = \frac{(\Delta m_{E,i})_{pl}}{c_i \cdot EI} \tag{3.13a}$$

$$\Delta\phi_j = \frac{(\Delta m_{E,j})_{pl}}{c_j \cdot EI} \tag{3.13b}$$

where the indices refer to ends *i* and *j* of the spread plastic subelement.

The curvature increments from Eqs. (3.13) are added to the curvatures at the end of the previous load step to obtain the current curvatures. These are then used to calculate the internal moments

$(m_R)_{n+1}$ of the spread plastic subelement from the moment-curvature relation at each corresponding end (Fig. 3.4). The incremental vector of internal resisting moments (Δm_R) can then be determined by subtracting from the current resisting moments those at the end of the previous load step

$$(\Delta m_R)_{pl} = [(m_R)_{n+1} - (m_R)_n]_{pl}$$

exactly as was done in the case of the concentrated plasticity subelement.

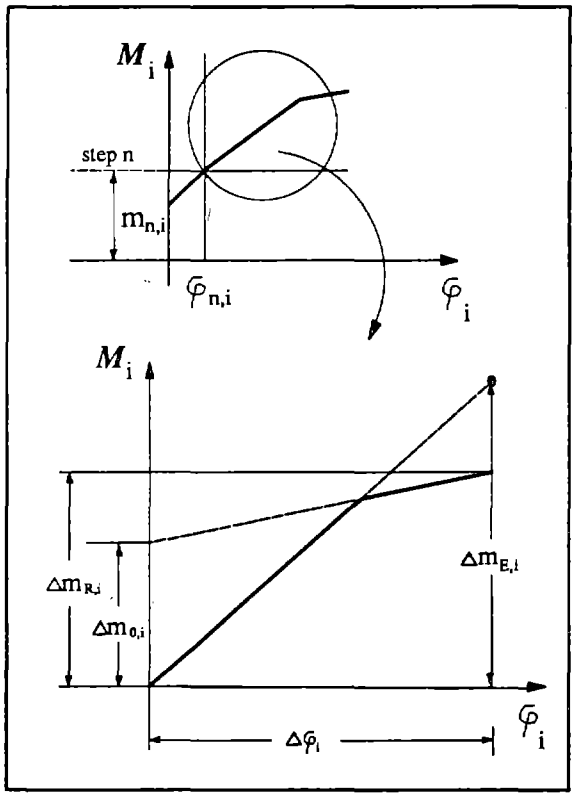

Fig. 3.4 ***State determination and initial moment calculation for spread plasticity subelement (stiffness change)***

By comparing the internal moment increments at the two ends of the element $(\Delta m_R)_{pl}$ to the external moment increments $(\Delta m_E)_{pl}$, it is determined whether a change of stiffness took place during the load step. If such a change is detected, the flexibility matrix of the spread plastic subelement is updated. Since Eq. (3.9b) no longer holds, initial moments at the ends of the element have to be introduced yielding a relation identical to Eq. (3.11a), which is then solved for the initial moments resulting in Eq. (3.12a).

If the external moment increments in Eqs. (3.7) and (3.8) result in a change in the plastic zone length at one or both ends of the beam subelement, then the process of determining the initial moments becomes considerably more involved.

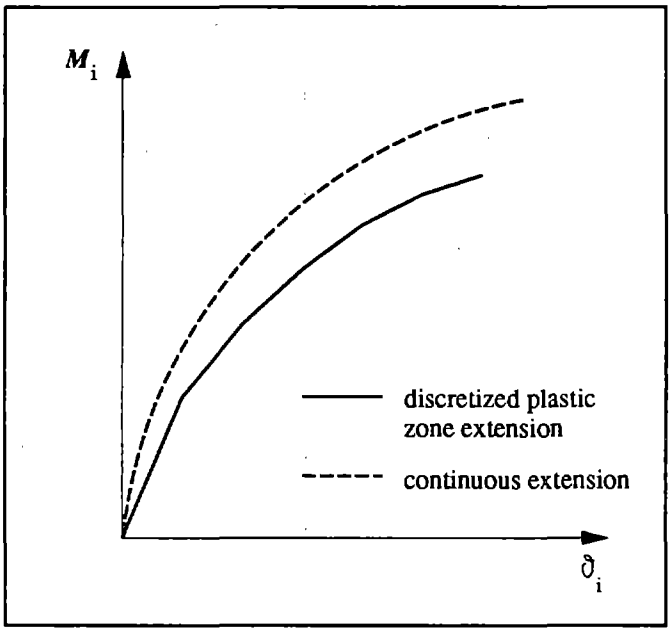

Fig. 3.5 Moment-rotation relation at one end of the spread plastic subelement

To illustrate the complexity of the problem the moment-rotation relation at one end of the spread plastic beam subelement is shown in Fig. 3.5. Since the plastic zone length is a continuous variable the moment-rotation relation is nonlinear, as shown by the broken line in Fig. 3.5. It should also be kept in mind that the moment-rotation relation at one end of the element also depends on the moment acting at the other end, because of the non-zero coupling terms in the element flexibility matrix. This leads to a moment-rotation relation which is not unique, thus requiring that both end moments be considered simultaneously. In order to reduce the computational effort the process of plastic zone extension is simplified by assuming that the change in length takes place in discrete increments z_d. The actual plastic zone length z_a thus follows the step function shown dashed in Fig. 3.6. This results in the moment-rotation relation being multi-linear instead of continuous as shown by the solid line in Fig. 3.5. The discrepancy between the actual and the idealized moment-rotation relation in Fig. 3.5 can be reduced by decreasing the size of z_d.

The basic problem in the state determination of the spread plastic subelement now lies in the fact that it is not possible to directly relate rotations with curvatures and, consequently, moments at each

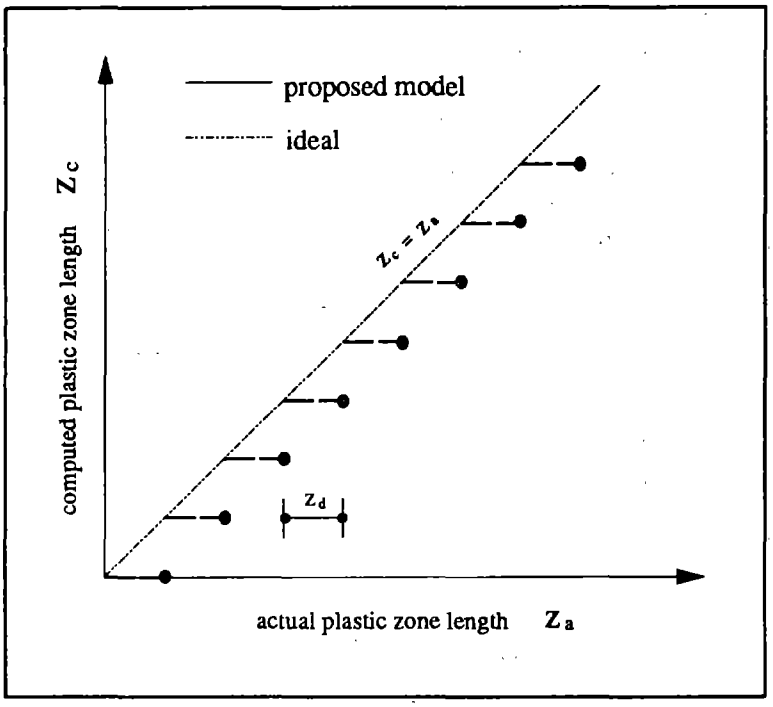

Fig. 3.6 Discretization of plastic zone extension

end of the element, as is the case in the joint and concentrated plasticity elements. This is illustrated in Fig. 3.7, where $(\Delta\theta_i)_{pl}$ denotes the increment of end rotation at end i of the element resulting from external moment increments Δm_E.

The internal resisting moment which corresponds to rotation increment $(\Delta\theta_i)_{pl}$ and is represented by a question mark in Fig. 3.7 cannot be determined for the simple reason that the exact moment-rotation relation (solid line in Fig. 3.7) is not known. This relation depends on the changes in the plastic zone length which cannot be determined without due account of the coupling that exists between the end moments of the element. Another way of looking at the problem is to recall that the resisting moments of the spread plastic subelement are related to the curvatures at the end sections. Since there is no closed form relation between the curvatures at the end sections and the end rotations, the direct determination of the internal resisting moments from the rotation increments $(\Delta\theta)_{pl}$ is not possible.

To solve this problem resort is made to concepts first introduced in the event-to-event method [SIM82-1].

At the beginning of the load step the plastic zone length z_a at ends i and j is known

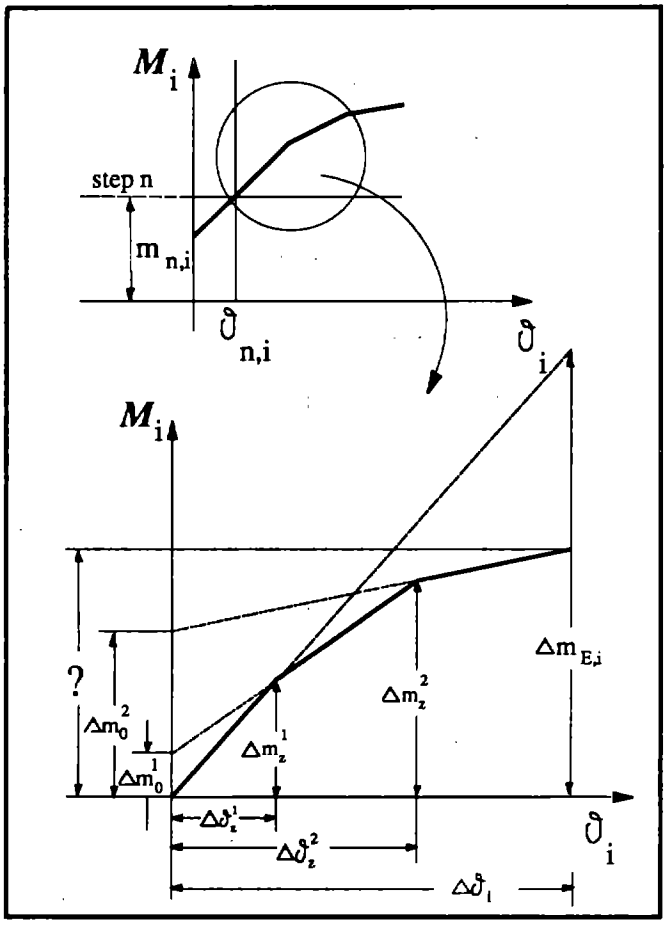

Fig. 3.7 ***Determination of initial moments at end i of the spread plasticity element (change in plastic zone length)***

$$z_a = \begin{Bmatrix} z_{a,i} \\ z_{a,j} \end{Bmatrix}$$

Given the external moment increments $(\Delta m_E)_{pl}$ the resulting shear increment ΔV can be determined

$$\Delta V = \frac{(\Delta m_{E,i} + \Delta m_{E,j})_{pl}}{L} \tag{3.14}$$

Thus the new theoretical plastic zone lengths z_c can be determined from

$$z_{c,i} = \frac{(m_{n,i} + \Delta m_{E,i})_{pl} - M_{y,i}}{V_n + \Delta V} \tag{3.15a}$$

$$z_{c,j} = \frac{(m_{n,j} + \Delta m_{E,j})_{pl} - M_{y,j}}{V_n + \Delta V} \tag{3.15b}$$

where M_y is the section yield moment (positive or negative), $\boldsymbol{m}_n$ is the vector of end moments of the beam subelement at the end of the previous load step and V_n is given by

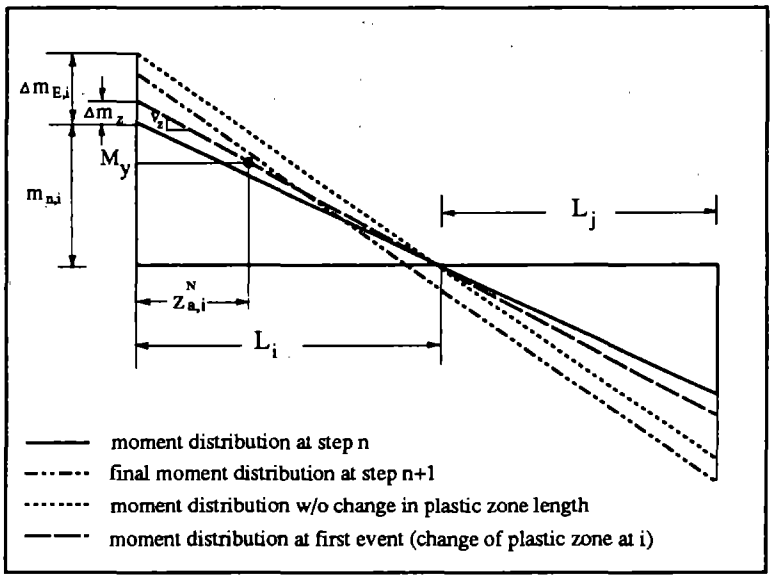

Fig. 3.8 ***Moment distributions in spread plasticity element during a given load step***

$$V_n = \frac{(m_{n,i} + m_{n,j})_{pl}}{L} \tag{3.16}$$

The theoretical plastic zone lengths z_c are compared against those at the end of the previous step z_a. If both plastic zone lengths in vector z_c are smaller than those in vector z_a, then no change in plastic zone length has taken place. If an increase in plastic zone length at one or both ends of the beam subelement is detected during the comparison of z_c with z_a, then the corresponding plastic zone length is updated to a new value z_a^N by adding a finite length increment z_d to the plastic zone value z_a at the end of the previous load step (Figs. 3.6 and 3.8)

$$z^N_{a,i} = z_{a,i} + z_d \qquad \text{if} \qquad z_{c,i} > z_{a,i}$$

$$z^N_{a,j} = z_{a,j} + z_d \qquad \text{if} \qquad z_{c,j} > z_{a,j}$$

If the plastic zones at both ends of the beam subelement extend during a load step, we need to establish which is going to do so first. This is the concept behind the event-to-event method. To do so we make use of the fact that the stiffness of the spread plastic subelement does not change until one of the plastic zones extends. Thus the point of inflection of the moment diagram does not change between the beginning of the load step and the instant when one of the plastic zones first extends. Using this fact we can establish which zone is going to spread first by calculating the moment distribution at the stage when this event takes place (Fig. 3.8). If we assume that the plastic zone length at end i will spread first, then the shear force corresponding to a discrete increment of the plastic zone by z_d is

$$V_i^* = \frac{M_{y,i}}{L_i - z_{a,i}^N} \tag{3.18a}$$

where L_i is the distance of the point of inflection from end i (Fig. 3.8). This is calculated using the current end moment values (Fig. 3.8)

$$L_i = \frac{m_{n,i} + \Delta m_{E,i}}{m_{n,i} + \Delta m_{E,i} + m_{n,j} + \Delta m_{E,j}} \cdot L$$

If, on the other hand, the plastic zone length at end j spreads out first by the discrete increment z_d, then the corresponding shear force is

$$V_j^* = \frac{M_{y,j}}{L_j - z_{a,j}^N} \tag{3.18c}$$

where L_j is the distance of the point of inflection from end j given by

$$L_j = \frac{m_{n,j} + \Delta m_{E,j}}{m_{n,i} + \Delta m_{E,i} + m_{n,j} + \Delta m_{E,j}} \cdot L$$

If the plastic zones at both ends of the beam subelement extend during a load step, then a comparison of the shear force values from Eqs. (3.18a) and (3.18c) establishes which event will take place first. The event to take place first is obviously associated with the smaller shear force value from Eqs. (3.18a) and (3.18c). This value is denoted by V_z.

Making use of the fact that the inflection point does not change until the first event takes place, also permits the determination of the moment and corresponding rotation increments at the ends of the element when the event occurs (Figs. 3.7 and 3.8)

$$\Delta \boldsymbol{m}_z = \begin{Bmatrix} V_z \cdot L_i \\ V_z \cdot L_j \end{Bmatrix} - \begin{Bmatrix} m_{n,i} \\ m_{n,j} \end{Bmatrix} \tag{3.19}$$

$$\Delta\theta_z = [\boldsymbol{f}]_{pl} \cdot \Delta \boldsymbol{m}_z \tag{3.20}$$

At this point the flexibility matrix of the spread plastic beam subelement is updated to account for the new plastic zone length. Since the flexibility matrix changes, Eq. (3.20) no longer holds. Instead, it has to be modified by introducing initial moments $(\Delta \boldsymbol{m}_0)_{pl}$ at the ends of the beam subelement as follows (Fig. 3.7)

$$\Delta\theta_z = [\boldsymbol{f}_u]_{pl} \cdot \{\Delta \boldsymbol{m}_z - \Delta \boldsymbol{m}_0\}_{pl} \tag{3.21a}$$

Eq. (3.21a) can be solved for the initial moments resulting in

$$(\Delta \boldsymbol{m}_0)_{pl} = \Delta \boldsymbol{m}_z - [\boldsymbol{k}_u]_{pl} \cdot \Delta\theta_z \tag{3.21b}$$

The outlined event-to-event procedure culminating in Eq. (3.21b) thus allows the determination of the initial moments at the ends of the spread plastic subelement, if a change of plastic zone length at one or both ends of the beam subelement takes place during the load step. The process is presented for one event only. Since the change of the plastic zone length at one end results in a change in the element flexibility matrix and an unbalance between external and internal end moments, a new iteration needs to be performed until no events are detected during an iteration. This entire process is presented in a summary form at the end of this chapter.

It is important to stress the difference between Eqs. (3.12a) and (3.21b). In the first case no change in plastic zone length takes place. Only the average section stiffness at one or both plastic zones of the element changes. In this case the internal resisting moments $(\Delta \boldsymbol{m}_R)_{pl}$ arising from the rotation increments $\Delta\theta_{pl}$ are determined by Eq. (3.9b) and are then used in calculating the initial moments. In the second case the internal resisting moments $\Delta \boldsymbol{m}_z$ *at the instant that the plastic zone at one end of the beam extends* are determined. These along with the corresponding end rotations are then used to determine the initial moments at the ends of the beam subelement.

Once the initial moments at the ends of all subelements in series are determined the initial moments at the ends of the girder superelement are established from the following relation

$$\Delta \boldsymbol{M}_0 = [\boldsymbol{K}]_g \cdot \{ [\boldsymbol{f}_u]_{pl} \cdot (\Delta \boldsymbol{m}_0)_{pl} + [\boldsymbol{f}_u]_{jnt} \cdot (\Delta \boldsymbol{m}_0)_{jnt} \} \tag{3.22}$$

Eq. (3.22) is derived in Appendix A.

The initial moments at the ends of the superelement are finally transformed to the global coordinate system using the transformation matrix [a].

$$\Delta R_0 = [a]^T \cdot \Delta M_0 \tag{3.23}$$

Eq. (3.23) gives the vector of initial load increments at the end of the first iteration (Fig. 3.2). These are then subtracted from the vector of external load increments $(\Delta R_E)_n$ according to Eq. (3.5) and the process is restarted by applying anew Eqs. (3.6)-(3.23) until the difference between internal resisting and applied moments at the ends of all subelements is smaller than a specified tolerance. It should be noted that Eqs. (3.9) and (3.13) have to be modified in the second iteration to include the initial end moments from the previous iteration (Fig. 3.7).

A complete description of the iterative process during a particular load step is given in the following algorithm summary with the help of iteration indices.

3.4 Summary of nonlinear analysis algorithm

For each load step

Step (1) Form the tangent flexibility matrix of all subelements which are the constituents of the girder superelements in the structure$[f]_{el}$, $[f]_{pl}$, $[f]_{jnt}$

Form the tangent stiffness of column $[K]_c$ and foundation elements $[K]_f$

Step (2) For all superelements in the structure add the flexibility matrices of the subelements to obtain the flexibility matrix of the girder superelement in local coordinates:

$$[F]_g = [f]_{el} + [f]_{pl} + [f]_{jnt}$$

Step (3) Invert the tangent flexibility matrix of each superelement to obtain the tangent stiffness matrix:

$$[K]_g = [F]_g^{-1}$$

Step (4) Transform the stiffness matrix of all structural elements to global coordinates, e.g. for girder superelements:

$$[K]_b = [a]^T \cdot [K]_g \cdot [a]$$

Step (5) Assemble the stiffness matrix of all elements into the tangent stiffness matrix of the whole structure (direct stiffness method) including the linear geometric matrix of column elements:

$$[K]_T = \Sigma\,[K]_b + [K]_c + [K]_G + [K]_f$$

Step (6) Given the vector of applied load increments $(\Delta R_E)_n$ solve for the displacement increments $\Delta\bar{r}_n$ relative to the converged solution at the previous load step n:

$$[K_T]^k \cdot \Delta\bar{r}_n^k = (\Delta R_E)_n - (\Delta R_0)^{k-1}$$

where k is the iteration index, $\Delta\bar{r}_n^k = (r_{n+1}^k - r_n)$ and $(\Delta R_0)^{k-1} = 0$ when k=1 (first iteration).

Step (7) From the global deformation increments Δr_m^k of each element calculate the local rotation increments $\Delta\Theta$:

$$\Delta\Theta^k = [a] \cdot \Delta r_m^k$$

Step (8) Calculate the moment increments at the ends of each superelement:

$\Delta M_E^k = [K]_g^k \cdot \Delta\Theta^k + \Delta M_0^{k-1}$ where $\Delta M_0^{k-1} = 0$ for k=1 (first iteration).

Step (9) Since all subelements are in series

$$\Delta M_E^k = (\Delta m_E)_{el}^k = (\Delta m_E)_{pl}^k = (\Delta m_E)_{jnt}^k$$

Step (10) Calculate the rotation increments at the ends of each subelement:

$$\Delta\theta_{el}^k = [f]_{el}^k \cdot (\Delta m_E)_{el}$$

$$\Delta\theta_{pl}^k = [f]_{pl}^k \cdot (\Delta m_E^k - \Delta m_0^{k-1})_{pl}$$

$$\Delta\theta_{jnt}^k = [f]_{jnt}^k \cdot (\Delta m_E - \Delta m_0^{k-1})_{jnt}$$

In the case of the spread plastic subelement calculate the curvature increments at the end sections:

$$\Delta\phi_i^k = \frac{(\Delta m_{E,i} - \Delta m_{0,i}^{k-1})_{pl}}{c_i^k \cdot EI}$$

$$\Delta\phi_j^k = \frac{(\Delta m_{E,j} - \Delta m_{0,j}^{k-1})_{pl}}{c_j^k \cdot EI}$$

where $\Delta m_0^{k-1} = 0$ for $k = 1$ (first iteration).

Step (11) Update the current end rotations/end curvatures and determine the internal resisting moments from the hysteretic moment-rotation/ moment-curvature relations:

$$(\theta_{n+1}^k)_{pl} = (\theta_n)_{pl} + \Delta\theta_{pl}^k \quad \rightarrow \quad (m_R^k)_{pl}$$

$$(\theta_{n+1}^k)_{jnt} = (\theta_n)_{jnt} + \Delta\theta_{jnt}^k \quad \rightarrow \quad (m_R^k)_{jnt}$$

$$(\phi_{n+1}^k) = (\phi_n) + \Delta\phi^k \quad \rightarrow \quad (m_R^k)_{pl}$$

The first relation applies to the concentrated plastic and the last to the spread plastic subelement. The calculation of internal resisting moments takes place at each end of the subelement independently.

Step (12) Calculate the increment of internal resisting moments and the moment unbalance between internal and external moment increments, if any

$$(\Delta m_R^k)_{pl} = \left\{ m_R^k - (m_R)_n \right\}_{pl} \quad \rightarrow \quad (\Delta m_U^k)_{pl} = (\Delta m_E^k - \Delta m_R^k)_{pl}$$

$$(\Delta m_R^k)_{jnt} = \left\{ m_R^k - (m_R)_n \right\}_{jnt} \quad \rightarrow \quad (\Delta m_U^k)_{jnt} = (\Delta m_E^k - \Delta m_R^k)_{jnt}$$

If the euklidean norm of Δm_U exceeds a prespecified tolerance then the flexibility matrix of the corresponding subelement is updated.

Step (13) For the spread plastic subelement calculate the new theoretical length of the plastic zones

$$z_{c,i}^k = \frac{(m_{n,i} + \Delta m_{E,i}^k)_{pl} - M_{y,i}}{V_n + \Delta V^k} \qquad \text{and} \qquad z_{c,j}^k = \frac{(m_{n,j} + \Delta m_{E,j}^k)_{pl} - M_{y,j}}{V_n + \Delta V^k}$$

where

$$V_n = \frac{(m_{n,i} + m_{n,j})_{pl}}{L} \qquad \text{and} \qquad \Delta V^k = \frac{(\Delta m_{E,i}^k + \Delta m_{E,j}^k)_{pl}}{L}$$

Compare the theoretical plastic zone lengths against the previous values and update these by a finite increment z_d, if necessary

$$z_{a,i}^N = z_{a,i} + z_d \qquad \text{if} \qquad z_{c,i} > z_{a,i}$$

$$z_{a,j}^N = z_{a,j} + z_d \qquad \text{if} \qquad z_{c,j} > z_{a,j}$$

where $z_d = 0.025 \cdot L$.

If a change in plastic zone length takes place at one or both ends of the spread plastic subelement, determine the end moment and the corresponding end rotation increments when the first event of a change in the plastic zone length is about to take place

$$\Delta m_z^k = \begin{Bmatrix} V_z^k \cdot L_i^k \\ V_z^k \cdot L_j^k \end{Bmatrix} - \begin{Bmatrix} m_{n,i} \\ m_{n,j} \end{Bmatrix} \qquad \text{and} \qquad \Delta\theta_z^k = [f]^k \cdot \Delta m_z^k$$

where

$$V_z^k = \min\left[(V_i^*)^k, (V_j^*)^k \right] = \min\left[\frac{M_{y,i}}{L_i^k - z_{a,i}}, \frac{M_{y,j}}{L_j^k - z_{a,j}} \right]$$

$$L_i^k = \frac{m_{n,i} + \Delta m_{E,i}^k}{m_{n,i} + \Delta m_{E,i}^k + m_{n,j} + \Delta m_{E,j}^k} \cdot L \qquad L_j^k = \frac{m_{n,j} + \Delta m_{E,j}^k}{m_{n,i} + \Delta m_{E,i}^k + m_{n,j} + \Delta m_{E,j}^k} \cdot L$$

Update the flexibility matrix of the spread plastic subelement to account for the extension of the plastic zone that takes place first.

Step (14) Invert the updated subelement flexibility matrices to obtain the corresponding stiffness matrices. Calculate the initial moments at the ends of each subelement

$$(\Delta m_0)_{pl}^k = (\Delta m_R)_{pl}^k - [k]_{pl}^{k+1} \cdot \Delta\theta_{pl}^k$$

$$(\Delta m_0)_{jnt}^k = (\Delta m_R)_{jnt}^k - [k]_{jnt}^{k+1} \cdot \Delta\theta_{jnt}^k$$

$$(\Delta m_0)_{pl}^k = \Delta m_z^k - [k]_{pl}^{k+1} \cdot \Delta\theta_z^k$$

The last equation only applies to the spread plastic subelement.

Step (15) Calculate the initial moments at the ends of all superelements

$$\Delta M_0^k = [K]_g^{k+1} \cdot \left\{ [f]_{pl}^{k+1} \cdot (\Delta m_0)_{pl}^k + [f]_{jnt}^{k+1} \cdot (\Delta m_0)_{jnt}^k \right\}$$

Step (16) Calculate the initial load vector

$$\Delta R_0^k = [a]^T \cdot \Delta M_0^k$$

go back to **Step 4**, set $k = k+1$ and $k-1 = k$ and continue until no unbalanced moments occur in **Step 12**.

CHAPTER 4

ANALYTICAL STUDIES OF NONLINEAR RESPONSE TO CYCLIC LOADS

4.1 Introduction

The nonlinear models and the analytical procedures presented in the previous chapters were implemented in a special purpose program which determines the nonlinear static response of reinforced concrete frames to cyclic alternating lateral loads. The program can also calculate the dynamic response of these structures to earthquake excitations. The present study focuses on analytical studies of static response, while the dynamic response studies will be presented in a following study.

To establish the validity of the proposed girder and beam-column joint models as well as the accuracy of the analytical procedures for calculating the nonlinear response of frame structures to cyclic static loads, the program was used in the simulation of the behavior of beam-column sub-assemblages for which experimental data were available. Two particular beam-column specimens were selected. These were cruciform shaped interior beam-column subassemblages subjected to a large number of cyclic deformation reversals. The first was designed and tested by Soleimani et. al. [SOL79-1] according to state-of-the-art concepts of earthquake resistant design, while the second was designed by Beckingsale [BEC80-1] to satisfy the requirements of the New Zealand Code of Practice [NZS82-1]. Because both specimens were designed according to the strong column-weak girder design philosophy, inelastic deformations were concentrated at the ends of the girders and the beam-column joint. The columns did not reach yielding and only exhibited minor cracking. Another important criterion for the selection of the specimens was the fact that the joints were designed so as to minimize the effects of shear transfer. As a result, shear cracking was limited and panel zone shear deformations were negligible. Thus data from both experimental studies were ideally suited to establish the validity of the proposed girder and beam-column joint models.

4.2 Beam-column subassemblages with a single joint

4.2.1 Beam-column subassemblage of Soleimani

The beam-column subassemblage designed and tested by Soleimani et. al. [SOL79-1] was a half scale model of a cruciform shaped portion from the third story of a twenty story, four bay ductile moment-resisting frame (Fig. 4.1). In the original report [SOL79-1] it is designated as specimen BC3.

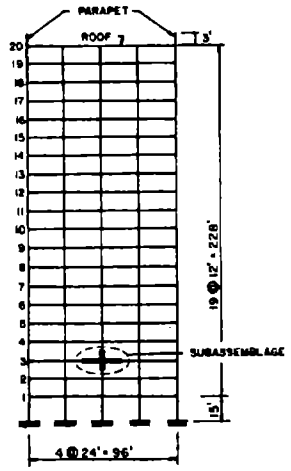

Fig. 4.1

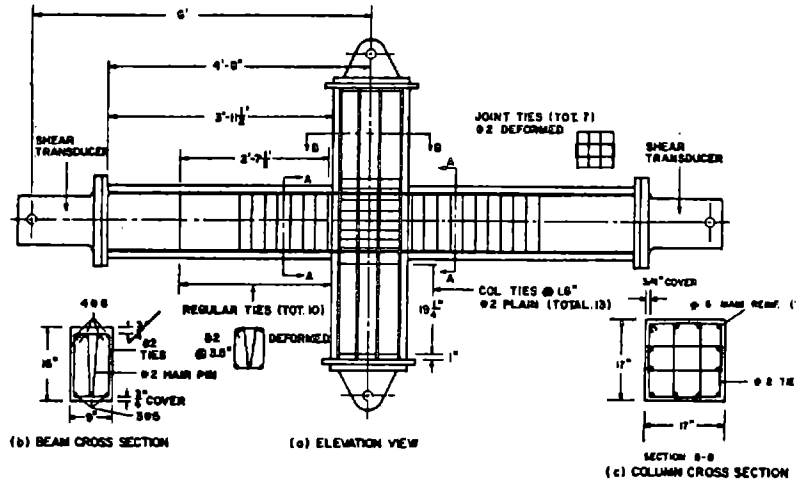

Fig. 4.2

Fig. 4.1 Selection of subassemblage from [VIW79-1]
Fig. 4.2 Reinforcement layout and details of beam-column subassemblage BC3 from [VIW79-1].

The frame was designed according to state-of-the-art concepts of earthquake resistant design. The design was based on the strong column-weak girder design philosophy and the joint was designed so as to minimize the effects of shear transfer. The specimen geometry and reinforcement layout are shown in Fig. 4.2. The subassemblage was subjected to constant gravity and cyclic lateral displacements of gradually increasing magnitude. The scheme of load application is shown in Fig. 4.3. The lateral displacement time history is shown in Fig. 4.4.

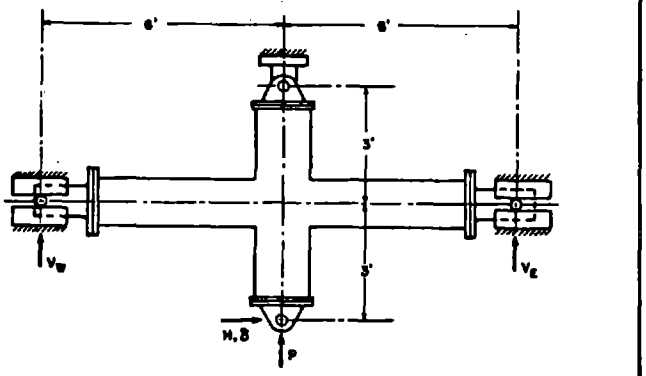

Fig. 4.3

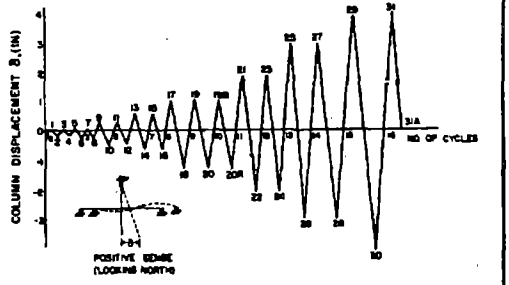

Fig. 4.4

Fig. 4.3 Scheme of load application for subassemblage BC3 from [VIW79-1]
Fig. 4.4 History of imposed lateral displacements of subassemblage BC3 from [VIW79-1]

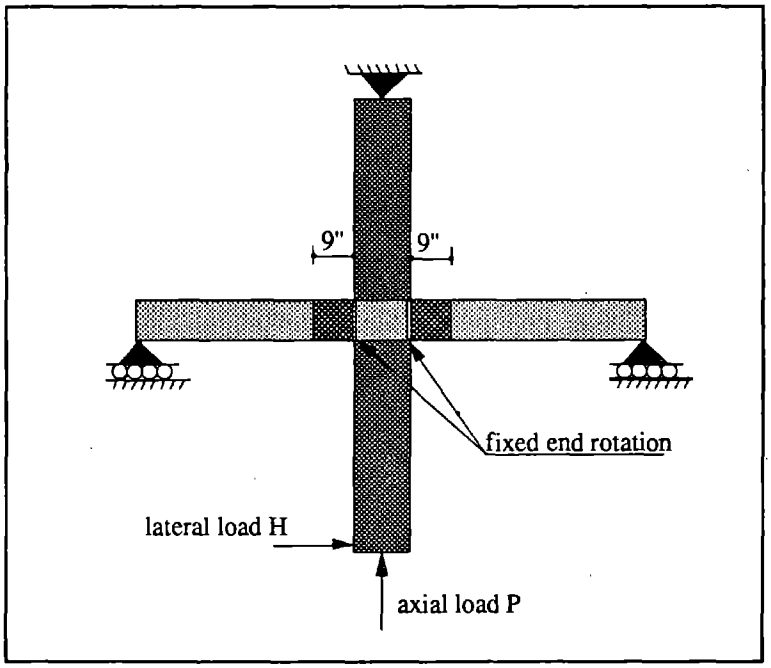

Fig. 4.5 Beam-column subassemblage BC3 tested by Soleimani

Soleimani's beam-column subassemblage was extensively instrumented. Of particular interest for the purposes of the correlations presented in this study is the fact that clip gages were used to measure the average curvature in the critical regions of the beams and columns. Each beam end zone where inelastic strains were expected to occur was subdivided into two regions. Hysteretic

moment-rotation relations were determined in each region by multiplying the measured average curvature by the length of the corresponding region. The region immediately adjacent to the beam-column joint had a length of 9", as shown in the schematic subassemblage drawing in Fig. 4.5.

The concentrated rotations which take place at the beam-column interface due to slippage of the reinforcing bars anchored in the joint were measured with eight precision linear potentiometers. Four of these potentiometers were rigidly connected to steel pins soldered to the reinforcing bars adjacent to the beam-column interface. These were used to measure the slippage of reinforcing bars. Four additional potentiometers mounted on steel rods which were encased in the concrete next to the beam-column interface were used to measure the size of cracks forming at the beam-column interface. These extensive measurements allowed the determination of the concentrated rotations (fixed-end rotations) at the beam-column interface of the subassemblage.

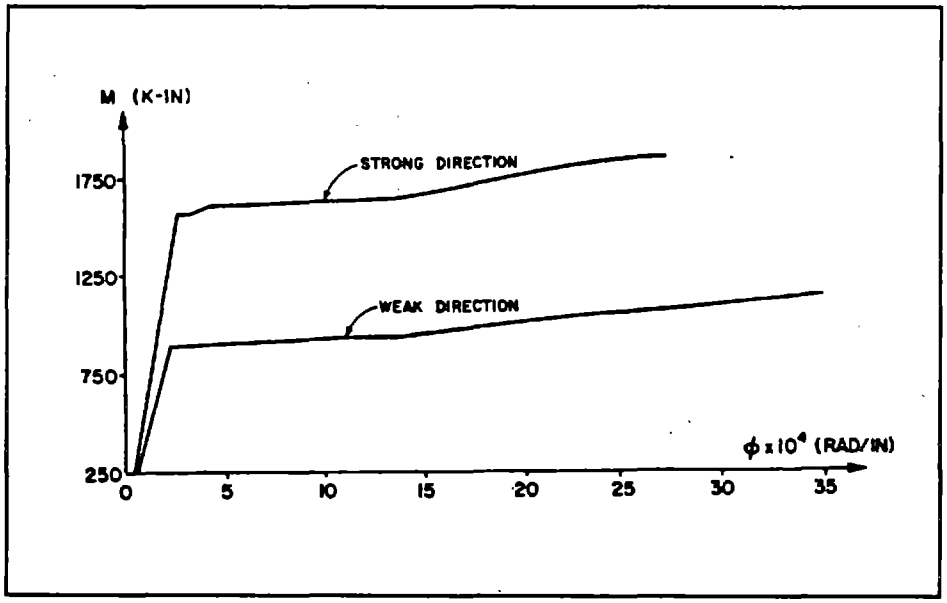

Fig. 4.6 Analytical moment-curvature relation in girder inelastic region from [VIW79-1]

The model used in the analytical studies consists of two girder superelements, two column elements and some fictitious elements to allow the computer program to simulate the test configuration and conditions. The girder superelements are each made up of an elastic, a spread plastic and a joint subelement.

The derivation of the properties of the girder and beam-column elements is based on the material properties measured in [SOL79-1]. Using the stress-strain relation of reinforcing steel and concrete, the section geometry and the reinforcement layout in the girder end region the monotonic

moment-curvature relation of a typical section is established using well-known principles of reinforced concrete analysis. The two curves depicted in Fig. 4.6 correspond to a negative bending moment inducing tension in the top reinforcement (strong-direction) and a positive bending moment leading to tension in the bottom reinforcement (weak-direction). The values which are extracted from the curves in Fig. 4.6 are summarized in Table 4.1.

Table 4.1

GIRDER MOMENT-CURVATURE RELATION

		yield moment [k-in]	initial stiffness [10^3 k-in^2 /rad]
positive M	west	880	3920
	east	880	3920
negative M	west	1570	5780
	east	1570	5780

The derivation of the flexural strength and stiffness properties of the girder superelement is based on a bilinear approximation of the moment-curvature relations in Fig. 4.6. The stiffness of the elastic subelement is determined as the average of the pre-yield stiffness of the moment-curvature relations in the strong and weak direction, since the spread plastic subelement is based on a single pre-yield stiffness. The post-yield stiffness of the beam subelement, on the other hand, can have different values in the two directions of bending. Even though the two curves in Fig. 4.6 exhibit different post-yield stiffness values, the strain hardening ratio which expresses the ratio of each of these values and the pre-yield stiffness of the element turned out to be equal to 0.016 for both directions of bending.

The properties of the beam-column joint element are determined using the joint finite element model proposed by Filippou in [FIL83-3]. The analytically predicted monotonic moment-rotation relation at the beam-column joint interface of specimen BC3 is shown in Fig. 4.7 [FIL83-2]. Two different envelopes correspond to positive and negative bending moments at the beam-column interface. The bilinear approximations to each cyclic envelope curve yield the values summarized in Table 4.2.

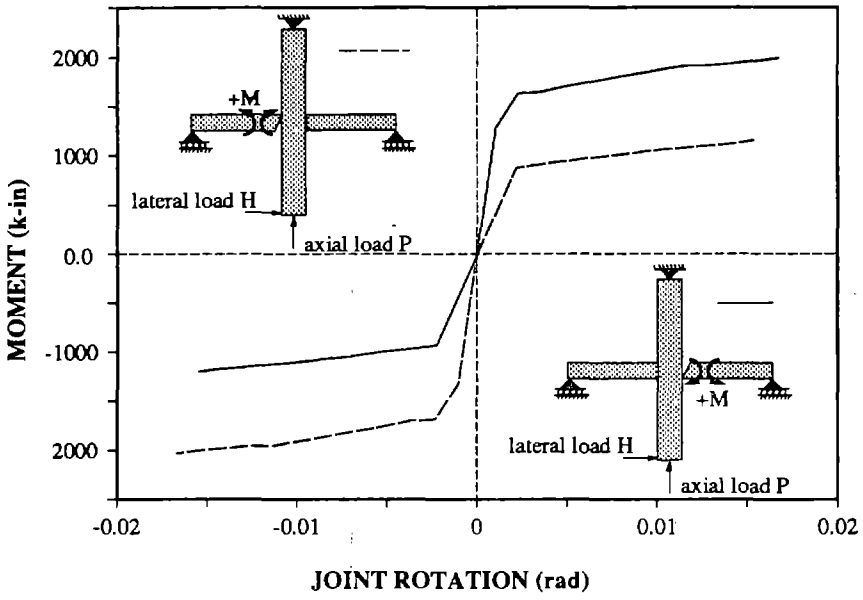

Fig. 4.7 Monotonic moment-rotation relation of beam-column joint

Table 4.2			
JOINT MOMENT-ROTATION RELATION			
		initial stiffness [10^3 k-in /rad]	strain hardening ratio
positive M	west	409	0.050
	east	409	0.050
negative M	west	730	0.034
	east	730	0.034

The analytical predictions of the frame model described above and subjected to the load history in Fig. 4.4 are shown in Figs. 4.8-4.11. Fig. 4.8 shows the load-displacement relation measured at the bottom of the column in Fig. 4.5. Even though the experiment was conducted under displacement controlled conditions, as is commonly the case for obvious reasons, the analysis was performed by specifying the magnitude of the lateral load measured at the moment of load reversal and then subdividing this load into a number of increments. There are two reasons for resorting to load controlled conditions in the analytical studies: first, in lateral-load-to-collapse analyses of multistory structures the lateral load pattern is either known or assumed. This is not the case with the lateral displacements. This fact makes a load controlled analysis more straightforward. Secondly,

slight discrepancies in the estimation of the post-yield stiffness of structural subassemblages result in considerable differences in predicted displacements under imposed load conditions. Thus a load controlled analysis is a much more severe test of the ability of various models to represent the post-yield stiffness of the structure.

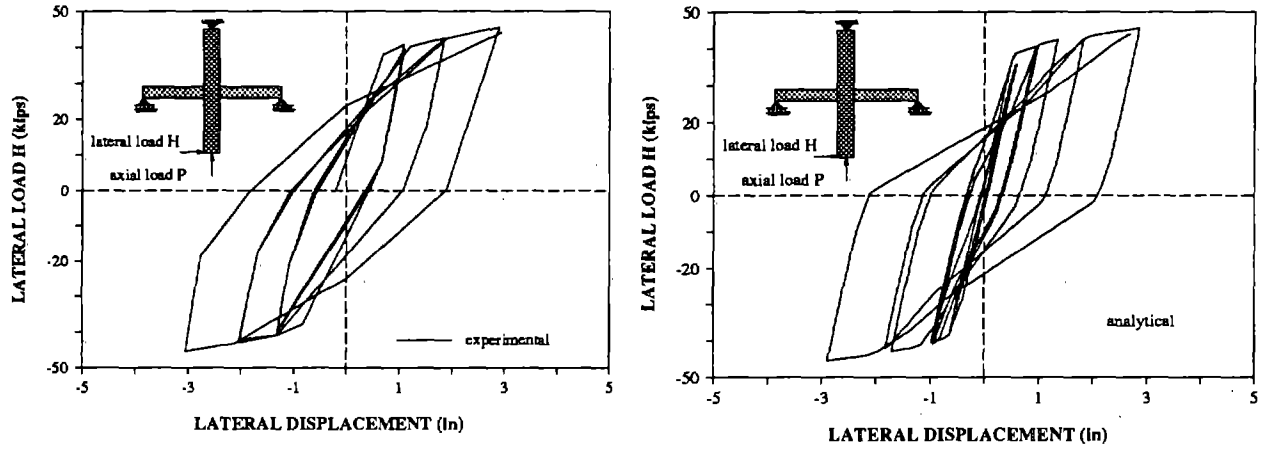

(a) *(b)*

Fig. 4.8 *Load-deformation relation of subassemblage BC3*
(a) experimental
(b) analytical

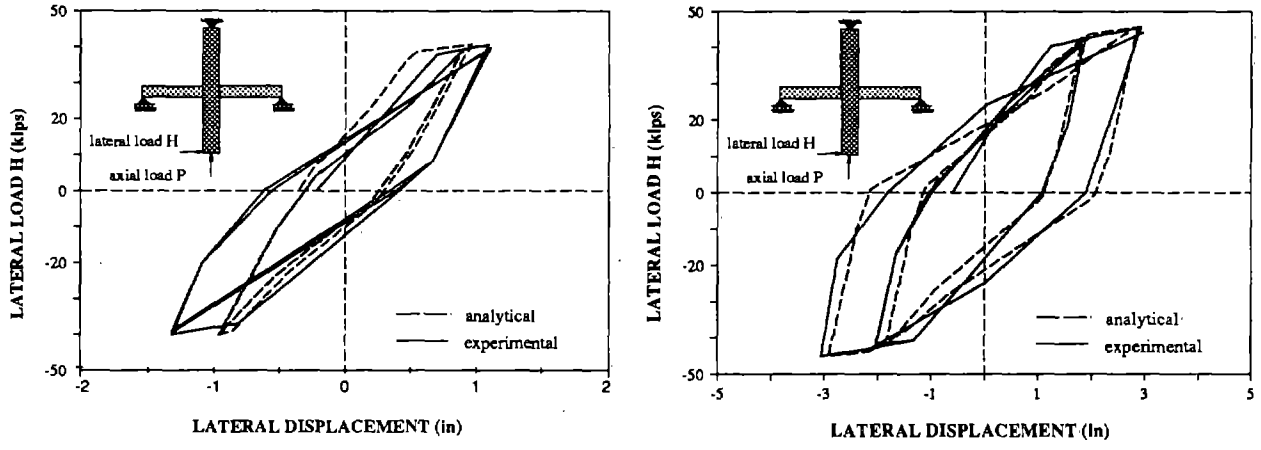

(a) *(b)*

Fig. 4.9 *Correlation of load-displacement relation of BC3*
(a) cycles with small lateral displacement
(b) cycles with large lateral displacement

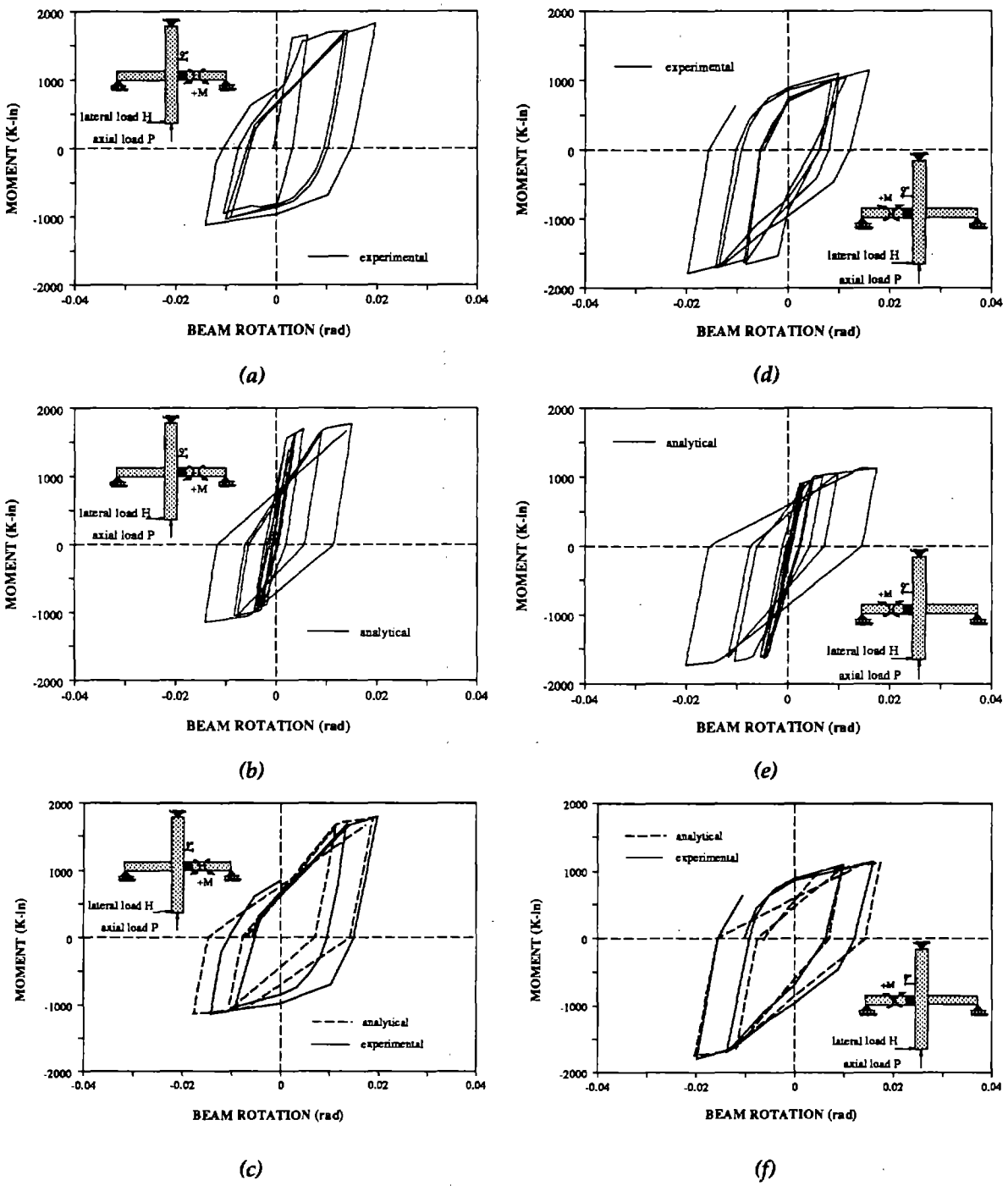

Fig. 4.10 *Moment-rotation relation in 9" girder end zones of subassemblage BC3*

(a),(d) Experimental

(b),(e) Analytical

(c),(f) Correlation of individual cycles

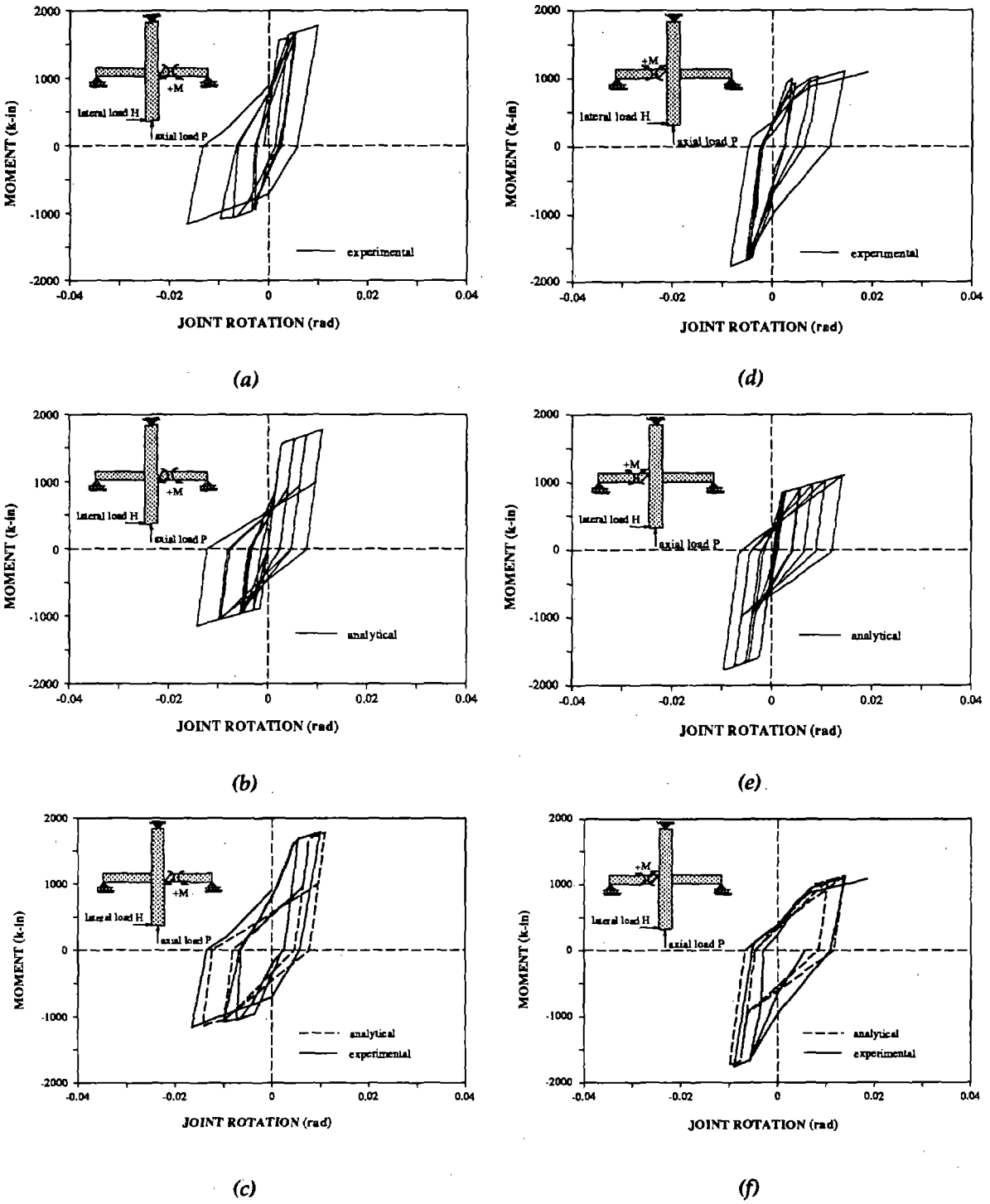

Fig. 4.11 *Moment-rotation relation at beam-column interfaces of subassemblage BC3*
(a),(d) Experimental
(b),(e) Analytical
(c),(f) Correlation of individual cycles

Fig. 4.8 shows the experimental and analytical load-displacement relation of subassemblage BC3 for the entire loading history. To facilitate the comparison between experimental and analytical results individual cycles are shown in Fig. 4.9. Fig. 4.10 shows the correlation of beam rotations in a 9" zone adjacent to the column and Fig. 4.11 the fixed-end rotations at the beam column interface due to pull-out of reinforcing bars anchored in the joint. A careful study of the results in Figs. 4.8-4.11 leads to the following observations:

(1) Excellent agreement between analytical and experimental results is found, particularly, if account is taken of the fact that the subassemblage is subjected to load-controlled loading conditions. This excellent agreement is not only limited to the global load-displacement response, but is also seen in the local rotations of the different critical regions of the subassemblage.

(2) The analytical model is capable of correctly representing the strength and stiffness of the subassemblage. This is of particular importance in the case of the post-yield stiffness where slight discrepancies can lead to large deviations between observed and predicted lateral displacements.

(3) The analytical model follows the hysteretic behavior of the critical regions of the subassemblage with satisfactory accuracy. Thus the energy dissipated in each critical region is predicted well. During reloading cycles with the same displacement ductility slight discrepancies in the moment-rotation relation of the girder inelastic regions are observed. These are caused by inaccuracies in the reloading stiffness of the beam model.

(4) The analytical model of the girder inelastic region shows a stiffer unloading slope than observed in the experimental results (Fig. 4.10). This results in a stiffer unloading slope of the entire subassemblage. This discrepancy in the unloading stiffness of Clough's hysteretic model has already been pointed out by Saiidi in [SAI82-1]. There is, however, as yet no rational model for predicting the unloading stiffness of inelastic girder regions.

(5) The correlation of analytical and experimental results of girder rotations shows considerable differences in the two directions of loading. When the girder end moments cause compression in the top reinforcing layer (bending in the weak direction) the cracks in the inelastic region do not close. This happens because of the unequal amount of top and bottom reinforcement. The applied moment is then resisted by a force couple in the top and bottom reinforcing steel. In this case the moment-rotation relation closely follows the stress-strain relation of reinforcement and Clough's hysteretic model underestimates the reloading stiffness under small moments. As can be seen in Fig. 4.10, an elasto-plastic reloading rule comes closer to the

actual behavior. This is not the case when the applied bending moments cause compression in the bottom steel. In this case satisfactory agreement between analysis and experiment is observed.

(6) The beam-column joint model shows excellent agreement with experimental results. No discrepancy in the reloading stiffness is observed in this case, because of the slippage of reinforcing bars through the joint.

4.2.2 Parametric studies on Soleimani's subassemblage

Because of the availability of extensive experimental measurements of the response of sub-assemblage BC3, it was selected for a detailed investigation of the effect of modeling parameters. Of considerable interest is the ability of the one-component model to predict the global and local response of the subassemblage, because of its wide-spread use in nonlinear studies to date. The accuracy of the one-component can be studied within the framework of the developed program by replacing the spread plasticity with the concentrated plasticity element.

The first question to be addressed in the case of the concentrated model is the selection of appropriate values for describing the monotonic moment-rotation relation. Particularly difficult is the selection of the post-yield stiffness of the model, as has been discussed in detail in [ANA81-1], [MAH76-1]. Typically, the monotonic moment-rotation relation of an equivalent cantilever beam having a span equal to half the span of the actual girder is used to derive the properties of the one-component model. This procedure is described in Section 1.2.2.1. Using this procedure in the case at hand results in a strain hardening ratio of 0.03. To test the sensitivity of the one-component model two additional values of the strain hardening ratio of the moment-rotation relation are used in this study. The first value was established by trial and error so as to give the best possible correlation with the experimental load-displacement relation of subassemblage BC3. This value of the strain hardening ratio is equal to 0.039. Finally, a strain hardening ratio equal to that of the moment-curvature relation was used as a lower bound. Previous studies [ANA81-1], [MAH76-1] have pointed out that setting the ratio of the moment-curvature relation equal to that of the moment-rotation relation results in a considerable underestimation of post-yield stiffness.

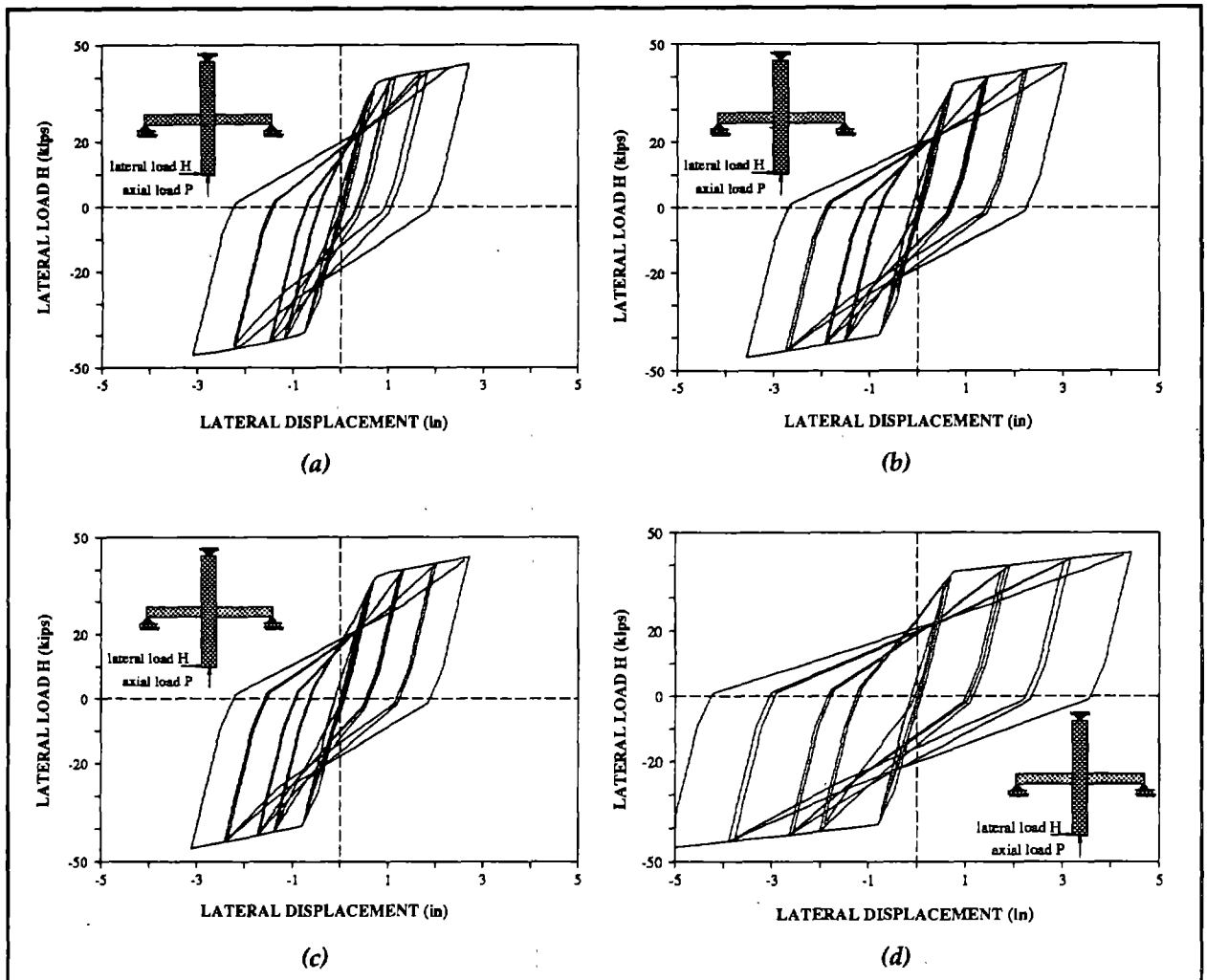

Fig. 4.12 ***Load displacement relation of subassemblage BC3.***
(a) Spread plasticity model
(b) Concentrated plasticity model. Strain hardening ratio = 0.03
(c) Concentrated plasticity model. Strain hardening ratio = 0.039
(d) Concentrated plasticity model. Strain hardening ratio = 0.016

The results of the parametric studies on Soleimani's subassemblage are presented in Figs. 4.12-4.16. Fig. 4.12 shows the lateral load-displacement relation of subassemblage BC3. Figs. 4.13 and 4.14 show the moment-rotation relation in the girders. It is to be noted that Figs. 4.13 and 4.14 show the **total** girder rotation, by contrast to Fig. 4.10 which shows the girder rotation in a 9" zone adjacent to the column. Finally, Figs. 4.15 and 4.16 show the rotation at the two beam-column interfaces of subassemblage BC3. Four different cases are presented identified by corresponding letters in the figures:

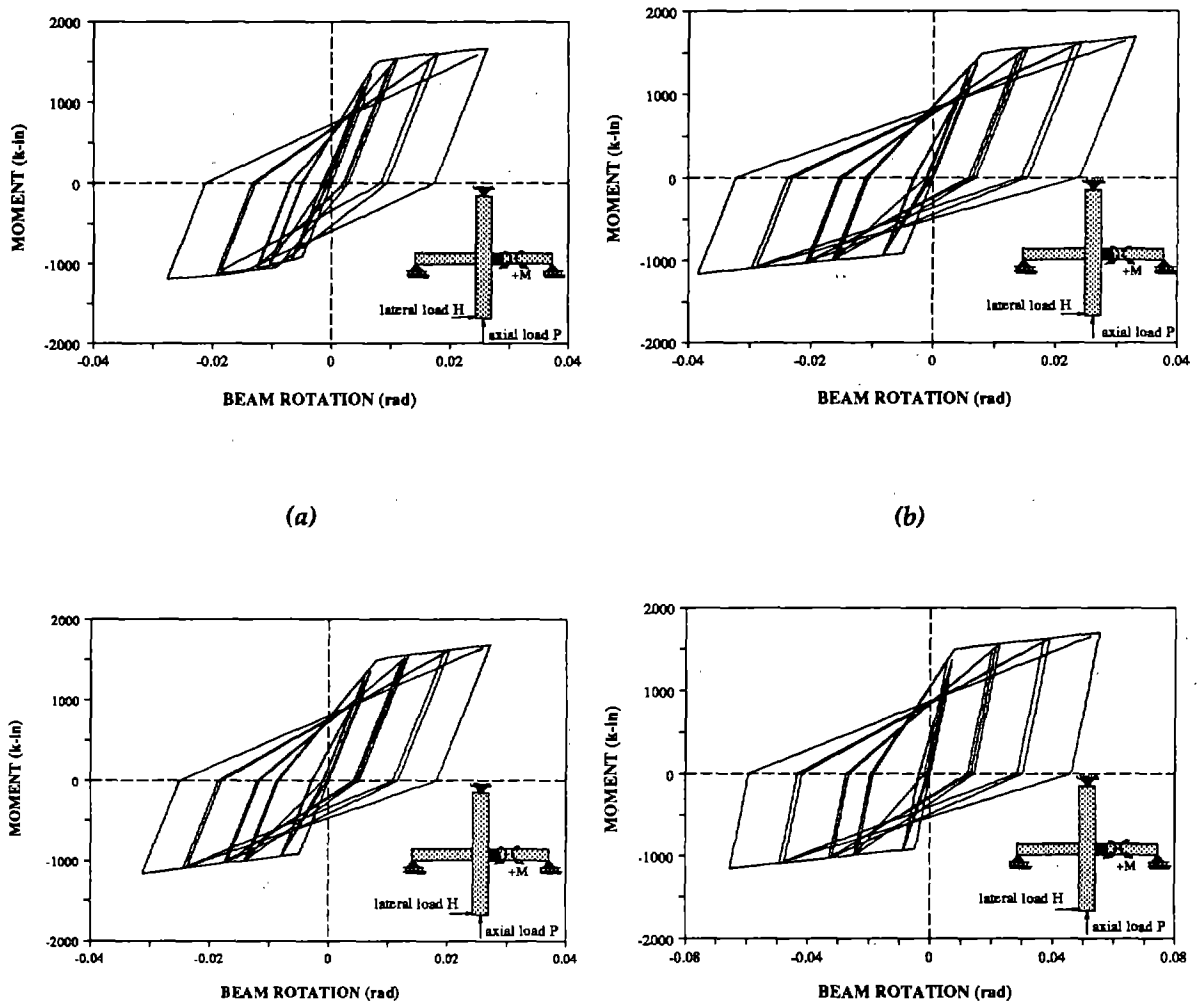

Fig. 4.13 *Girder moment-rotation relation of subassemblage BC3.*
(a) Spread plasticity model
(b) Concentrated plasticity model. Strain hardening ratio = 0.03
(c) Concentrated plasticity model. Strain hardening ratio = 0.039
(d) Concentrated plasticity model. Strain hardening ratio = 0.016

Case (a) Spread plasticity beam model using the values presented in the correlation with experimental results.

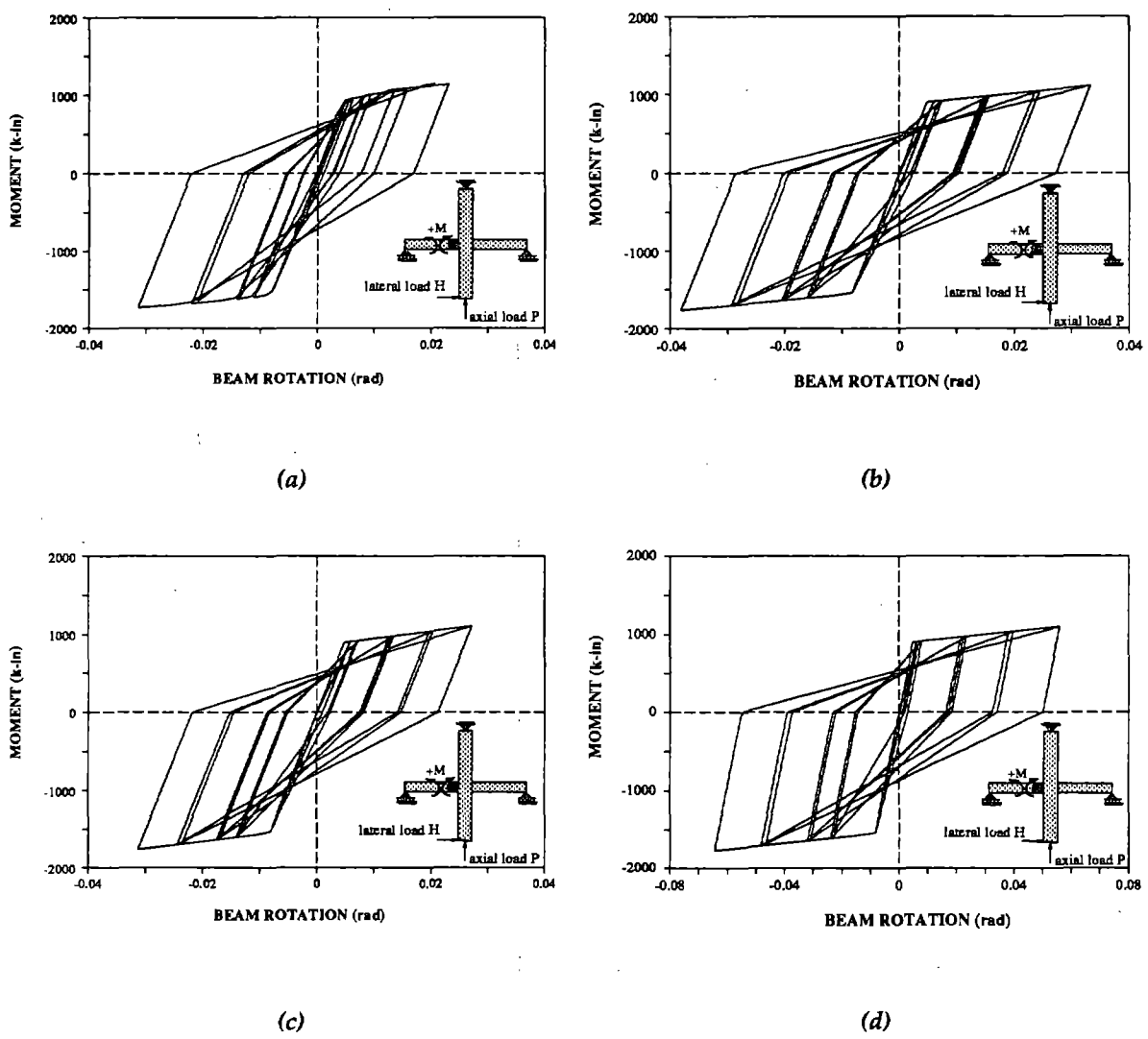

Fig. 4.14 *Girder moment-rotation relation of subassemblage BC3.*
(a) Spread plasticity model
(b) Concentrated plasticity model. Strain hardening ratio = 0.03
(c) Concentrated plasticity model. Strain hardening ratio = 0.039
(d) Concentrated plasticity model. Strain hardening ratio = 0.016

Case (b) Concentrated plasticity model with a strain hardening ratio of 0.03.

Case (c) Concentrated plasticity model with a strain hardening ratio of 0.039.

Case (d) Concentrated plasticity model with a strain hardening ratio of 0.016.

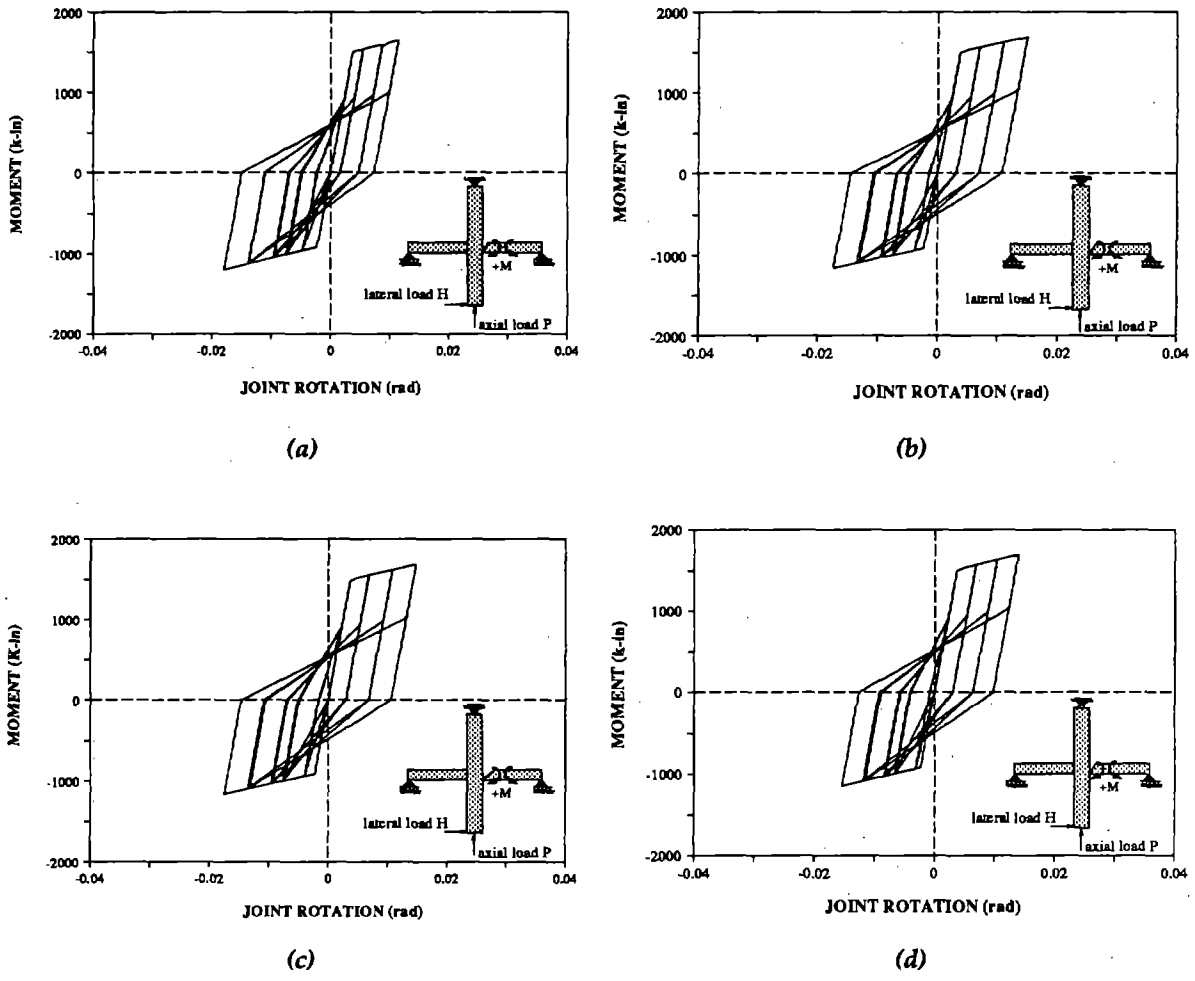

Fig. 4.15 ***Beam-column joint moment-rotation relation of subassemblage BC3.***
(a) Spread plasticity model
(b) Concentrated plasticity model. Strain hardening ratio = 0.03
(c) Concentrated plasticity model. Strain hardening ratio = 0.039
(d) Concentrated plasticity model. Strain hardening ratio = 0.016

The beam-column joint model described in the correlation with experimental results is used in all four cases. A careful study of the results in Figs. 4.12-4.16 leads to the following observations:

(1) When the strain hardening ratio of the concentrated plasticity model is selected equal to 0.039 an almost perfect correlation of the global load-displacement relation is obtained between spread plasticity and concentrated plasticity model. Even so, local rotation values in the girder critical regions do not show such an excellent match. The concentrated plasticity model overestimates the maximum local girder rotations by as much as 15% (compare Figs. 4.13a

and c and 4.14a and c). This can be basically attributed to inherent differences in the monotonic and hysteretic behavior between the spread plastic and the point hinge model. This differences will be discussed in more detail later.

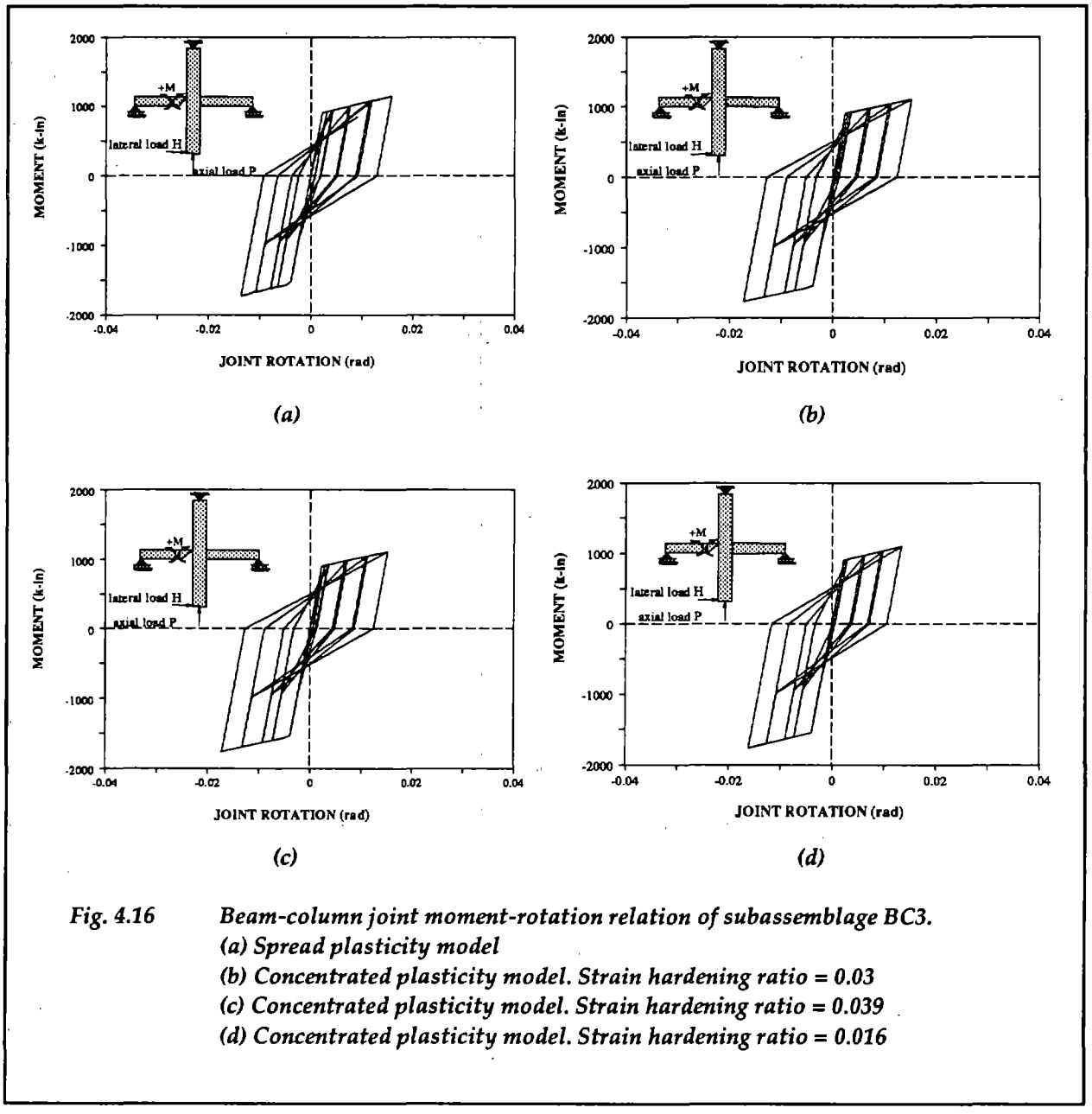

Fig. 4.16 *Beam-column joint moment-rotation relation of subassemblage BC3.*
(a) Spread plasticity model
(b) Concentrated plasticity model. Strain hardening ratio = 0.03
(c) Concentrated plasticity model. Strain hardening ratio = 0.039
(d) Concentrated plasticity model. Strain hardening ratio = 0.016

(2) The strain hardening ratio of 0.03 which is selected on the basis of the procedure described in Chapter 2 does not yield very accurate results in spite of the fact that the assumption of the point of inflection lying at girder midspan is correct in the case of a cruciform shaped subassemblage loaded as shown in Fig. 4.3. There is a small underestimation of the post-yield

stiffness of the subassemblage leading to a discrepancy in maximum lateral displacement on the order of 15-20% (compare Figs. 4.12a and b). This discrepancy is even more pronounced in the case of girder rotation values amounting to approximately 40% (compare Figs. 4.13a and b and 4.14a and c).

(3) The strain hardening ratio of 0.016, which is equal to the strain hardening ratio of the girder moment-curvature relation, leads to a considerable underestimation of post-yield stiffness. This results in an overestimation of maximum lateral displacement by as much as 50% and an overestimation of maximum girder rotation values by almost 100%. This fact has already been pointed out in [MAH76-1] and [ANA81-1].

(4) The beam-column joint behavior does not show much difference in the four cases studied. There is a slight increase in maximum fixed-end rotations between the concentrated plasticity and the spread plasticity model. This increase is almost the same for the three strain hardening ratios of the concentrated plasticity model. This happens because the joint properties are the same in the four cases and the moments at the beam-column interface do not vary much from one case to the other due to the load-controlled nature of the parametric studies. In a displacement-controlled arrangement the concentrated plasticity model leads to an underestimation of fixed-end rotations due to the increase of the relative flexibility of the girder inelastic region with respect to the beam-column joint.

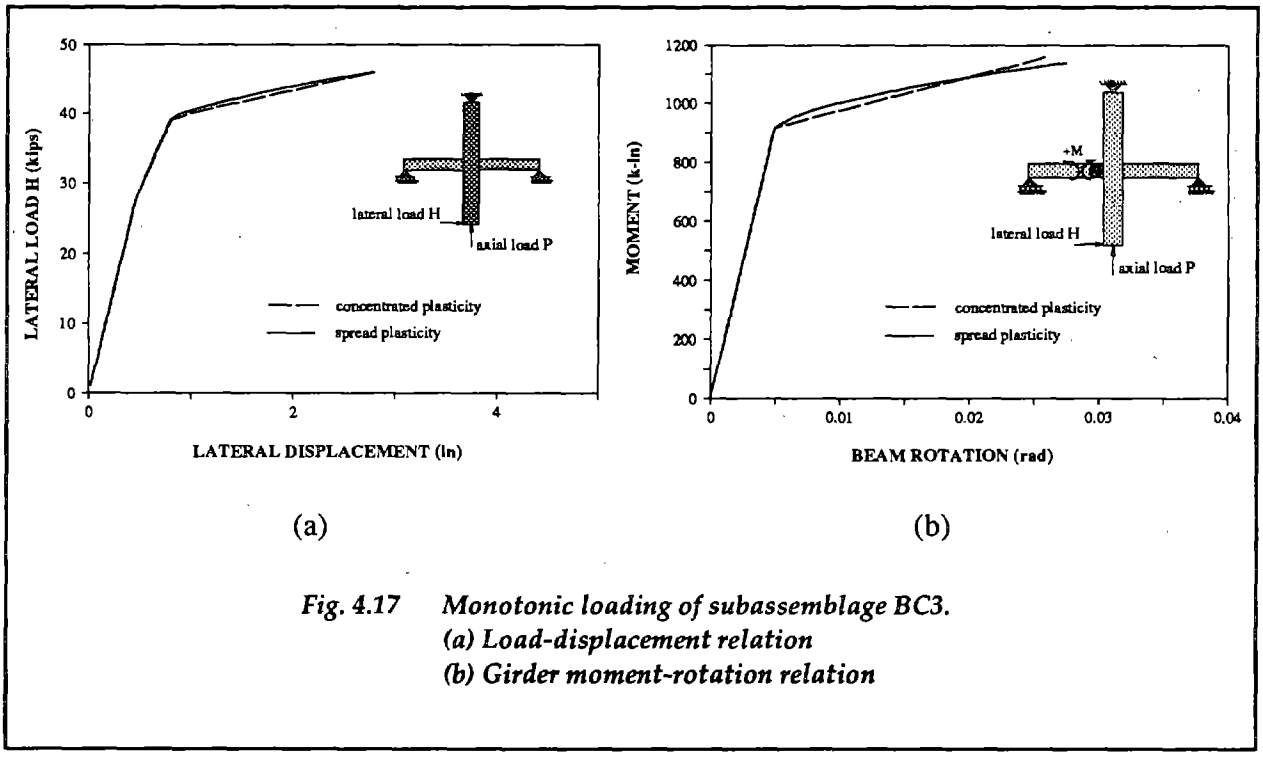

Fig. 4.17 Monotonic loading of subassemblage BC3.
(a) Load-displacement relation
(b) Girder moment-rotation relation

To shed some light on these observations it is useful to study the monotonic behavior of the subassemblage. The lateral load displacement relation is shown in Fig. 4.17a and the resulting girder moment-rotation relation is shown in Fig. 4.17b. The post-yield stiffness of the concentrated plasticity model was determined so as to match the lateral load-displacement predictions of the spread plasticity model as well as possible. The resulting strain hardening ratio is equal to 0.05 in this case. Fig. 4.17b shows well the gradual change of post-yield stiffness of the spread plasticity model, as the length of the plastic zone spreads gradually, and the inability of the concentrated plasticity model to match this behavior.

The different post-yield stiffness values of the concentrated plasticity model which are obtained under different loading conditions help explain the discrepancy of the maximum girder rotation values observed in Figs. 4.13 and 4.14. There is first the strain hardening ratio of 0.05 for which the monotonic lateral load-displacement relation of the concentrated plasticity model best matches that of the spread plasticity model. This is followed by the ratio of 0.039 which yields the best fit of the cyclic lateral load-displacement relation between spread and concentrated plasticity model. Finally, there is the ratio of 0.03 determined by the procedure in Chapter 2 which matches the maximum value of girder rotation of the spread plasticity model under a certain level of monotonic loading. These different values clearly point out the difficulty associated with the selection of appropriate parameters for the concentrated plasticity model. Most importantly, model parameters are loading dependent, as has been pointed out already in [ANA81-1]. This fact results in unreliable predictions of the global and, in particular, the local response of frame structures which are subjected to cyclic static and dynamic lateral loads, unless the loading history of the critical regions in the structure can be established a priori and the model parameters can be tuned accordingly. By contrast, the spread plasticity model relies on the moment-curvature relation of a girder section, which can be derived by well established procedures. This is a considerable advantage of the spread plasticity model over the concentrated plasticity counterpart.

An interesting feature of the hysteretic behavior of the spread plasticity model can be seen in the last cycle of Fig. 4.14a. To illustrate the point Fig. 4.18 is used which shows that the spread plasticity model does not reload towards the point of maximum previous inelastic rotation. Instead the reloading stiffness is slightly higher. This happens in spite of the fact that the moment-curvature relation at each section along the inelastic zone follows Clough's hysteretic model, which prescribes that reloading take place towards the point of maximum previous inelastic curvature. This higher reloading stiffness of beam inelastic regions has been observed in several experiments. Researchers have attempted to take this effect into account by introducing a reloading stiffness factor into the

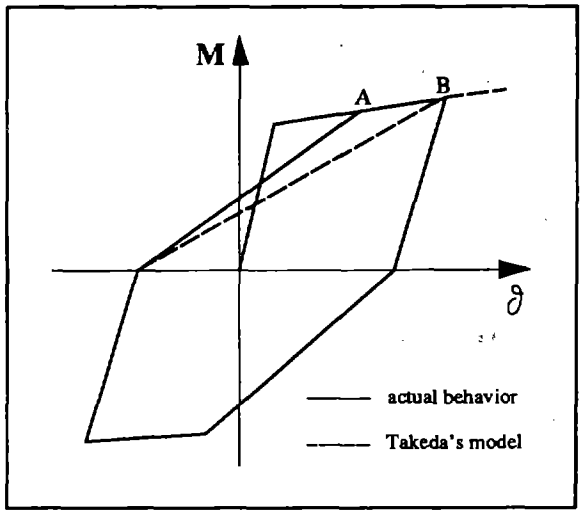

Fig. 4.18 Hysteretic behavior of spread plasticity model

one-component model [KAN73-1]. The spread plastic subelement accounts for this effect without the introduction of additional empirical factors. Fig. 4.14a shows that the spread plasticity model also exhibits a slight increase in strength during reloading.

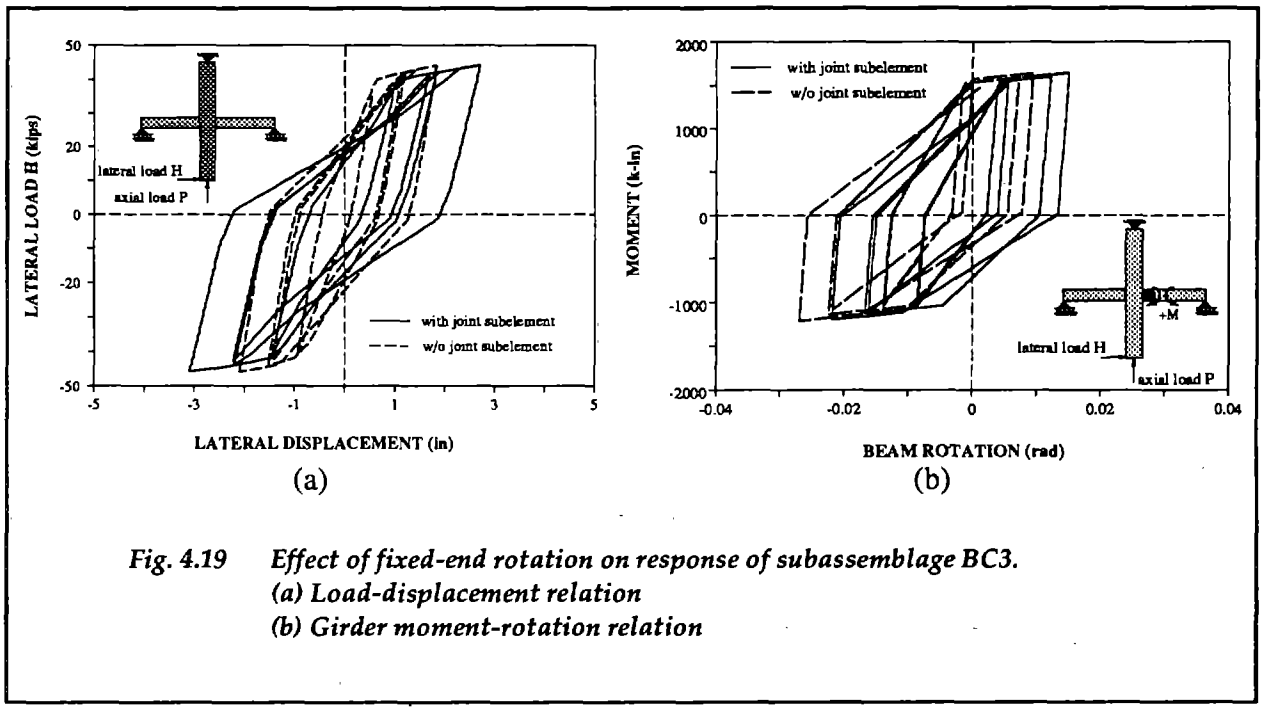

Fig. 4.19 Effect of fixed-end rotation on response of subassemblage BC3.
(a) Load-displacement relation
(b) Girder moment-rotation relation

The contribution of fixed-end rotations at the beam-column interface to the global response of the subassemblage is illustrated in Fig. 4.19a. It is clearly seen that the contribution of fixed-end rotations makes up about 50% of the lateral displacement of the subassemblage in the later cycles.

This compares well with the observations of Soleimani et. al. [SOL79-1] and several other investigators [DUR82-1]. It is interesting to note that the maximum rotation values of the girder inelastic region are not affected much by the inclusion of the beam-column joint subelement (Fig. 4.19b), because of the load-controlled arrangement adopted in the numerical testing. There is, however, a clear shift of one hysteretic relation with respect to the other. This occurs, because of an excursion into the inelastic range in one direction of loading, which is not recovered during load reversal.

4.2.3 Beam-column subassemblage of Beckingsale

The reliability of the proposed models was further tested by comparing the analytical predictions with the experimental data for one of the specimens tested by Beckingsale [BEC80-1]. The specimen was designed according to the requirements of the New Zealand Building Code [NZS82-1] and represents an approximately two-third scale model of a cruciform-shaped beam-column subassemblage from the lower stories of a typical frame of 10 to 15 stories height.

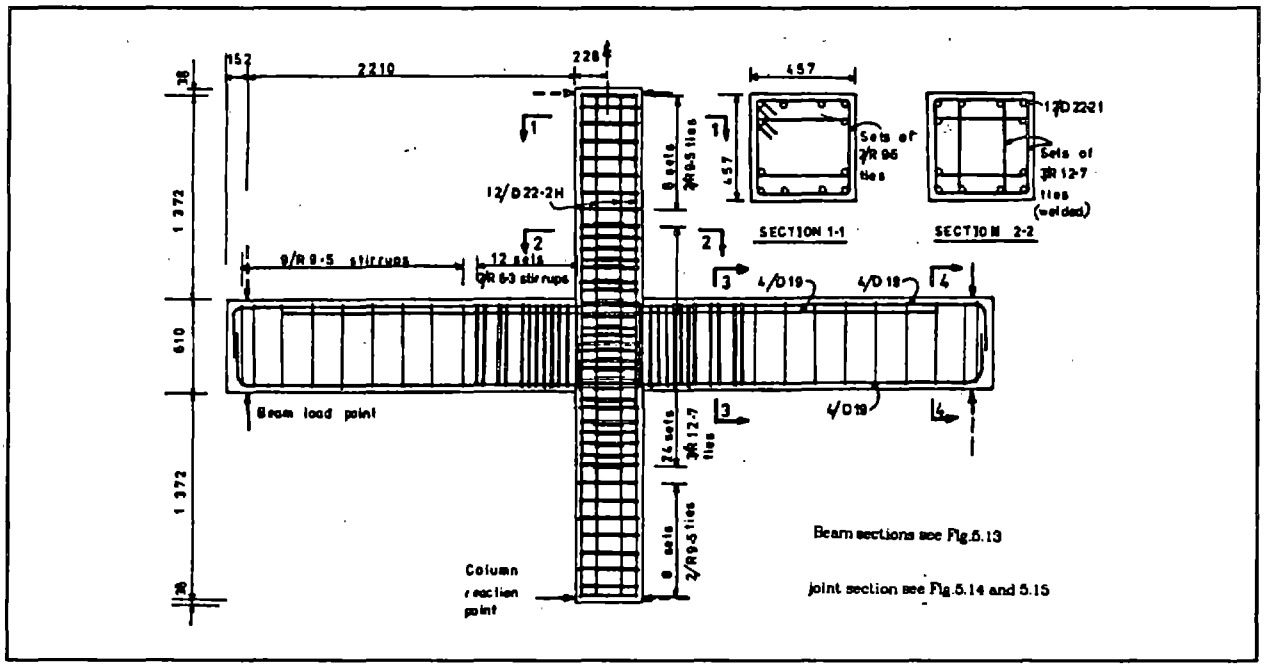

Fig. 4.20 Beam-column subassemblage tested by Beckingsale in [BEC80-1]

The size of the members and the amount and detailing of reinforcement (Figs. 4.20 and 4.21) were determined so as to ensure that inelastic deformations would develop in the girder end zones and the beam-column joint. The axial load level of the columns was very low ($0.05 \cdot f_c' \cdot A_g$).

Adequate shear reinforcement was provided in the beam-column joint region and the contribution of concrete to the joint shear resistance was neglected, thus ensuring that shear cracking was kept to a minimum and joint deformations due to diagonal shear cracks were negligibly small.

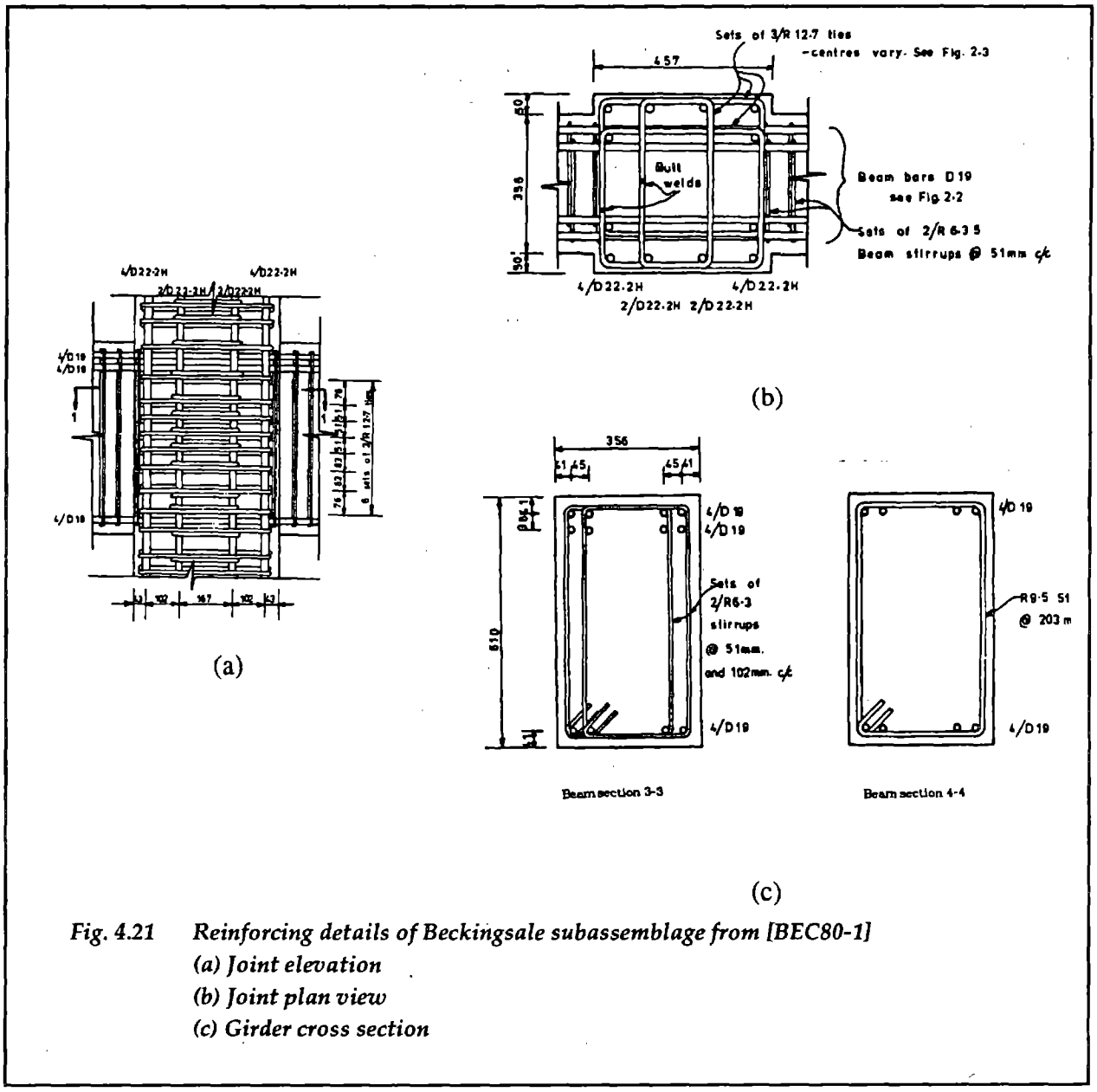

Fig. 4.21 Reinforcing details of Beckingsale subassemblage from [BEC80-1]
(a) Joint elevation
(b) Joint plan view
(c) Girder cross section

The specimen geometry and reinforcement layout are shown in Figs. 4.20 and 4.21. Lateral loading of the subassemblage was simulated by loading one beam upwards and the other downwards until reaching the prescribed displacements, then releasing and applying the loads in the opposite direction. The induced column shear loading sequence is shown in Fig. 4.22.

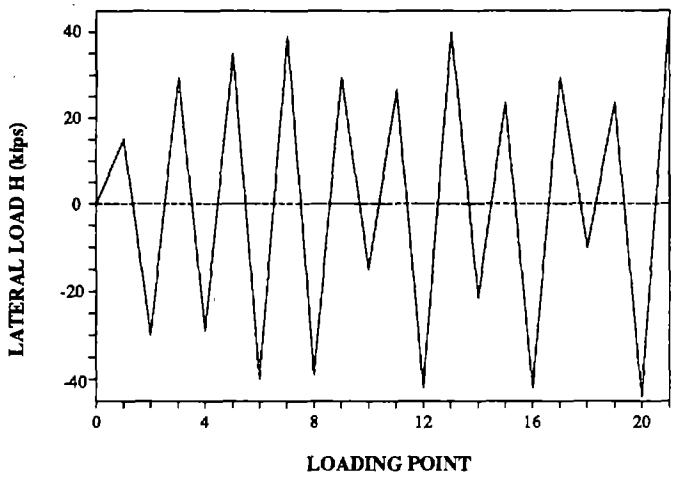

Fig. 4.22 Loading sequence applied to Beckingsale subassemblage

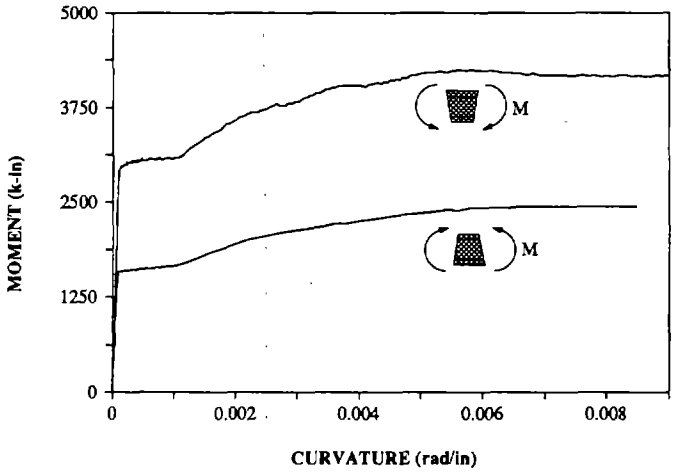

Fig. 4.23 Monotonic moment-curvature relation in girder end region of Beckingsale subassemblage

The parameters of the spread plastic and beam-column joint subelements were derived analytically based on the actual material properties reported in [BEC80-1]. The parameters used in the spread plastic subelement were derived by fitting a bilinear envelope curve to the actual monotonic moment-curvature relation of a girder section. This was determined with the aid of the nonlinear section analysis program described in [FIL89-1] (Fig. 4.23). The beam model parameters are summarized in Table 4.3. The strain hardening ratio was equal to 0.016 in both directions of bending.

Table 4.3			
GIRDER MOMENT-CURVATURE RELATION			
		yield moment [k-in]	initial stiffness [10^3 k-in^2 /rad]
positive M	west	1562	17280
	east	1562	17280
negative M	west	3043	30420
	east	3043	30420

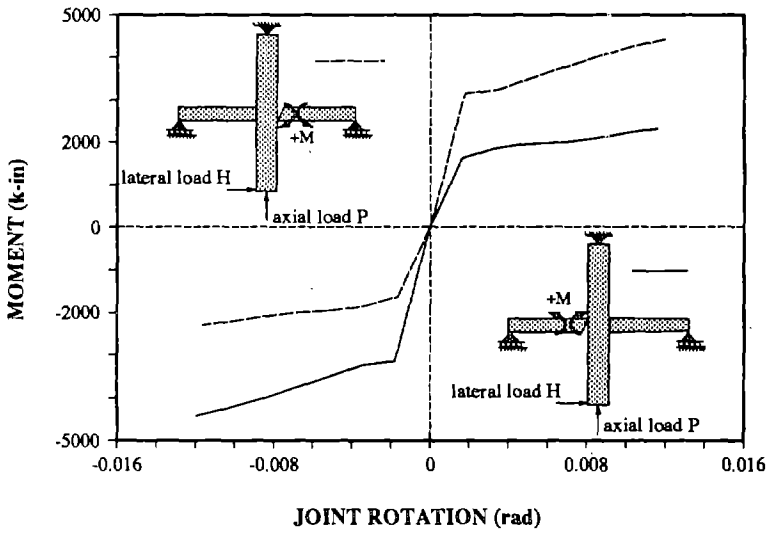

Fig. 4.24 Monotonic moment-rotation relation at beam-column interfaces of Beckingsale subassemblage

The parameters of the beam-column joint subelement were derived by fitting a bilinear envelope curve to the actual monotonic moment-rotation relation of the beam-column joint. This was determined with the aid of the finite element program presented in [FIL83-2] based on the geometry and reinforcement layout of the joint (Fig. 4.24). The beam-column joint model parameters are summarized in Table 4.4. The strain hardening ratio of the moment-rotation relation was taken equal to 0.06 in both directions of bending.

Table 4.4			
JOINT MOMENT-ROTATION RELATION			
		yield moment [k-in]	initial stiffness [10^3 k-in /rad]
positive M	west	1562	960
	east	1562	960
negative M	west	3043	1780
	east	3043	1780

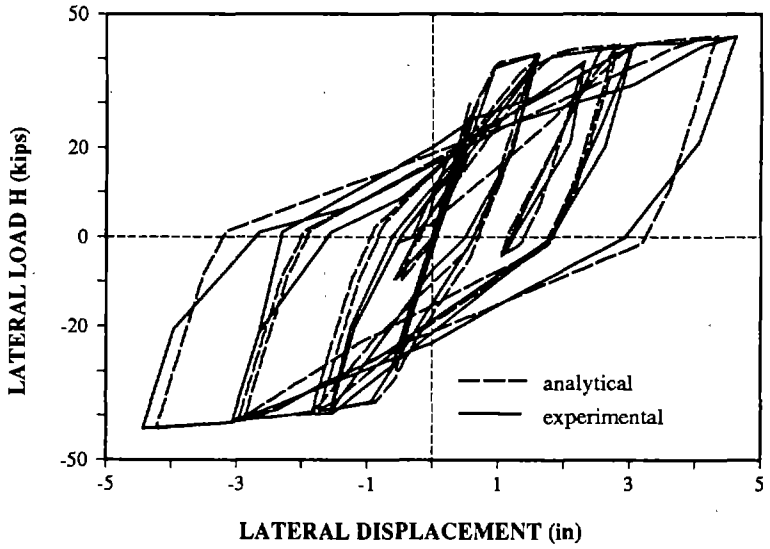

Fig. 4.25 Load-displacement response of Beckingsale subassemblage

The global load displacement relation of the subassemblage is shown in Fig. 4.25. Excellent agreement between analytically predicted values and experimental results is generally observed, particularly, if account is taken of the fact that the subassemblage is subjected to load-controlled loading conditions. The analytical model is capable of very satisfactorily representing the strength and stiffness of the subassemblage. There is a discrepancy in the prediction of the unloading stiffness of the subassemblage, which can be mostly attributed to the stiff unloading slope of the beam subelement model.

4.3 Beam-column subassemblage with two joints

The difference between the spread plasticity and the concentrated plasticity model can be further illustrated by studying the lateral response of a statically indeterminate beam-column subassemblage. In order to retain some reference to the results of the statically determinate subassemblage studied earlier, the statically indeterminate subassemblage is formed by using two cruciform shaped subassemblages which are made continuous at one end, as shown in Fig. 4.26. The geometry and reinforcement layout of each subassemblage are identical to those of the cruciform shaped subassemblage BC3.

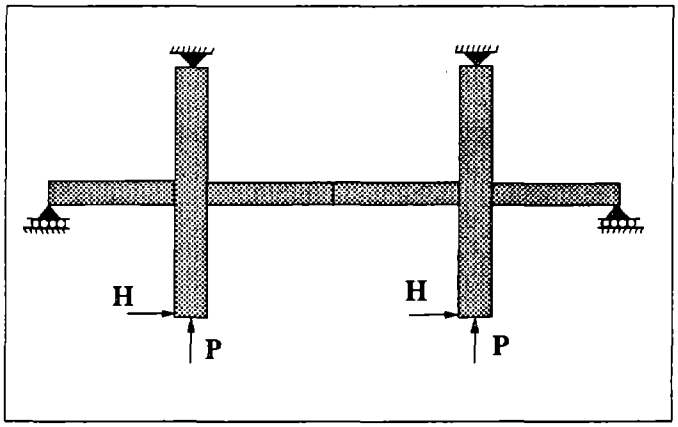

Fig. 4.26 Geometry of statically indeterminate beam-column subassemblage

The intent of these studies is to investigate the performance of the different models when coupling is present between the girder end moments. Since the amount of top reinforcement is different from that of bottom reinforcement, as is typically the case in practice, the point of inflection of the moment distribution under lateral loads does not lie at girder midspan. Moreover, the point of inflection shifts continuously as stiffness changes take place in the girders and the joints and as the loading direction is reversed. Such a shift is not accounted for in the concentrated plasticity model. The presence of coupling also leads to an interaction between the girder end moments, such that the moment-rotation relation at one end is affected by the moment at the other end. This effect is caused by the off-diagonal elements in the stiffness matrix of the spread plastic beam model.

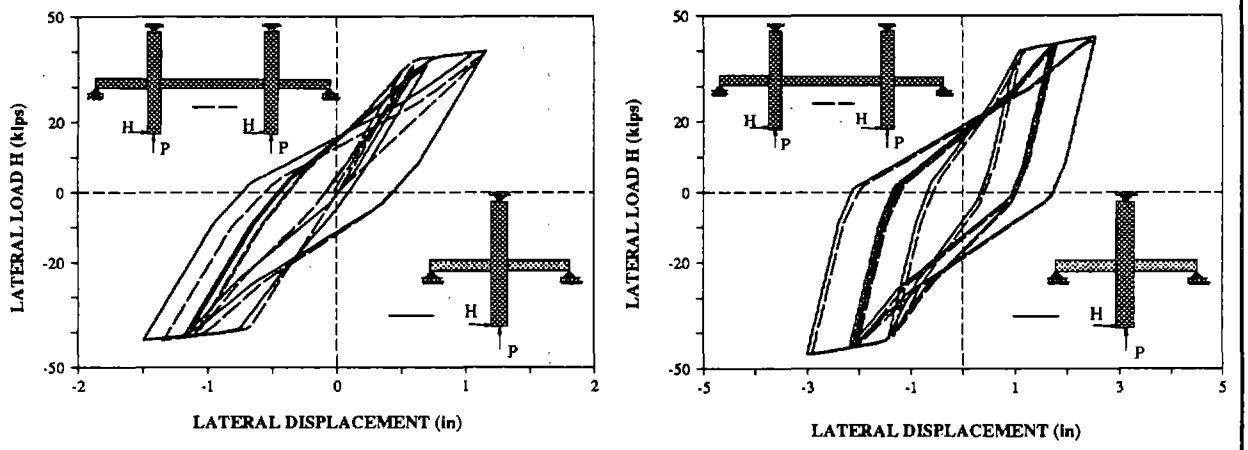

Fig. 4.27 Comparison of load-displacement relation between statically determinate and indeterminate subassemblage
(a) cycles with small displacement ductility
(b) cycles with large displacement ductility

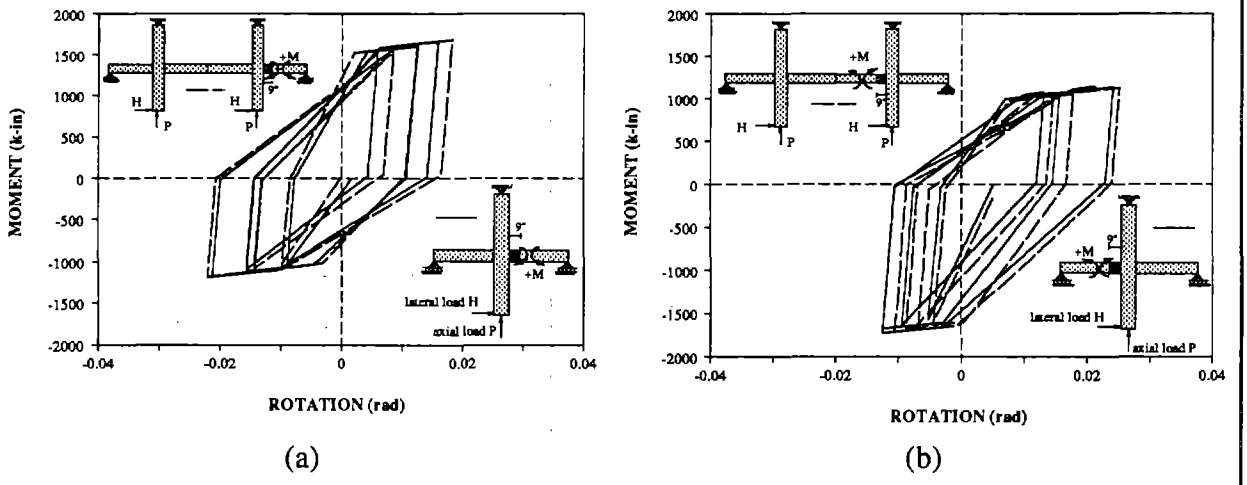

Fig. 4.28 Comparison of girder moment-rotation relation between statically determinate and indeterminate subassemblage

The statically indeterminate subassemblage is subjected to the same loading history as subassemblage BC3. It should be noted that the total lateral load acting on the subassemblage with two joints is twice that acting on specimen BC3. A comparison of the lateral load-displacement response of the two subassemblages is presented in Fig. 4.27. The resulting hysteretic moment-rotation relation in two 9" zones on either side of one column is compared in Fig. 4.28. There is a slight

difference in the response of the two subassemblages. This difference is caused by the shift in the point of inflection and the coupling between the moments acting at the ends of the interior girder, since all model parameters are kept the same in both cases and the model does not account for axial deformations of the girder elements. The effect of one end moment on the moment-rotation relation at the other end can be barely seen in Fig. 4.28. It is interesting to note, however, the small outward shift of the moment-rotation envelope curve upon reloading of the girder inelastic region in both subassemblages. This shift is partly caused by the definition of an average reloading stiffness for the entire inelastic zone and partly by the effect of the end moment at the other end of the girder.

Figs. 4.29-4.31 compare the response of the statically indeterminate subassemblage in three cases:

Case (a) Spread plasticity beam model using the same values used in the correlation with experimental results of subassemblage BC3.

Case (b) Concentrated plasticity model with a strain hardening ratio of 0.03.

Case (c) Concentrated plasticity model with a strain hardening ratio of 0.039.

A strain hardening ratio of 0.016 results in too large a discrepancy with the results of the spread plasticity model and is not considered further. A careful study of Figs. 4.29-4.31 results in the following observations:

(1) The concentrated plasticity model overestimates the maximum lateral displacement of the subassemblage. This overestimation amounts to 50% for a strain hardening ratio of 0.03 and to about 20% for a strain hardening ratio of 0.039. It is important to note that the latter strain hardening ratio gave excellent agreement of global response between concentrated and spread plasticity model in the case of subassemblage BC3 (statically determinate).

(2) The overestimation of maximum girder rotation values by the concentrated plasticity model is even larger. It is as large as 150% for a strain hardening ratio of 0.03 and as large as 100% for a ratio of 0.039.

(3) There is almost no difference of the maximum fixed-end rotation values between the different cases.

This considerable discrepancy between concentrated plasticity and spread plasticity model can be attributed to two basic factors:

(a)

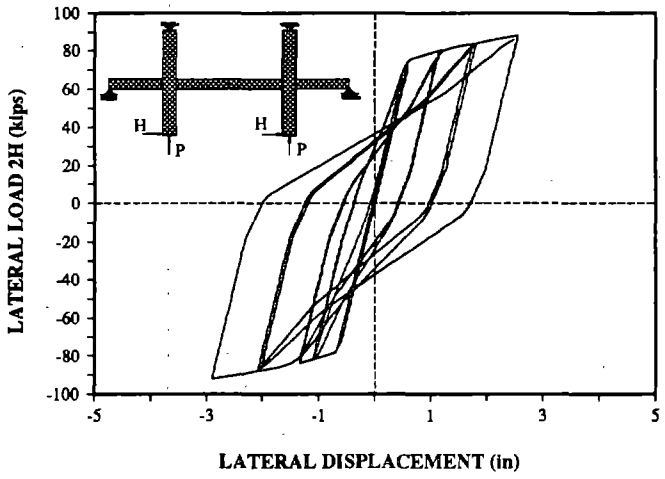

(b)

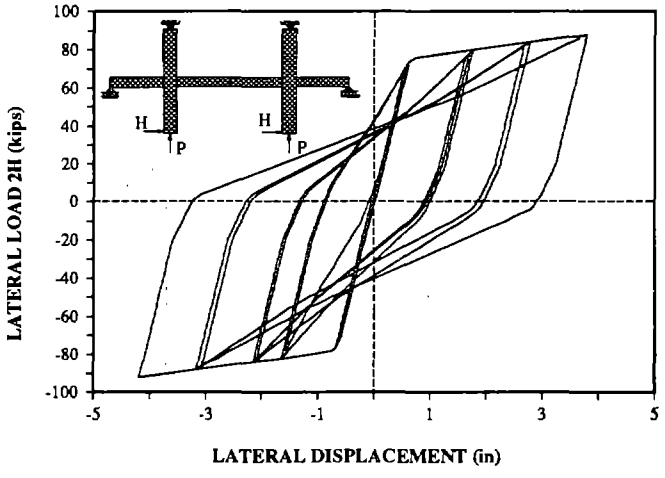

(c)

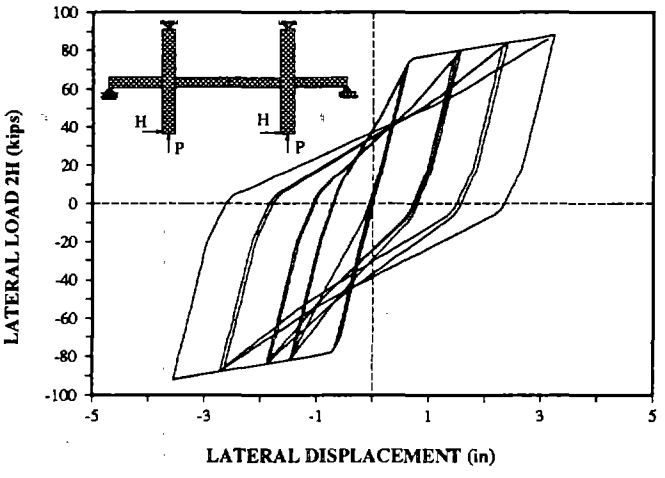

Fig. 4.29 Load-displacement relation of statically indeterminate subassemblage
(a) Spread plasticity model
(b) Concentrated plasticity model. Strain hardening ratio: 0.03
(c) Concentrated plasticity model. Strain hardening ratio: 0.039

(a)

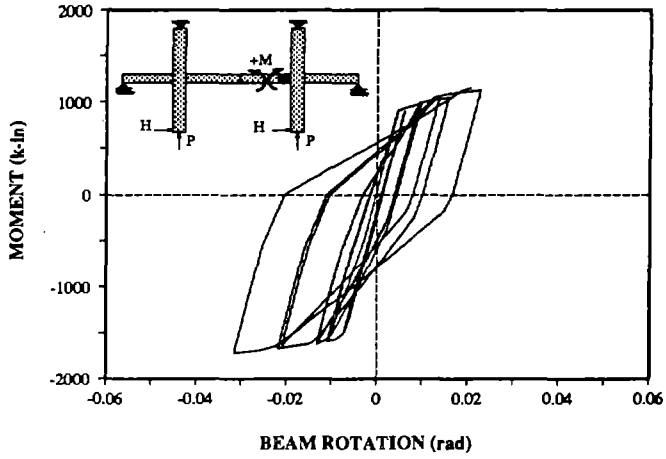

(b)

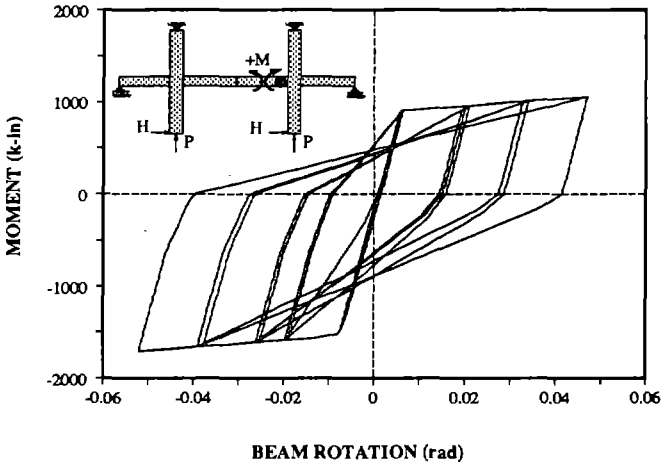

(c)

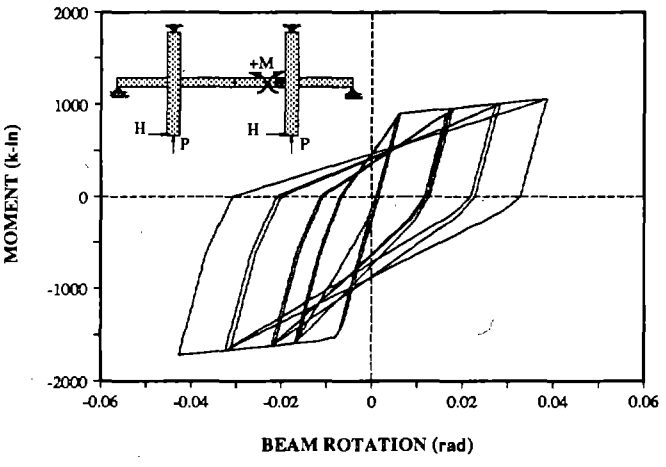

Fig. 4.30 *Girder moment-rotation relation of statically indeterminate subassemblage*
(a) Spread plasticity model
(b) Concentrated plasticity model. Strain hardening ratio: 0.03
(c) Concentrated plasticity model. Strain hardening ratio: 0.039

(a)

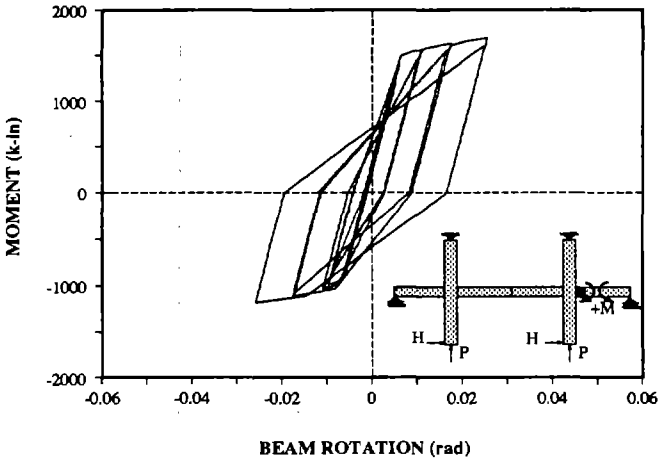

(b)

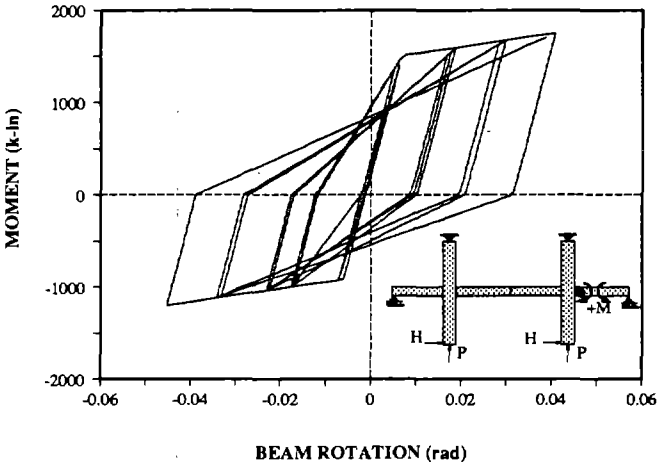

(c)

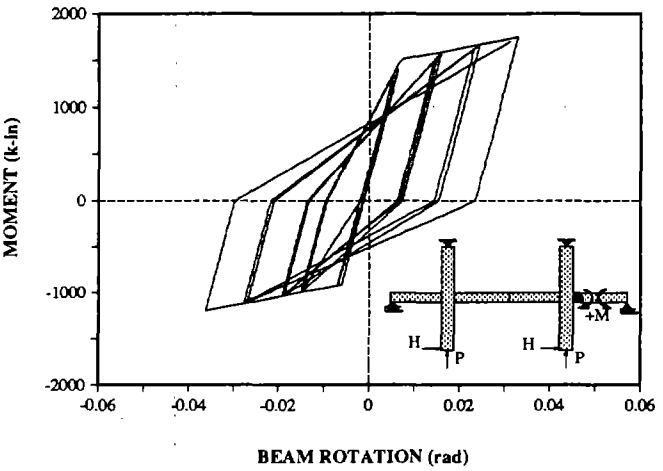

Fig. 4.31 *Girder moment-rotation relation of statically indeterminate subassemblage*
(a) Spread plasticity model
(b) Concentrated plasticity model. Strain hardening ratio: 0.03
(c) Concentrated plasticity model. Strain hardening ratio: 0.039

(a)

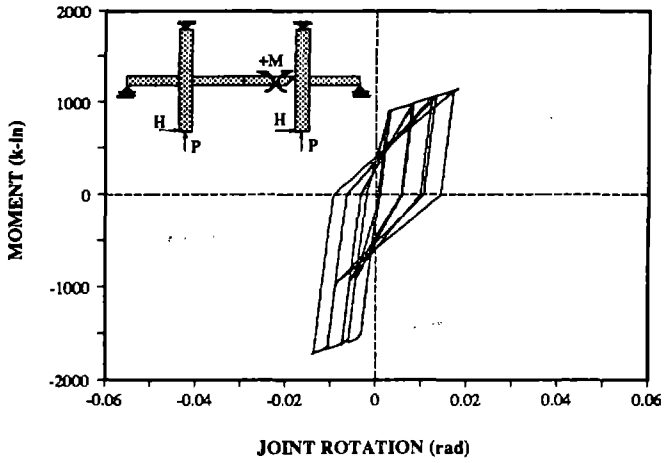

(b)

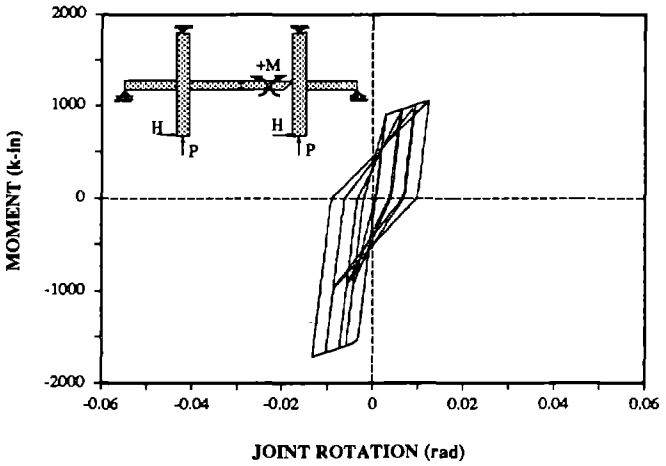

(c)

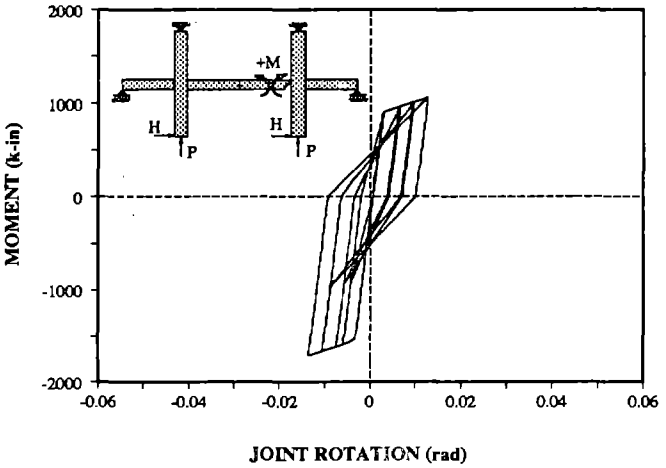

Fig. 4.32 Beam-column joint moment-rotation relation of statically indeterminate subassemblage
(a) Spread plasticity model
(b) Concentrated plasticity model. Strain hardening ratio: 0.03
(c) Concentrated plasticity model. Strain hardening ratio: 0.039

(a)

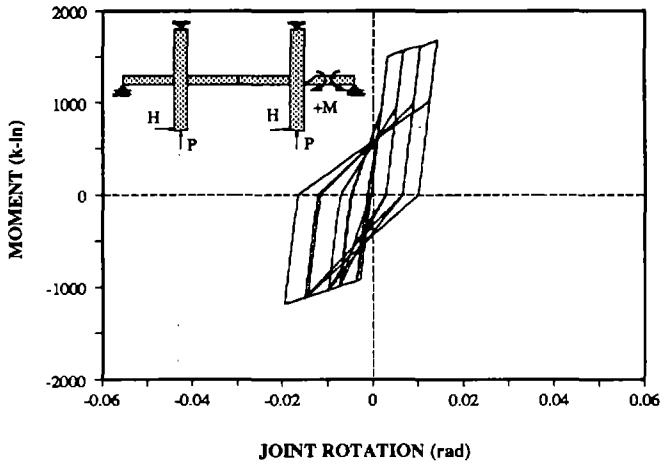

(b)

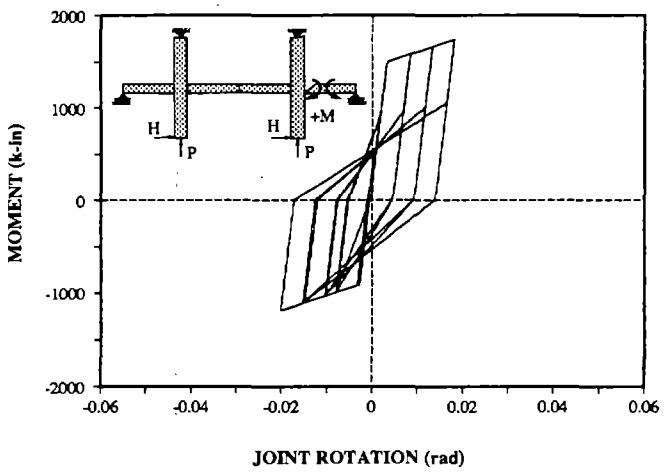

(c)

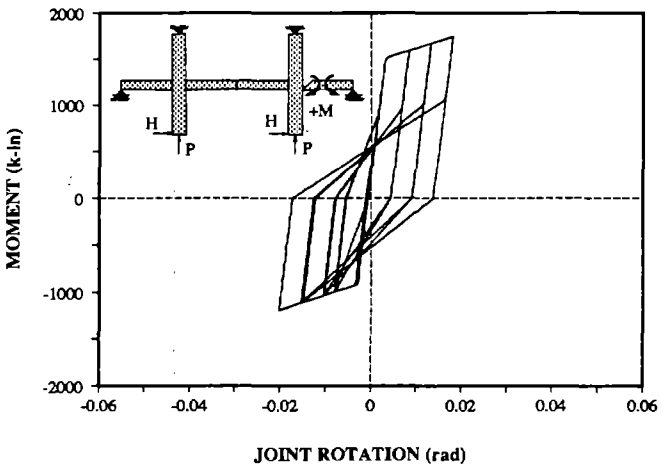

Fig. 4.33 Beam-column joint moment-rotation relation of statically indeterminate subassemblage
(a) Spread plasticity model
(b) Concentrated plasticity model. Strain hardening ratio: 0.03
(c) Concentrated plasticity model. Strain hardening ratio: 0.039

(a) The inability of the concentrated plasticity model to account for the shift of the point of inflection that takes place in the statically indeterminate subassemblage.

(b) The change in stiffness and moment strength that takes place during reloading of the spread plasticity model (Fig. 4.30a), which does not occur in the concentrated plasticity model. These changes are related to the definition of reloading stiffness and the coupling between the end moments at the girder ends.

The results of the response of statically indeterminate subassemblages further stress the limitations of the concentrated plasticity model in accurately predicting the behavior of reinforced concrete frame structures without having to adjust the model parameters in each case. Since such adjustment has to be done by trial and error and does not follow a rational procedure, it appears highly undesirable. By contrast, the spread plasticity model is based on parameters which can be derived by well established procedures, while not resulting in unreasonable computational expense. It is, therefore, believed to be a good compromise between accuracy of local and global response predictions on one hand, and computational efficiency on the other.

CHAPTER 5
CONCLUSIONS

5.1 Summary

This study has focused on the development of improved analytical methods for predicting the nonlinear static and dynamic response of multistory reinforced concrete frames. The present report is limited to the study of static response. An extensive study on the dynamic response of these structures will be presented in a following report.

A new approach in describing the nonlinear hysteretic behavior of reinforced concrete frame elements has been proposed. This approach consists of isolating the basic mechanisms controlling the hysteretic behavior of girders and columns into individual subelements which are connected in series to form the girder or column superelement. Two particular subelement models were proposed in this study: one describes the inelastic behavior along the girder accounting for the gradual spread of inelastic deformations at the girder ends, while the other models the fixed-end rotations that arise at the beam-column interface due to bond deterioration and slippage of reinforcing bars in the beam-column joint region. The properties of these elements can be derived from basic principles or refined finite element models.

Because several subelements are connected in series and each of these follows a different hysteretic rule, internal unbalanced moments might arise between these elements at any given load step. The implementation of the proposed superelement model thus requires the development of a numerical scheme which accounts for these unbalanced moments between subelements. Such a scheme was developed in this study within the framework of a special purpose analysis program for the nonlinear static and dynamic analysis of reinforced concrete moment-resisting frames.

To establish the validity of the proposed models correlation studies of analytical predictions with experimental evidence of the load-displacement response of beam-column subassemblages under static load reversals were conducted.

The predictions of the proposed model were also compared with those of the widely used one-component model. The two models were compared by investigating the local and global

response of simple structural subassemblages under cyclic load reversals. One of the key parameters of the one-component model, namely, the post-yield stiffness of the moment-rotation envelope curve was varied in these studies.

5.2 Conclusions

A careful analysis of the methods and results which were presented in the preceding chapters leads to the following conclusions:

(1) The proposed modeling approach of decomposing a structural element into subelements connected in series represents a flexible platform for the development of analytical models of any desired level of complexity. Such complexity can be achieved in two ways: first by adding any number of subelements into an existing structural element or, secondly, by refining the hysteretic law of a single subelement. Clearly, a combination of these two schemes is also possible. Studies to date have been limited to the second approach adopting a single element and refining the hysteretic law to account for various effects. This study points to the advantages of the first modeling scheme. This approach results in simple hysteretic laws which can be derived from physical behavior rather than curve fitting.

(2) By isolating mechanisms of hysteretic behavior in separate subelements it is possible to establish improved analytical models of such behavior. These models are based on parameters which are derived from the physical properties of the structural elements by well established procedures or by very refined local models.

(3) The exchange of results between refined local models suitable for a detailed analysis of small regions and more simplified component models which are suitable for global analysis of multistory structures provides a powerful tool for the study of the seismic response of reinforced concrete structures.

(4) The proposed girder superelement correlates very well with available experimental evidence of the response of beam-column subassemblages to cyclic load reversals. Excellent agreement with experimental results is observed, both, at the local as well as the global level. The girder element currently consists of two subelements: one describes the inelastic behavior along the girder accounting for the gradual spread of inelastic deformations at the girder ends, while the other models the fixed-end rotations that arise at the beam-column interface due to bond deterioration and slippage of reinforcing bars in the beam-column joint region.

(5) The monotonic envelope of the spread plastic subelement is derived from the moment-curvature relation of a section in the inelastic region of the girder. It depends on three values, namely, initial section stiffness, flexural strength and strain hardening ratio and can thus be readily established from first principles. The law governing the hysteretic behavior of the spread plastic subelement is very simple with no additional parameters introduced. It is based on Clough's hysteretic model.

(6) The properties of the beam-column joint subelement are established with the aid of a previously developed refined model of the hysteretic behavior of beam-column joints. The monotonic envelope depends on three parameters in each direction of bending: the initial stiffness, the yield strength and the strain hardening ratio. The law governing the hysteretic behavior of the beam-column joint subelement is very simple with no additional parameters introduced. It is based on a modification of Clough's hysteretic model so as to account for the characteristic "pinching" effect observed in one direction of bending.

(7) In spite of the simplicity of hysteretic behavior of both subelement models, excellent agreement of the predicted local behavior of beam-column subassemblages with experimental evidence is found. The only limitation of the hysteretic models appears to be the unloading stiffness which is consistently higher than observed in experiments.

(8) The widely used one-component model shows limitations with respect to the spread plasticity model. These limitations appear in spite the fact that the fixed-end rotations were modeled in a separate element in the present study. The limitations are:

   (a) There is no single rational method for deriving the post-yield stiffness of the moment-rotation relation of the model. In the most commonly used method the derivation of the post-yield stiffness hinges on several assumptions and depends on the load magnitude.

   (b) The post-yield stiffness depends on the loading history and the structural system of the subassemblage. Even though this parameter can be "tuned" to match the experimental results of a particular subassemblage under a given load history, the same post-yield stiffness yields poor results under different loading conditions.

   (c) Even in a case of excellent agreement of global response values between one-component model and experimental results, the local moment-rotation of the girder inelastic region does not show such good agreement. This is due to the inherent inability of the model to follow the gradual change of post-yield stiffness associated with the spread of inelastic deformations into the girder.

(d) The model does not account for the shift in the point of inflection of the girder during the response time history. Reinforced concrete girders are commonly reinforced so that the bottom steel area at the girder ends is only about half that at the top. When both ends yield, the point of inflection lies closer to the third span than the midspan point of the girder, as is assumed in the derivation of the post-yield stiffness of the one-component model. When the loading is reversed until both ends yield in the opposite direction, the inflection point shifts to the third span point at the other end of the girder.

(e) The model does not account for the coupling between the moments acting at the two ends of the girder. Even though this effect is relatively small, it leads to a more complex hysteretic behavior than anticipated by the model. Previous research efforts have attempted to account for this phenomenon by introducing additional parameters into the hysteretic law of the one-component model.

(9) The spread plasticity girder element overcomes all these limitations. An important advantage over the one-component model derives from fact that all parameters of the spread plasticity element are directly related with the physical properties of the structural element and can be derived by well established methods.

(10) In addition to the excellent agreement with experimental results, the spread plasticity element maintains computational efficiency. This is achieved in three ways:

(a) Each inelastic region possesses a single average effective stiffness. This concept, originally proposed by Soleimani et. al. in [SOL79-2], results in a symmetric element stiffness matrix.

(b) The continuous process of plastic zone extension is discretized, as described in Chapter 3.

(c) An efficient nonlinear analysis algorithm is developed which accounts for the non-linearities due to the gradual spread of the plastic zone length and the coupling between the end moments of the girder.

(11) The spread plasticity model only approximately accounts for the effect of gravity loads. The effect of gravity loads on the location of plastic hinges is not accounted for. Since inelastic zones are assumed to form at the ends of the member, the girder needs to be subdivided into several elements, if plastic zones can form along the span.

(12) A new global algorithm of nonlinear analysis is proposed. This algorithm is based on the initial stress modification of the Newton-Raphson method. It solves satisfactorily the problem of possible internal unbalanced moments between the various subelements. These arise, because the subelements are connected in series, while each follows an independent hysteretic rule. Since this situation is encountered in many studies, the algorithm is generally applicable.

(13) Finally, it is important to note that the proposed algorithm guarantees within a specified tolerance *exact equilibrium between internal resisting moments and external loads at each load step*.

5.3 Recommendations for further research

The proposed model provides a platform for the addition of new subelements which account for mechanisms of hysteretic behavior that have not been considered in this study. Among these are:

(1) The effect of inelastic deformations in columns with due account of the interaction between bending moment and axial load.

(2) The effect of shear in short span girders.

(3) The effect of shear in short columns.

(4) The effect of pull-out of column reinforcement from the foundation.

In addition, the effect of various models on the local and global response of reinforced concrete frame structures subjected to earthquake excitations should be studied in detail. In this context the inclusion or not of a particular subelement will help establish the effect of the corresponding mechanism on the local and global response of reinforced concrete moment-resisting frames.

REFERENCES

[ACI85-1] ACI-ASCE committee 352, "Design of Beam-Column Joints in Monolithic Reinforced Structures," *ACI Journal*, v. 82, no. 3, May-June 1985.

[ACI83-1] ACI Committee 318, Building Code Requirements for Reinforced Concrete, American Concrete Institute, Detroit, MI, 1983.

[ANA81-1] Anagnostopoulos, S.A., "Inelastic Beams for Seismic Analyses of Structures", *Journal of the Structural Division, ASCE,* Vol. 107, No. ST7, July 1981.

[AND77-1] Anderson, J.C. and Townsend, W.H., "Models for RC Frames with Degrading Stiffness", *Journal of the Structural Division, ASCE,* Vol. 103, No. ST12, Dec. 1977.

[ASC82-1] American Society of Civil Engineers, Finite Element Analysis of Reinforced Concrete Structures, New York, 1982.

[BAN81-1] Banon, H., Biggs, J.M. and Irvine, M.H., "Seismic Damage in Reinforced Concrete Frames", *Journal of the Structural Division, ASCE,* Vol. 107, No. ST9, Sept. 1981.

[BEC80-1] Beckingsale, C.W., "Post Elastic Behaviour of Reinforced Concrete Beam-Column Joints," *Research Report 80-20, Department of Civil Engineering,* University of Canterbury, New Zealand, Aug. 1980.

[BER73-1] Bergan, P.G. and Soreide, T., "A Comparative Study of Different Solution Techniques as applied to a Nonlinear Structural Problem", *Computer Methods in Applied Mechanics and Engineering,* Vol. 2, pp. 185-201, Feb. 1973

[BER75-1] Bertero, V.V. and Mahin, S.A., "An Evaluation of Some Methods for Predicting the Seismic Behavior of Reinforced Concrete Buildings", *Earthquake Engineering Research Center, Report No. EERC 75-5,* University of California, Berkeley, Feb. 1975.

[BER75-2] Bertero, V.V. and Popov, E.P., "Hysteretic Behavior of Ductile Moment Resisting Reinforced Concrete Frame Components", *Earthquake Engineering Research Center, Report No. EERC 75-16,* University of California, Berkeley, April 1975.

[BER79-1] Bertero, V.V., "Seismic Behavior of Structural Concrete Linear Elements (Beams, Columns) and Their Connections", Introductory Report to Theme II, *AICAP-CEB Symposium, Structural Concrete Under Seismic Actions, Rome 1979;* Comité Euro-International Du Béton, Bulletin D' Information No. 131, Vol. 1, pp. 125-212.

[BRE73-1] Bresler, B., "Behavior of Structural Elements," Proceedings of a Workshop on Building Practices for Disaster Mitigation, Boulder, Colorado, Aug., 1972, published by the U.S. Department of Commerce, National Bureau of Standards, Building Science Series No. 6, Feb. 1973.

[CEB83-1] Comité Euro-International du Beton, "Response of R.C. Critical Regions under Large Amplitude Reversed Actions", *Bulletin d'Information No. 161,* Lausanne, Switzerland, August 1983.

[CHO73-1] Chopra, A.K., Kan. C, "Effect of Stiffness Degradation On Earthquake Ductility Requirement of Multistory Buildings," *International Journal of Earthquake Engineering and Structural Dynamics,* Vol.2, No. 1, July 1973.

[CLO65-1] Clough, R.W., Benuska, K.L. and Wilson, E.L., "Inelastic Earthquake Response of Tall Buildings", *Proceedings, Third World Conference on Earthquake Engineering, New Zealand,* Vol. 11, New Zealand National Committee on Earthquake Engineering, 1965.

[CLO66-1] Clough, R.W., Benuska, K.L. and Lin, T.Y., "FHA Study of Seismic Design Criteria for High Rise Buildings", HUDTS-3, Aug. 1966, Federal Housing Administration, Washington D.C.

[CLO75-1] Clough, R.W. and Penzien, J., ***"Dynamics of Structures",*** McGraw Hill Book Co., New York, 1975.

[DUR82-1] Durrani, A.J. and Wight, J.K., "Experimental and Analytical Study of Internal Beam to Column Connections Subjected to Reversed Cyclic Loading," *Department of Civil Engineering Report No. UMCE82R3,* University of Michigan, July 1982, p. 275.

[EMO81-1] Emori, K. and Schnobrich, W.C., "Inelastic Behavior of Concrete Frame-Wall Structures", *Journal of the Structural Division, ASCE,* Vol. 107, No. ST1, Jan. 1981.

[FIL83-1] Filippou, F., "Effects of Bond Deterioration on Seismic Response of R/C Frames," *Ph.D. Dissertation,* University of California, Berkeley, 1983.

[FIL83-2] Filippou, F.C., Popov, E.V. and Bertero, V.V., "Effects of Bond Deterioration on Hysteretic Behaviour of Reinforced Concrete Joints," *Earthquake Engineering Research Center, Report No. UCB/EERC-83/19,* University of California, Berkeley, p. 191.

[FIL83-3] Filippou, F.C., Popov, E.P. and Bertero, V.V., "Modeling of Reinforced Concrete Joints under Cyclic Excitations", *Journal of Structural Engineering, ASCE,* Vol. 109, No. 11, Nov. 1983.

[FILI89-1] Filippou, F.C., "Microcomputer-Aided Design of Reinforced and Prestressed Concrete Elements", *ACI-Special Publication,* State-of-the-Art Computer Applications in Concrete Technology, ACI SP-111, 1989.

[GIB74-1] Giberson, M.F., "Two Nonlinear Beams with Definition of Ductility", *Journal of the Structural Division, ASCE,* Vol. 95, No. ST7, July 1974.

[HAD86-1] Mohammad S. Al Haddad and Wight, J.K., "Feasibility and Consequences of Moving Beam Plastic Hinging Zones for Earthquake Resistant Design of Reinforced Concrete Buildings", *Department of Civil Engineering Report No. UMCE86-1,* University of Michigan, July 1986.

[HAI74-1] Haisler, W.E. and Stricklin, J.A., "Computational Methods for Solving Nonlinear Structural Mechanics Problems", *Proceedings of the International Conference in Nonlinear Mechanics,* University of Texas at Austin, Sept. 1974.

[JIR77-1] Jirsa, J.O., "Behavior of Elements and Subassemblages-R.C. Frames", *Proceedings of a Workshop on Earthquake Resistant Reinforced Concrete Building Construction,* Vol. III, pp.1196-1214, University of California, Berkeley, July 1977.

[KAN73-1] Kanaan, A.E. and Powell, G.H., "General Purpose Computer Program for Inelastic Dynamic Response of Plane Structures", *Earthquake Engineering Research Center, Report No. EERC 73-6,* University of California, Berkeley, April 1973.

[KES84-1] Keshavarzian, M. and Schnobrich, W.C., "Computed Nonlinear Seismic Response of R/C Frame-Wall Structures", *Civil Engineering Studies, Structural Research Series No. 515,* University of Illinois at Urbana-Champaign, Urbana, Ill., May 1984.

[MA76-1] Ma, S.Y., Bertero, V.V. and Popov, E.P., "Experimental and Analytical Studies on the Hysteretic Behavior of Reinforced Concrete Rectangular and T-Beams," *Earthquake Engineering Research Center, Report No. EERC 76-2,* University of California, Berkeley, 1976.

[MAH76-1] Mahin, S.A. and Bertero, V.V., "Problems in Establishing and Predicting Ductility in Seismic Design", *International Symposium on Earthquake Structural Engineering*, St. Louis, Missouri, USA, Aug. 1976.

[MEY83-1] Meyer, C., Roufaiel, M.S. and Arzoumanidis, S.G., "Analysis of Damaged Concrete Frames for Cyclic Loads", *Earthquake Engineering and Structural Dynamics*, Vol. 11, 1983, pag. 207-228.

[NZS82-1] NZS 3101-1982, "Code of Practice for the Design of Concrete Structures", Standards Association of New Zealand, Wellington, Part 1, p. 127, Part 2, p. 156.

[OTA74-1] Otani, S., "Inelastic Analysis of R/C Frame Structures", *Journal of the Structural Division, ASCE*, Vol. 100, No. ST7, July 1974.

[OTA85-1] Otani, S., Kitayama, K. and Aoyama, H., "Beam Bar Bond Stress and Behaviour of Reinforced Concrete Interior Beam-Column Joints", *Second US-NZ-Japan Seminar on Design of Reinforced Concrete Beam-Column Joints*, Tokyo, Japan, May 29-30 1985.

[PAN87-1] Pantazopoulou, S., "Three-Dimensional Aspects of Nonlinear Response of Reinforced Concrete Structures", thesis submitted in partial satisfaction of the requirements of the degree of Doctor of Philosophy, Univ. of California, Berkeley, Oct. 1987.

[PAR85-1] Park, Y.J. and Ang, A.H.S., "Mechanistic Seismic Damage Model for Reinforced Concrete", *Journal of Structural Engineering, ASCE*, Vol. 111, No. 4, April 1985.

[PAR75-1] Park, P. and Paulay, T., "***Reinforced Concrete Structures,***" John Wiley & Sons, New York 1975.

[PAR84-1] Park, R. and Paulay, T., "Joints in Reinforced Concrete Frames Designed for Earthquake Resistance," *Research Report 84-9*, Department of Civil Engineering, University of Canterbury, Christchurch, June 1984.

[PAU77-1] Paulay, T., "Capacity Design of Reinforced Concrete Ductile Frames," *Proceedings of a Workshop on Earthquake-Resistant Reinforced Concrete Building Construction*, University of California, Berkeley, Vol. 3, July 1977, pp. 1043-1075.

[POW85-1] Powell, G.H., "Notes on Computer Methods for Nonlinear Structural Analysis", Class notes of course CE 223B, University Of California, Berkeley, Spring 1985.

[ROU87-1] Roufaiel, M.S.L. and Meyer, C., "Analytical Modeling of Hysteretic Behavior of R/C Frames", *Journal of Structural Engineering, ASCE,* Vol. 113, No. 3, March 1987.

[SAI82-1] Saiidi, M., "Hysteresis Models for Reinforced Concrete", *Journal of the Structural Division, ASCE,* Vol. 108, No. ST5, May 1982.

[SIM82-1] Simons, J.W. and Powell, G.H., "Solution Strategies for Statically Loaded Nonlinear Structures", *Earthquake Engineering Research Center, Report No. EERC 82-22,* University of California, Berkeley, November 1982.

[SOL79-1] Soleimani, D., "Reinforced Concrete Ductile Frames Under Earthquke Loading with Stiffness Degradation", *Ph.D. Dissertation,* University of California, Berkeley, 1979.

[SOL79-2] Soleimani, D., Popov, E.P. and Bertero, V.V., "Nonlinear Beam Model for R/C Frame Analysis", *Seventh Conference on Electronic Computation,* St. Louis, Missouri, Aug. 1979, ASCE, New York 1979.

[SUK71-1] Suko, M., Adams, P.F.,"Dynamic Analysis of Multistory Frames," *Journal of the Structural Division, ASCE,* Vol. 97, No. ST10, Oct. 1971.

[TAK79-1] Takayanagi, T. and Schnobrich, W.C., "Non-Linear Analysis of Coupled Wall Systems", *Earthquake Engineering and Structural Dynamics,* Vol. 7, 1979, pag. 1-22.

[TAK70-1] Takeda, T., Sozen,M.A. and Nielsen, N.N., "Reinforced Concrete Response to Simulated Earthquakes", *Journal of the Structural Division, ASCE,* Vol. 96, ST12, Dec. 1970.

[UME82-1] Umemura, H. and Takizawa, H., "Dynamic Response of Reinforced Concrete Buildings", *Document 2, International Association of Bridge and Structural Engineering,* Zürich, Switzerland, 1982.

[VIW79-1] Viwathanatepa, S., Popov, E.P. and Bertero, V.V., "Seismic Behavior of Reinforced Concrete Interior Subassemblages", *Earthquake Engineering Research Center, Report No. EERC 79-14,* University of California, Berkeley, June 1979.

[ZER88-1] Zeris, C.A. and Mahin, S.A., "Analysis of Reinforced Concrete Beam-Columns under Uniaxial Excitations", *Journal of Structural Engineering, ASCE,* Vol. 114, No. 4, April 1988.

APPENDIX A

Derivation of Eq. (3.22)

The relation between the moment increments $\Delta \boldsymbol{M}_E$ at the ends of the superelement and the corresponding rotation increments $\Delta\Theta$ is given by

$$\Delta \boldsymbol{M}_E = [\boldsymbol{K}]_g \cdot \Delta\Theta + \Delta \boldsymbol{M}_0 \tag{A.1}$$

Let us define

$$\Delta \overline{\boldsymbol{M}} = [\boldsymbol{K}] \cdot \Delta\Theta \tag{A.2}$$

Since all subelements are in series the end moments are all equal

$$\Delta \boldsymbol{M}_E = (\Delta \boldsymbol{m}_E)_{el} = (\Delta \boldsymbol{m}_E)_{pl} = (\Delta \boldsymbol{m}_E)_{jnt} \tag{A.3}$$

The rotation increments at the ends of each subelements are given by the following relations

$$\Delta\theta_{el} = [f]_{el} \cdot (\Delta \boldsymbol{m}_E)_{el} \tag{A.4a}$$

$$\Delta\theta_{pl} = [f]_{pl} \cdot (\Delta \boldsymbol{m}_E - \Delta \boldsymbol{m}_0)_{pl} \tag{A.4b}$$

$$\Delta\theta_{jnt} = [f]_{jnt} \cdot (\Delta \boldsymbol{m}_E - \Delta \boldsymbol{m}_0)_{jnt} \tag{A.4c}$$

Using Eqs. (A.1)-(A.3) we obtain

$$\Delta\theta_{el} = [f]_{el} \cdot [\Delta \overline{\boldsymbol{M}} + \Delta \boldsymbol{M}_0] \tag{A.5a}$$

$$\Delta\theta_{pl} = [f]_{pl} \cdot \left[\Delta \overline{\boldsymbol{M}} + \Delta \boldsymbol{M}_0 - (\Delta \boldsymbol{m}_0)_{pl}\right] \tag{A.5b}$$

$$\Delta\theta_{jnt} = [f]_{jnt} \cdot \left[\Delta \overline{\boldsymbol{M}} + \Delta \boldsymbol{M}_0 - (\Delta \boldsymbol{m}_0)_{jnt}\right] \tag{A.5b}$$

Adding up Eqs. (A.5a-c) and noting that

$$\Delta\theta_{el} + \Delta\theta_{pl} + \Delta\theta_{jnt} = \Delta\Theta$$

$$[\boldsymbol{F}]_g = [f]_{el} + [f]_{pl} + [f]_{jnt}$$

we obtain

$$\Delta\Theta = [\boldsymbol{F}] \cdot (\Delta\overline{\boldsymbol{M}} + \Delta\boldsymbol{M}_0) - [\boldsymbol{f}]_{pl} \cdot (\Delta\boldsymbol{m}_0)_{pl} - [\boldsymbol{f}]_{jnt} \cdot (\Delta\boldsymbol{m}_0)_{jnt} \qquad (A.6)$$

Multiplying both sides of Eq. (A.6) by $[\boldsymbol{K}]_g$ and noting that $[\boldsymbol{F}]_g \cdot [\boldsymbol{K}]_g = [\boldsymbol{I}]$, where $[\boldsymbol{I}]$ is the identity matrix, we can solve for $\Delta\boldsymbol{M}_0$ and obtain

$$\Delta\boldsymbol{M}_0 = [\boldsymbol{K}] \cdot \{ [\boldsymbol{f}]_{pl} \cdot (\Delta\boldsymbol{m}_0)_{pl} + [\boldsymbol{f}]_{jnt} \cdot (\Delta\boldsymbol{m}_0)_{jnt} \} \qquad (A.7)$$

which is the desired Eq. (3.22).

EARTHQUAKE ENGINEERING RESEARCH CENTER REPORT SERIES

EERC reports are available from the National Information Service for Earthquake Engineering(NISEE) and from the National Technical Information Service(NTIS). Numbers in parentheses are Accession Numbers assigned by the National Technical Information Service; these are followed by a price code. Contact NTIS, 5285 Port Royal Road, Springfield Virginia, 22161 for more information. Reports without Accession Numbers were not available from NTIS at the time of printing. For a current complete list of EERC reports (from EERC 67-1) and availablity information, please contact University of California, EERC, NISEE, 1301 South 46th Street, Richmond, California 94804.

UCB/EERC-80/01 "Earthquake Response of Concrete Gravity Dams Including Hydrodynamic and Foundation Interaction Effects," by Chopra, A.K., Chakrabarti, P. and Gupta, S., January 1980, (AD-A087297)A10.

UCB/EERC-80/02 "Rocking Response of Rigid Blocks to Earthquakes," by Yim, C.S., Chopra, A.K. and Penzien, J., January 1980, (PB80 166 002)A04.

UCB/EERC-80/03 "Optimum Inelastic Design of Seismic-Resistant Reinforced Concrete Frame Structures," by Zagajeski, S.W. and Bertero, V.V., January 1980, (PB80 164 635)A06.

UCB/EERC-80/04 "Effects of Amount and Arrangement of Wall-Panel Reinforcement on Hysteretic Behavior of Reinforced Concrete Walls," by Iliya, R. and Bertero, V.V., February 1980, (PB81 122 525)A09.

UCB/EERC-80/05 "Shaking Table Research on Concrete Dam Models," by Niwa, A. and Clough, R.W., September 1980, (PB81 122 368)A06.

UCB/EERC-80/06 "The Design of Steel Energy-Absorbing Restrainers and their Incorporation into Nuclear Power Plants for Enhanced Safety (Vol 1a): Piping with Energy Absorbing Restrainers: Parameter Study on Small Systems," by Powell, G.H., Oughourlian, C. and Simons, J., June 1980.

UCB/EERC-80/07 "Inelastic Torsional Response of Structures Subjected to Earthquake Ground Motions," by Yamazaki, Y., April 1980, (PB81 122 327)A08.

UCB/EERC-80/08 "Study of X-Braced Steel Frame Structures under Earthquake Simulation," by Ghanaat, Y., April 1980, (PB81 122 335)A11.

UCB/EERC-80/09 "Hybrid Modelling of Soil-Structure Interaction," by Gupta, S., Lin, T.W. and Penzien, J., May 1980, (PB81 122 319)A07.

UCB/EERC-80/10 "General Applicability of a Nonlinear Model of a One Story Steel Frame," by Sveinsson, B.I. and McNiven, H.D., May 1980, (PB81 124 877)A06.

UCB/EERC-80/11 "A Green-Function Method for Wave Interaction with a Submerged Body," by Kioka, W., April 1980, (PB81 122 269)A07.

UCB/EERC-80/12 "Hydrodynamic Pressure and Added Mass for Axisymmetric Bodies.," by Nilrat, F., May 1980, (PB81 122 343)A08.

UCB/EERC-80/13 "Treatment of Non-Linear Drag Forces Acting on Offshore Platforms," by Dao, B.V. and Penzien, J., May 1980, (PB81 153 413)A07.

UCB/EERC-80/14 "2D Plane/Axisymmetric Solid Element (Type 3-Elastic or Elastic-Perfectly Plastic)for the ANSR-II Program," by Mondkar, D.P. and Powell, G.H., July 1980, (PB81 122 350)A03.

UCB/EERC-80/15 "A Response Spectrum Method for Random Vibrations," by Der Kiureghian, A., June 1981, (PB81 122 301)A03.

UCB/EERC-80/16 "Cyclic Inelastic Buckling of Tubular Steel Braces," by Zayas, V.A., Popov, E.P. and Mahin, S.A., June 1981, (PB81 124 885)A10.

UCB/EERC-80/17 "Dynamic Response of Simple Arch Dams Including Hydrodynamic Interaction," by Porter, C.S. and Chopra, A.K., July 1981, (PB81 124 000)A13.

UCB/EERC-80/18 "Experimental Testing of a Friction Damped Aseismic Base Isolation System with Fail-Safe Characteristics," by Kelly, J.M., Beucke, K.E. and Skinner, M.S., July 1980, (PB81 148 595)A04.

UCB/EERC-80/19 "The Design of Steel Energy-Absorbing Restrainers and their Incorporation into Nuclear Power Plants for Enhanced Safety (Vol.1B): Stochastic Seismic Analyses of Nuclear Power Plant Structures and Piping Systems Subjected to Multiple Supported Excitations," by Lee, M.C. and Penzien, J., June 1980, (PB82 201 872)A08.

UCB/EERC-80/20 "The Design of Steel Energy-Absorbing Restrainers and their Incorporation into Nuclear Power Plants for Enhanced Safety (Vol 1C): Numerical Method for Dynamic Substructure Analysis," by Dickens, J.M. and Wilson, E.L., June 1980.

UCB/EERC-80/21 "The Design of Steel Energy-Absorbing Restrainers and their Incorporation into Nuclear Power Plants for Enhanced Safety (Vol 2): Development and Testing of Restraints for Nuclear Piping Systems," by Kelly, J.M. and Skinner, M.S., June 1980.

UCB/EERC-80/22 "3D Solid Element (Type 4-Elastic or Elastic-Perfectly-Plastic) for the ANSR-II Program," by Mondkar, D.P. and Powell, G.H., July 1980, (PB81 123 242)A03.

UCB/EERC-80/23 "Gap-Friction Element (Type 5) for the Ansr-II Program," by Mondkar, D.P. and Powell, G.H., July 1980, (PB81 122 285)A03.

UCB/EERC-80/24 "U-Bar Restraint Element (Type 11) for the ANSR-II Program," by Oughourlian, C. and Powell, G.H., July 1980, (PB81 122 293)A03.

UCB/EERC-80/25 "Testing of a Natural Rubber Base Isolation System by an Explosively Simulated Earthquake," by Kelly, J.M., August 1980, (PB81 201 360)A04.

UCB/EERC-80/26 "Input Identification from Structural Vibrational Response," by Hu, Y., August 1980, (PB81 152 308)A05.

UCB/EERC-80/27 "Cyclic Inelastic Behavior of Steel Offshore Structures," by Zayas, V.A., Mahin, S.A. and Popov, E.P., August 1980, (PB81 196 180)A15.

UCB/EERC-80/28 "Shaking Table Testing of a Reinforced Concrete Frame with Biaxial Response," by Oliva, M.G., October 1980, (PB81 154 304)A10.

UCB/EERC-80/29 "Dynamic Properties of a Twelve-Story Prefabricated Panel Building," by Bouwkamp, J.G., Kollegger, J.P. and Stephen, R.M., October 1980, (PB82 138 777)A07.

UCB/EERC-80/30 "Dynamic Properties of an Eight-Story Prefabricated Panel Building," by Bouwkamp, J.G., Kollegger, J.P. and Stephen, R.M., October 1980, (PB81 200 313)A05.

UCB/EERC-80/31 "Predictive Dynamic Response of Panel Type Structures under Earthquakes," by Kollegger, J.P. and Bouwkamp, J.G., October 1980, (PB81 152 316)A04.

UCB/EERC-80/32 "The Design of Steel Energy-Absorbing Restrainers and their Incorporation into Nuclear Power Plants for Enhanced Safety (Vol 3): Testing of Commercial Steels in Low-Cycle Torsional Fatigue," by Spanner, P., Parker, E.R., Jongewaard, E. and Dory, M., 1980.

UCB/EERC-80/33 "The Design of Steel Energy-Absorbing Restrainers and their Incorporation into Nuclear Power Plants for Enhanced Safety (Vol 4): Shaking Table Tests of Piping Systems with Energy-Absorbing Restrainers," by Stiemer, S.F. and Godden, W.G., September 1980, (PB82 201 880)A05.

UCB/EERC-80/34 "The Design of Steel Energy-Absorbing Restrainers and their Incorporation into Nuclear Power Plants for Enhanced Safety (Vol 5): Summary Report," by Spencer, P., 1980.

UCB/EERC-80/35 "Experimental Testing of an Energy-Absorbing Base Isolation System," by Kelly, J.M., Skinner, M.S. and Beucke, K.E., October 1980, (PB81 154 072)A04.

UCB/EERC-80/36 "Simulating and Analyzing Artificial Non-Stationary Earth Ground Motions," by Nau, R.F., Oliver, R.M. and Pister, K.S., October 1980, (PB81 153 397)A04.

UCB/EERC-80/37 "Earthquake Engineering at Berkeley - 1980," by , September 1980, (PB81 205 674)A09.

UCB/EERC-80/38 "Inelastic Seismic Analysis of Large Panel Buildings," by Schricker, V. and Powell, G.H., September 1980, (PB81 154 338)A13.

UCB/EERC-80/39 "Dynamic Response of Embankment, Concrete-Gavity and Arch Dams Including Hydrodynamic Interation," by Hall, J.F. and Chopra, A.K., October 1980, (PB81 152 324)A11.

UCB/EERC-80/40 "Inelastic Buckling of Steel Struts under Cyclic Load Reversal.," by Black, R.G., Wenger, W.A. and Popov, E.P., October 1980, (PB81 154 312)A08.

UCB/EERC-80/41 "Influence of Site Characteristics on Buildings Damage during the October 3,1974 Lima Earthquake," by Repetto, P., Arango, I. and Seed, H.B., September 1980, (PB81 161 739)A05.

UCB/EERC-80/42 "Evaluation of a Shaking Table Test Program on Response Behavior of a Two Story Reinforced Concrete Frame," by Blondet, J.M., Clough, R.W. and Mahin, S.A., December 1980, (PB82 196 544)A11.

UCB/EERC-80/43 "Modelling of Soil-Structure Interaction by Finite and Infinite Elements," by Medina, F., December 1980, (PB81 229 270)A04.

UCB/EERC-81/01 "Control of Seismic Response of Piping Systems and Other Structures by Base Isolation," by Kelly, J.M., January 1981, (PB81 200 735)A05.

UCB/EERC-81/02 "OPTNSR- An Interactive Software System for Optimal Design of Statically and Dynamically Loaded Structures with Nonlinear Response," by Bhatti, M.A., Ciampi, V. and Pister, K.S., January 1981, (PB81 218 851)A09.

UCB/EERC-81/03 "Analysis of Local Variations in Free Field Seismic Ground Motions," by Chen, J.-C., Lysmer, J. and Seed, H.B., January 1981, (AD-A099508)A13.

UCB/EERC-81/04 "Inelastic Structural Modeling of Braced Offshore Platforms for Seismic Loading," by Zayas, V.A., Shing, P.-S.B., Mahin, S.A. and Popov, E.P., January 1981, (PB82 138 777)A07.

UCB/EERC-81/05 "Dynamic Response of Light Equipment in Structures," by Der Kiureghian, A., Sackman, J.L. and Nour-Omid, B., April 1981, (PB81 218 497)A04.

UCB/EERC-81/06 "Preliminary Experimental Investigation of a Broad Base Liquid Storage Tank," by Bouwkamp, J.G., Kollegger, J.P. and Stephen, R.M., May 1981, (PB82 140 385)A03.

UCB/EERC-81/07 "The Seismic Resistant Design of Reinforced Concrete Coupled Structural Walls," by Aktan, A.E. and Bertero, V.V., June 1981, (PB82 113 358)A11.

UCB/EERC-81/08 "Unassigned," by Unassigned, 1981.

UCB/EERC-81/09 "Experimental Behavior of a Spatial Piping System with Steel Energy Absorbers Subjected to a Simulated Differential Seismic Input," by Stiemer, S.F., Godden, W.G. and Kelly, J.M., July 1981, (PB82 201 898)A04.

UCB/EERC-81/10 "Evaluation of Seismic Design Provisions for Masonry in the United States," by Sveinsson, B.I., Mayes, R.L. and McNiven, H.D., August 1981, (PB82 166 075)A08.

UCB/EERC-81/11 "Two-Dimensional Hybrid Modelling of Soil-Structure Interaction," by Tzong, T.-J., Gupta, S. and Penzien, J., August 1981, (PB82 142 118)A04.

UCB/EERC-81/12 "Studies on Effects of Infills in Seismic Resistant R/C Construction," by Brokken, S. and Bertero, V.V., October 1981, (PB82 166 190)A09.

UCB/EERC-81/13 "Linear Models to Predict the Nonlinear Seismic Behavior of a One-Story Steel Frame," by Valdimarsson, H., Shah, A.H. and McNiven, H.D., September 1981, (PB82 138 793)A07.

UCB/EERC-81/14 "TLUSH: A Computer Program for the Three-Dimensional Dynamic Analysis of Earth Dams," by Kagawa, T., Mejia, L.H., Seed, H.B. and Lysmer, J., September 1981, (PB82 139 940)A06.

UCB/EERC-81/15 "Three Dimensional Dynamic Response Analysis of Earth Dams," by Mejia, L.H. and Seed, H.B., September 1981, (PB82 137 274)A12.

UCB/EERC-81/16 "Experimental Study of Lead and Elastomeric Dampers for Base Isolation Systems," by Kelly, J.M. and Hodder, S.B., October 1981, (PB82 166 182)A05.

UCB/EERC-81/17 "The Influence of Base Isolation on the Seismic Response of Light Secondary Equipment," by Kelly, J.M., April 1981, (PB82 255 266)A04.

UCB/EERC-81/18 "Studies on Evaluation of Shaking Table Response Analysis Procedures," by Blondet, J. M., November 1981, (PB82 197 278)A10.

UCB/EERC-81/19 "DELIGHT.STRUCT: A Computer-Aided Design Environment for Structural Engineering," by Balling, R.J., Pister, K.S. and Polak, E., December 1981, (PB82 218 496)A07.

UCB/EERC-81/20 "Optimal Design of Seismic-Resistant Planar Steel Frames," by Balling, R.J., Ciampi, V. and Pister, K.S., December 1981, (PB82 220 179)A07.

UCB/EERC-82/01 "Dynamic Behavior of Ground for Seismic Analysis of Lifeline Systems," by Sato, T. and Der Kiureghian, A., January 1982, (PB82 218 926)A05.

UCB/EERC-82/02 "Shaking Table Tests of a Tubular Steel Frame Model," by Ghanaat, Y. and Clough, R.W., January 1982, (PB82 220 161)A07.

UCB/EERC-82/03 "Behavior of a Piping System under Seismic Excitation: Experimental Investigations of a Spatial Piping System supported by Mechanical Shock Arrestors," by Schneider, S., Lee, H.-M. and Godden, W. G., May 1982, (PB83 172 544)A09.

UCB/EERC-82/04 "New Approaches for the Dynamic Analysis of Large Structural Systems," by Wilson, E.L., June 1982, (PB83 148 080)A05.

UCB/EERC-82/05 "Model Study of Effects of Damage on the Vibration Properties of Steel Offshore Platforms," by Shahrivar, F. and Bouwkamp, J.G., June 1982, (PB83 148 742)A10.

UCB/EERC-82/06 "States of the Art and Pratice in the Optimum Seismic Design and Analytical Response Prediction of R/C Frame Wall Structures," by Aktan, A.E. and Bertero, V.V., July 1982, (PB83 147 736)A05.

UCB/EERC-82/07 "Further Study of the Earthquake Response of a Broad Cylindrical Liquid-Storage Tank Model," by Manos, G.C. and Clough, R.W., July 1982, (PB83 147 744)A11.

UCB/EERC-82/08 "An Evaluation of the Design and Analytical Seismic Response of a Seven Story Reinforced Concrete Frame," by Charney, F.A. and Bertero, V.V., July 1982, (PB83 157 628)A09.

UCB/EERC-82/09 "Fluid-Structure Interactions: Added Mass Computations for Incompressible Fluid," by Kuo, J.S.-H., August 1982, (PB83 156 281)A07.

UCB/EERC-82/10 "Joint-Opening Nonlinear Mechanism: Interface Smeared Crack Model," by Kuo, J.S.-H., August 1982, (PB83 149 195)A05.

UCB/EERC-82/11 "Dynamic Response Analysis of Techi Dam," by Clough, R.W., Stephen, R.M. and Kuo, J.S.-H., August 1982, (PB83 147 496)A06.

UCB/EERC-82/12 "Prediction of the Seismic Response of R/C Frame-Coupled Wall Structures," by Aktan, A.E., Bertero, V.V. and Piazzo, M., August 1982, (PB83 149 203)A09.

UCB/EERC-82/13 "Preliminary Report on the Smart 1 Strong Motion Array in Taiwan," by Bolt, B.A., Loh, C.H., Penzien, J. and Tsai, Y.B., August 1982, (PB83 159 400)A10.

UCB/EERC-82/14 "Shaking-Table Studies of an Eccentrically X-Braced Steel Structure," by Yang, M.S., September 1982, (PB83 260 778)A12.

UCB/EERC-82/15 "The Performance of Stairways in Earthquakes," by Roha, C., Axley, J.W. and Bertero, V.V., September 1982, (PB83 157 693)A07.

UCB/EERC-82/16 "The Behavior of Submerged Multiple Bodies in Earthquakes," by Liao, W.-G., September 1982, (PB83 158 709)A07.

UCB/EERC-82/17 "Effects of Concrete Types and Loading Conditions on Local Bond-Slip Relationships," by Cowell, A.D., Popov, E.P. and Bertero, V.V., September 1982, (PB83 153 577)A04.

UCB/EERC-82/18 "Mechanical Behavior of Shear Wall Vertical Boundary Members: An Experimental Investigation," by Wagner, M.T. and Bertero, V.V., October 1982, (PB83 159 764)A05.

UCB/EERC-82/19 "Experimental Studies of Multi-support Seismic Loading on Piping Systems," by Kelly, J.M. and Cowell, A.D., November 1982.

UCB/EERC-82/20 "Generalized Plastic Hinge Concepts for 3D Beam-Column Elements," by Chen, P. F.-S. and Powell, G.H., November 1982, (PB83 247 981)A13.

UCB/EERC-82/21 "ANSR-II: General Computer Program for Nonlinear Structural Analysis," by Oughourlian, C.V. and Powell, G.H., November 1982, (PB83 251 330)A12.

UCB/EERC-82/22 "Solution Strategies for Statically Loaded Nonlinear Structures," by Simons, J.W. and Powell, G.H., November 1982, (PB83 197 970)A06.

UCB/EERC-82/23 "Analytical Model of Deformed Bar Anchorages under Generalized Excitations," by Ciampi, V., Eligehausen, R., Bertero, V.V. and Popov, E.P., November 1982, (PB83 169 532)A06.

UCB/EERC-82/24 "A Mathematical Model for the Response of Masonry Walls to Dynamic Excitations," by Sucuoglu, H., Mengi, Y. and McNiven, H.D., November 1982, (PB83 169 011)A07.

UCB/EERC-82/25 "Earthquake Response Considerations of Broad Liquid Storage Tanks," by Cambra, F.J., November 1982, (PB83 251 215)A09.

UCB/EERC-82/26 "Computational Models for Cyclic Plasticity, Rate Dependence and Creep," by Mosaddad, B. and Powell, G.H., November 1982, (PB83 245 829)A08.

UCB/EERC-82/27 "Inelastic Analysis of Piping and Tubular Structures," by Mahasuverachai, M. and Powell, G.H., November 1982, (PB83 249 987)A07.

UCB/EERC-83/01 "The Economic Feasibility of Seismic Rehabilitation of Buildings by Base Isolation," by Kelly, J.M., January 1983, (PB83 197 988)A05.

UCB/EERC-83/02 "Seismic Moment Connections for Moment-Resisting Steel Frames.," by Popov, E.P., January 1983, (PB83 195 412)A04.

UCB/EERC-83/03 "Design of Links and Beam-to-Column Connections for Eccentrically Braced Steel Frames," by Popov, E.P. and Malley, J.O., January 1983, (PB83 194 811)A04.

UCB/EERC-83/04 "Numerical Techniques for the Evaluation of Soil-Structure Interaction Effects in the Time Domain," by Bayo, E. and Wilson, E.L., February 1983, (PB83 245 605)A09.

UCB/EERC-83/05 "A Transducer for Measuring the Internal Forces in the Columns of a Frame-Wall Reinforced Concrete Structure," by Sause, R. and Bertero, V.V., May 1983, (PB84 119 494)A06.

UCB/EERC-83/06 "Dynamic Interactions Between Floating Ice and Offshore Structures," by Croteau, P., May 1983, (PB84 119 486)A16.

UCB/EERC-83/07 "Dynamic Analysis of Multiply Tuned and Arbitrarily Supported Secondary Systems," by Igusa, T. and Der Kiureghian, A., July 1983, (PB84 118 272)A11.

UCB/EERC-83/08 "A Laboratory Study of Submerged Multi-body Systems in Earthquakes," by Ansari, G.R., June 1983, (PB83 261 842)A17.

UCB/EERC-83/09 "Effects of Transient Foundation Uplift on Earthquake Response of Structures," by Yim, C.-S. and Chopra, A.K., June 1983, (PB83 261 396)A07.

UCB/EERC-83/10 "Optimal Design of Friction-Braced Frames under Seismic Loading," by Austin, M.A. and Pister, K.S., June 1983, (PB84 119 288)A06.

UCB/EERC-83/11 "Shaking Table Study of Single-Story Masonry Houses: Dynamic Performance under Three Component Seismic Input and Recommendations," by Manos, G.C., Clough, R.W. and Mayes, R.L., July 1983, (UCB/EERC-83/11)A08.

UCB/EERC-83/12 "Experimental Error Propagation in Pseudodynamic Testing," by Shiing, P.B. and Mahin, S.A., June 1983, (PB84 119 270)A09.

UCB/EERC-83/13 "Experimental and Analytical Predictions of the Mechanical Characteristics of a 1/5-scale Model of a 7-story R/C Frame-Wall Building Structure," by Aktan, A.E., Bertero, V.V., Chowdhury, A.A. and Nagashima, T., June 1983, (PB84 119 213)A07.

UCB/EERC-83/14 "Shaking Table Tests of Large-Panel Precast Concrete Building System Assemblages," by Oliva, M.G. and Clough, R.W., June 1983, (PB86 110 210/AS)A11.

UCB/EERC-83/15 "Seismic Behavior of Active Beam Links in Eccentrically Braced Frames," by Hjelmstad, K.D. and Popov, E.P., July 1983, (PB84 119 676)A09.

UCB/EERC-83/16 "System Identification of Structures with Joint Rotation," by Dimsdale, J.S., July 1983, (PB84 192 210)A06.

UCB/EERC-83/17 "Construction of Inelastic Response Spectra for Single-Degree-of-Freedom Systems," by Mahin, S. and Lin, J., June 1983, (PB84 208 834)A05.

UCB/EERC-83/18 "Interactive Computer Analysis Methods for Predicting the Inelastic Cyclic Behaviour of Structural Sections," by Kaba, S. and Mahin, S., July 1983, (PB84 192 012)A06.

UCB/EERC-83/19 "Effects of Bond Deterioration on Hysteretic Behavior of Reinforced Concrete Joints," by Filippou, F.C., Popov, E.P. and Bertero, V.V., August 1983, (PB84 192 020)A10.

UCB/EERC-83/20 "Analytical and Experimental Correlation of Large-Panel Precast Building System Performance," by Oliva, M.G., Clough, R.W., Velkov, M. and Gavrilovic, P., November 1983.

UCB/EERC-83/21 "Mechanical Characteristics of Materials Used in a 1/5 Scale Model of a 7-Story Reinforced Concrete Test Structure," by Bertero, V.V., Aktan, A.E., Harris, H.G. and Chowdhury, A.A., October 1983, (PB84 193 697)A05.

UCB/EERC-83/22 "Hybrid Modelling of Soil-Structure Interaction in Layered Media," by Tzong, T.-J. and Penzien, J., October 1983, (PB84 192 178)A08.

UCB/EERC-83/23 "Local Bond Stress-Slip Relationships of Deformed Bars under Generalized Excitations," by Eligehausen, R., Popov, E.P. and Bertero, V.V., October 1983, (PB84 192 848)A09.

UCB/EERC-83/24 "Design Considerations for Shear Links in Eccentrically Braced Frames," by Malley, J.O. and Popov, E.P., November 1983, (PB84 192 186)A07.

UCB/EERC-84/01 "Pseudodynamic Test Method for Seismic Performance Evaluation: Theory and Implementation," by Shing, P.-S.B. and Mahin, S.A., January 1984, (PB84 190 644)A08.

UCB/EERC-84/02 "Dynamic Response Behavior of Kiang Hong Dian Dam," by Clough, R.W., Chang, K.-T., Chen, H.-Q. and Stephen, R.M., April 1984, (PB84 209 402)A08.

UCB/EERC-84/03 "Refined Modelling of Reinforced Concrete Columns for Seismic Analysis," by Kaba, S.A. and Mahin, S.A., April 1984, (PB84 234 384)A06.

UCB/EERC-84/04 "A New Floor Response Spectrum Method for Seismic Analysis of Multiply Supported Secondary Systems," by Asfura, A. and Der Kiureghian, A., June 1984, (PB84 239 417)A06.

UCB/EERC-84/05 "Earthquake Simulation Tests and Associated Studies of a 1/5th-scale Model of a 7-Story R/C Frame-Wall Test Structure," by Bertero, V.V., Aktan, A.E., Charney, F.A. and Sause, R., June 1984, (PB84 239 409)A09.

UCB/EERC-84/06 "R/C Structural Walls: Seismic Design for Shear," by Aktan, A.E. and Bertero, V.V., 1984.

UCB/EERC-84/07 "Behavior of Interior and Exterior Flat-Plate Connections subjected to Inelastic Load Reversals," by Zee, H.L. and Moehle, J.P., August 1984, (PB86 117 629/AS)A07.

UCB/EERC-84/08 "Experimental Study of the Seismic Behavior of a Two-Story Flat-Plate Structure," by Moehle, J.P. and Diebold, J.W., August 1984, (PB86 122 553/AS)A12.

UCB/EERC-84/09 "Phenomenological Modeling of Steel Braces under Cyclic Loading," by Ikeda, K., Mahin, S.A. and Dermitzakis, S.N., May 1984, (PB86 132 198/AS)A08.

UCB/EERC-84/10 "Earthquake Analysis and Response of Concrete Gravity Dams," by Fenves, G. and Chopra, A.K., August 1984, (PB85 193 902/AS)A11.

UCB/EERC-84/11 "EAGD-84: A Computer Program for Earthquake Analysis of Concrete Gravity Dams," by Fenves, G. and Chopra, A.K., August 1984, (PB85 193 613/AS)A05.

UCB/EERC-84/12 "A Refined Physical Theory Model for Predicting the Seismic Behavior of Braced Steel Frames," by Ikeda, K. and Mahin, S.A., July 1984, (PB85 191 450/AS)A09.

UCB/EERC-84/13 "Earthquake Engineering Research at Berkeley - 1984," by , August 1984, (PB85 197 341/AS)A10.

UCB/EERC-84/14 "Moduli and Damping Factors for Dynamic Analyses of Cohesionless Soils," by Seed, H.B., Wong, R.T., Idriss, I.M. and Tokimatsu, K., September 1984, (PB85 191 468/AS)A04.

UCB/EERC-84/15 "The Influence of SPT Procedures in Soil Liquefaction Resistance Evaluations," by Seed, H.B., Tokimatsu, K., Harder, L.F. and Chung, R.M., October 1984, (PB85 191 732/AS)A04.

UCB/EERC-84/16 "Simplified Procedures for the Evaluation of Settlements in Sands Due to Earthquake Shaking," by Tokimatsu, K. and Seed, H.B., October 1984, (PB85 197 887/AS)A03.

UCB/EERC-84/17 "Evaluation of Energy Absorption Characteristics of Bridges under Seismic Conditions," by Imbsen, R.A. and Penzien, J., November 1984.

UCB/EERC-84/18 "Structure-Foundation Interactions under Dynamic Loads," by Liu, W.D. and Penzien, J., November 1984, (PB87 124 889/AS)A11.

UCB/EERC-84/19 "Seismic Modelling of Deep Foundations," by Chen, C.-H. and Penzien, J., November 1984, (PB87 124 798/AS)A07.

UCB/EERC-84/20 "Dynamic Response Behavior of Quan Shui Dam," by Clough, R.W., Chang, K.-T., Chen, H.-Q., Stephen, R.M., Ghanaat, Y. and Qi, J.-H., November 1984, (PB86 115177/AS)A07.

UCB/EERC-85/01 "Simplified Methods of Analysis for Earthquake Resistant Design of Buildings," by Cruz, E.F. and Chopra, A.K., February 1985, (PB86 112299/AS)A12.

UCB/EERC-85/02 "Estimation of Seismic Wave Coherency and Rupture Velocity using the SMART 1 Strong-Motion Array Recordings," by Abrahamson, N.A., March 1985, (PB86 214 343)A07.

UCB/EERC-85/03 "Dynamic Properties of a Thirty Story Condominium Tower Building," by Stephen, R.M., Wilson, E.L. and Stander, N., April 1985, (PB86 118965/AS)A06.

UCB/EERC-85/04 "Development of Substructuring Techniques for On-Line Computer Controlled Seismic Performance Testing," by Dermitzakis, S. and Mahin, S., February 1985, (PB86 132941/AS)A08.

UCB/EERC-85/05 "A Simple Model for Reinforcing Bar Anchorages under Cyclic Excitations," by Filippou, F.C., March 1985, (PB86 112 919/AS)A05.

UCB/EERC-85/06 "Racking Behavior of Wood-framed Gypsum Panels under Dynamic Load," by Oliva, M.G., June 1985.

UCB/EERC-85/07 "Earthquake Analysis and Response of Concrete Arch Dams," by Fok, K.-L. and Chopra, A.K., June 1985, (PB86 139672/AS)A10.

UCB/EERC-85/08 "Effect of Inelastic Behavior on the Analysis and Design of Earthquake Resistant Structures," by Lin, J.P. and Mahin, S.A., June 1985, (PB86 135340/AS)A08.

UCB/EERC-85/09 "Earthquake Simulator Testing of a Base-Isolated Bridge Deck," by Kelly, J.M., Buckle, I.G. and Tsai, H.-C., January 1986, (PB87 124 152/AS)A06.

UCB/EERC-85/10 "Simplified Analysis for Earthquake Resistant Design of Concrete Gravity Dams," by Fenves, G. and Chopra, A.K., June 1986, (PB87 124 160/AS)A08.

UCB/EERC-85/11 "Dynamic Interaction Effects in Arch Dams," by Clough, R.W., Chang, K.-T., Chen, H.-Q. and Ghanaat, Y., October 1985, (PB86 135027/AS)A05.

UCB/EERC-85/12 "Dynamic Response of Long Valley Dam in the Mammoth Lake Earthquake Series of May 25-27, 1980," by Lai, S. and Seed, H.B., November 1985, (PB86 142304/AS)A05.

UCB/EERC-85/13 "A Methodology for Computer-Aided Design of Earthquake-Resistant Steel Structures," by Austin, M.A., Pister, K.S. and Mahin, S.A., December 1985, (PB86 159480/AS)A10 .

UCB/EERC-85/14 "Response of Tension-Leg Platforms to Vertical Seismic Excitations," by Liou, G.-S., Penzien, J. and Yeung, R.W., December 1985, (PB87 124 871/AS)A08.

UCB/EERC-85/15 "Cyclic Loading Tests of Masonry Single Piers: Volume 4 - Additional Tests with Height to Width Ratio of 1," by Sveinsson, B., McNiven, H.D. and Sucuoglu, H., December 1985.

UCB/EERC-85/16 "An Experimental Program for Studying the Dynamic Response of a Steel Frame with a Variety of Infill Partitions," by Yanev, B. and McNiven, H.D., December 1985.

UCB/EERC-86/01 "A Study of Seismically Resistant Eccentrically Braced Steel Frame Systems," by Kasai, K. and Popov, E.P., January 1986, (PB87 124 178/AS)A14.

UCB/EERC-86/02 "Design Problems in Soil Liquefaction," by Seed, H.B., February 1986, (PB87 124 186/AS)A03.

UCB/EERC-86/03 "Implications of Recent Earthquakes and Research on Earthquake-Resistant Design and Construction of Buildings," by Bertero, V.V., March 1986, (PB87 124 194/AS)A05.

UCB/EERC-86/04 "The Use of Load Dependent Vectors for Dynamic and Earthquake Analyses," by Leger, P., Wilson, E.L. and Clough, R.W., March 1986, (PB87 124 202/AS)A12.

UCB/EERC-86/05 "Two Beam-To-Column Web Connections," by Tsai, K.-C. and Popov, E.P., April 1986, (PB87 124 301/AS)A04.

UCB/EERC-86/06 "Determination of Penetration Resistance for Coarse-Grained Soils using the Becker Hammer Drill," by Harder, L.F. and Seed, H.B., May 1986, (PB87 124 210/AS)A07.

UCB/EERC-86/07 "A Mathematical Model for Predicting the Nonlinear Response of Unreinforced Masonry Walls to In-Plane Earthquake Excitations," by Mengi, Y. and McNiven, H.D., May 1986, (PB87 124 780/AS)A06.

UCB/EERC-86/08 "The 19 September 1985 Mexico Earthquake: Building Behavior," by Bertero, V.V., July 1986.

UCB/EERC-86/09 "EACD-3D: A Computer Program for Three-Dimensional Earthquake Analysis of Concrete Dams," by Fok, K.-L., Hall, J.F. and Chopra, A.K., July 1986, (PB87 124 228/AS)A08.

UCB/EERC-86/10 "Earthquake Simulation Tests and Associated Studies of a 0.3-Scale Model of a Six-Story Concentrically Braced Steel Structure," by Uang, C.-M. and Bertero, V.V., December 1986, (PB87 163 564/AS)A17.

UCB/EERC-86/11 "Mechanical Characteristics of Base Isolation Bearings for a Bridge Deck Model Test," by Kelly, J.M., Buckle, I.G. and Koh, C.-G., 1987.

UCB/EERC-86/12 "Effects of Axial Load on Elastomeric Isolation Bearings," by Koh, C.-G. and Kelly, J.M., November 1987.

UCB/EERC-87/01 "The FPS Earthquake Resisting System: Experimental Report," by Zayas, V.A., Low, S.S. and Mahin, S.A., June 1987.

UCB/EERC-87/02 "Earthquake Simulator Tests and Associated Studies of a 0.3-Scale Model of a Six-Story Eccentrically Braced Steel Structure," by Whittaker, A., Uang, C.-M. and Bertero, V.V., July 1987.

UCB/EERC-87/03 "A Displacement Control and Uplift Restraint Device for Base-Isolated Structures," by Kelly, J.M., Griffith, M.C. and Aiken, I.D., April 1987.

UCB/EERC-87/04 "Earthquake Simulator Testing of a Combined Sliding Bearing and Rubber Bearing Isolation System," by Kelly, J.M. and Chalhoub, M.S., 1987.

UCB/EERC-87/05 "Three-Dimensional Inelastic Analysis of Reinforced Concrete Frame-Wall Structures," by Moazzami, S. and Bertero, V.V., May 1987.

UCB/EERC-87/06 "Experiments on Eccentrically Braced Frames with Composite Floors," by Ricles, J. and Popov, E., June 1987.

UCB/EERC-87/07 "Dynamic Analysis of Seismically Resistant Eccentrically Braced Frames," by Ricles, J. and Popov, E., June 1987.

UCB/EERC-87/08 "Undrained Cyclic Triaxial Testing of Gravels-The Effect of Membrane Compliance," by Evans, M.D. and Seed, H.B., July 1987.

UCB/EERC-87/09 "Hybrid Solution Techniques for Generalized Pseudo-Dynamic Testing," by Thewalt, C. and Mahin, S.A., July 1987.

UCB/EERC-87/10 "Ultimate Behavior of Butt Welded Splices in Heavy Rolled Steel Sections," by Bruneau, M., Mahin, S.A. and Popov, E.P., July 1987.

UCB/EERC-87/11 "Residual Strength of Sand from Dam Failures in the Chilean Earthquake of March 3, 1985," by De Alba, P., Seed, H.B., Retamal, E. and Seed, R.B., September 1987.

UCB/EERC-87/12 "Inelastic Seismic Response of Structures with Mass or Stiffness Eccentricities in Plan," by Bruneau, M. and Mahin, S.A., September 1987.

UCB/EERC-87/13 "CSTRUCT: An Interactive Computer Environment for the Design and Analysis of Earthquake Resistant Steel Structures," by Austin, M.A., Mahin, S.A. and Pister, K.S., September 1987.

UCB/EERC-87/14 "Experimental Study of Reinforced Concrete Columns Subjected to Multi-Axial Loading," by Low, S.S. and Moehle, J.P., September 1987.

UCB/EERC-87/15 "Relationships between Soil Conditions and Earthquake Ground Motions in Mexico City in the Earthquake of Sept. 19, 1985," by Seed, H.B., Romo, M.P., Sun, J., Jaime, A. and Lysmer, J., October 1987.

UCB/EERC-87/16 "Experimental Study of Seismic Response of R. C. Setback Buildings," by Shahrooz, B.M. and Moehle, J.P., October 1987.

UCB/EERC-87/17 "The Effect of Slabs on the Flexural Behavior of Beams," by Pantazopoulou, S.J. and Moehle, J.P., October 1987.

UCB/EERC-87/18 "Design Procedure for R-FBI Bearings," by Mostaghel, N. and Kelly, J.M., November 1987.

UCB/EERC-87/19 "Analytical Models for Predicting the Lateral Response of R C Shear Walls: Evaluation of their Reliability," by Vulcano, A. and Bertero, V.V., November 1987.

UCB/EERC-87/20 "Earthquake Response of Torsionally-Coupled Buildings," by Hejal, R. and Chopra, A.K., December 1987.

UCB/EERC-87/21 "Dynamic Reservoir Interaction with Monticello Dam," by Clough, R.W., Ghanaat, Y. and Qiu, X-F., December 1987.

UCB/EERC-87/22 "Strength Evaluation of Coarse-Grained Soils," by Siddiqi, F.H., Seed, R.B., Chan, C.K., Seed, H.B. and Pyke, R.M., December 1987.

UCB/EERC-88/01 "Seismic Behavior of Concentrically Braced Steel Frames," by Khatib, I., Mahin, S.A. and Pister, K.S., January 1988.

UCB/EERC-88/02 "Experimental Evaluation of Seismic Isolation of Medium-Rise Structures Subject to Uplift," by Griffith, M.C., Kelly, J.M., Coveney, V.A. and Koh, C.G., January 1988.

UCB/EERC-88/03 "Cyclic Behavior of Steel Double Angle Connections," by Astaneh-Asl, A. and Nader, M.N., January 1988.

UCB/EERC-88/04 "Re-evaluation of the Slide in the Lower San Fernando Dam in the Earthquake of Feb. 9, 1971," by Seed, H.B., Seed, R.B., Harder, L.F. and Jong, H.-L., April 1988.

UCB/EERC-88/05 "Experimental Evaluation of Seismic Isolation of a Nine-Story Braced Steel Frame Subject to Uplift," by Griffith, M.C., Kelly, J.M. and Aiken, I.D., May 1988.

UCB/EERC-88/06 "DRAIN-2DX User Guide.," by Allahabadi, R. and Powell, G.H., March 1988.

UCB/EERC-88/07 "Cylindrical Fluid Containers in Base-Isolated Structures," by Chalhoub, M.S. and Kelly, J.M. , April 1988.

UCB/EERC-88/08 "Analysis of Near-Source Waves: Separation of Wave Types using Strong Motion Array Recordings," by Darragh, R.B., June 1988.

UCB/EERC-88/09 "Alternatives to Standard Mode Superposition for Analysis of Non-Classically Damped Systems," by Kusainov, A.A. and Clough, R.W., June 1988.

UCB/EERC-88/10 "The Landslide at the Port of Nice on October 16, 1979," by Seed, H.B., Seed, R.B., Schlosser, F., Blondeau, F. and Juran, I., June 1988.

UCB/EERC-88/11 "Liquefaction Potential of Sand Deposits Under Low Levels of Excitation," by Carter, D.P. and Seed, H.B., August 1988.

UCB/EERC-88/12 "Nonlinear Analysis of Reinforced Concrete Frames Under Cyclic Load Reversals," by Filippou, F.C. and Issa, A., September 1988.